AN ABSTRACT OF THE THESIS OF

Clifford Lyons Trump for the degree of Doctor of Philosophy

in Oceanography presented on August 19, 1976

Title: EFFECTS OF MESOSCALE ATMOSPHERIC CONVECTIVE CELLS ON THE WATERS OF THE EAST CHINA SEA

Abstract approved: Redacted for Privacy

Stephen J. Neshyba

Currents and atmospheric parameters were measured in the East China Sea in February, 1975 as part of the AMTEX'75 program. These data were used to describe outbreaks of cold continental air over this warm and shallow sea. Particular emphasis was placed on describing the structure of mesoscale atmospheric cells embedded in the outbreaks and the effects of these cells on the water column. The general current features were also described.

Two cold air outbreaks were recorded. Heat fluxes (latent plus sensible) as high as 1430 cal/cm^{2}day were calculated. Evidence of mesoscale atmospheric cells was found during outbreaks in satellite imagery and in solarimeter data. The development of mesoscale cells was described by correlating fluctuations in the air temperature and absolute humidity records. The cells were found to be best developed when satellite imagery showed they were of the closed variety. The data suggest that cellular activity matures from open to closed cell types.

During the period of greatest cellular development a representative closed cell was 22 km in diameter, moved at 8 m/sec over the spar buoy, had a temperature fluctuation of .4°C, an absolute humidity fluctuation of .4 g/kg, and wind speed and heat flux fluctuations of $\approx$ 12%.

A non-dimensional index, formed from the fluctuations of the air temperature and absolute humidity records, was used to indicate the passage of mesoscale atmospheric cells over the measuring site. Using this index as input and the fluctuations in the oceanic parameters at a depth of 20 meters as output, it was found that the passage of mature cells was significantly correlated with temperature fluctuations and current fluctuations aligned 25° to the right of the wind about 45 minutes later.

The currents were heavily dominated by the semi-diurnal tide. The current records were noisier during cold air outbreaks. A weak mean flow existed parallel to the Kuroshio flowing towards the northeast. This mean flow exhibited meandering characteristics that approached closed loop currents. Shorter period current fluctuations (less than 5 hours) were aligned 25° to the right of the wind indicative of Ekman veering. The waters were basically isothermal in the vertical, at least to 75 meters (total water depth $\approx$110 meters), though vertical temperature gradients appeared in Thermistor chain data with periods of 12.4 and 24 hours. The water temperature decreased during cold air outbreaks.

Effects of Mesoscale Atmospheric Convective Cells on the Waters of the East China Sea

by

Clifford Lyons Trump

A THESIS

submitted to

Oregon State University

in partial fulfillment of
the requirements for the
degree of

Doctor of Philosophy

Completed August 1976

Commencement June 1977

APPROVED:

Redacted for Privacy

Professor of Oceanography
in charge of major

Redacted for Privacy

Dean of School of Oceanography

Redacted for Privacy

Dean of Graduate School

Date thesis is presented August 19, 1976

Typed by Mary Jo Stratton for Clifford Lyons Trump

TABLE OF CONTENTS

LIST OF FIGURES

LIST OF SYMBOLS AND ABBREVIATIONS

AH	Absolute humidity calculated at AMTEX station 10
AMTEX	Air Mass Transformation Experiment
BR	Bowens Ratio = HS/HL
CM4	Current meter at AMTEX station 4
CS(4)	Current speed measured by CM4
CM7	Current meter at AMTEX station 7
CS(7)	Current speed measured by CM7
CD(7)	Current direction measured by CM7
CU(7)	U current component measured by CM7, positive east
CV(7)	V current component measured by CM7, positive north
CUE(7)	Current component measured by CM7 115° to right of mean wind direction
CVE(7)	Current component measured by CM7 25° to right of mean wind direction
CM10	Current meter at AMTEX station 10
CS(10)	Current speed measured by CM10
CD(10)	Current direction measured by CM10
CU(10)	U current component measured by CM10, positive east
CV(10)	V current component measured by CM10, positive north
CUE(10)	Current component measured by CM10 115° to right of mean wind direction
CVE(10)	Current component measured by CM10 25° to right of mean wind direction

DB	Dry bulb air temperature measured on SB10
HS	Sensible heat flux calculated at AMTEX station 10
HL	Latent heat flux calculated at AMTEX station 10
HF	HS + HL
MSI	Dimensionless index of mesoscale cellular activity at AMTEX station 10
SB10	Spar buoy at AMTEX station 10
SOL	Solarimeter data, a measure of incoming solar radiation at AMTEX station 10
ST0(10)	Sea temperature near surface measured on SB10
ST5(10)	Sea temperature at a depth of 5 meters measured on SB10
ST15(10)	Sea temperature at a depth of 15 meters measured on SB10
ST20(10)	Sea temperature at a depth of 20 meters measured on CM10
ST20(4)	Sea temperature at a depth of 20 meters measured on CM4
ST20(7)	Sea temperature at a depth of 20 meters measured on CM7
STD	Salinity, temperature, depth record
TC1	Thermistor chain at AMTEX station 1
TC1(20)	Sea temperature, at a depth of 20 meters measured by TC1
TC1(70)	Sea temperature at a depth of 70 meters measured by TC1
TC3	Thermistor chain at AMTEX station 3
TC3(20)	Sea temperature at a depth of 20 meters measured by TC3
TC3(70)	Sea temperature at a depth of 70 meters measured by TC3

TC11	Thermistor chain at AMTEX station 11
TC11(20)	Sea temperature at a depth of 20 meters measured by TC11
TC11(70)	Sea temperature at a depth of 70 meters measured by TC11
TS	Temperature-salinity values of sea water
V(7)	Current velocity measured by CM7
V(10)	Current velocity measured by CM10
WS	Wind speed measured by SB10
WD	Wind direction measured by SB10
WB	Wet bulb air temperature measured by SB10

EFFECTS OF MESOSCALE ATMOSPHERIC CONVECTIVE CELLS ON THE WATERS OF THE EAST CHINA SEA

I. INTRODUCTION

During the winter season cold, dry air builds up over continental land masses and periodically breaks out and flows over the adjacent waters. If the waters are warm, as is the case off the east coasts of North America and Asia, situations develop in which massive amounts of energy are transferred from the ocean to the atmosphere. Since these areas are also areas of cyclonic storm formation and strengthening it has been felt that this input of oceanic energy played a significant role. Although this phenomenon has been studied for years in the waters around Japan (e.g. Malkus, 1962), the actual mechanisms of organizing oceanic energy into cyclonic disturbances remain unclear.

In the 1960's satellite photographs revealed that when convective clouds formed over oceanic waters they often grouped into ring-like structures, about 30 to 80 kilometers in diameter, somewhat analogous to Bénard cells. This phenomenon was pronounced during cold air outbreaks. Meterologists became interested in these mesoscale cloud rings as a possible intermediate step in the organization of oceanic energy into storms. As a result an international research

program, AMTEX (Air Mass Transformation Experiment), was organized to study intensively the cold air outbreaks in general and mesoscale convective cells in particular. The area chosen for AMTEX was the East China Sea to the southwest of Japan, where cold air outbreaks, cyclogenesis, mesoscale cloud rings and large upward heat fluxes are prevalent.

In February, 1975, as part of the AMTEX '75 program, Oregon State University deployed an array of meterological spar buoys in the East China Sea to measure atmospheric parameters where they would be unaffected by the presence of land or ships. AMTEX was mainly concerned with how the cold dry air was modified by the warm ocean waters, while the subject of this dissertation is how the warm ocean reacts to the cold, dry air in general, and how it reacts to the passage of mesoscale atmospheric cells in particular.

To study this the spar buoy array was supplemented with three current meters. The current meter data were examined to see if the water movements and sea temperatures reflected the passage of the cells. The meteorological spar buoy data were used to determine when the cells were present, when they significantly affected surface conditions, and what form these surface effects took.

The current meter data were also used to describe the general features of the currents in the area, both to provide a setting for studying the effects of mesoscale cells and also because accurate

current meter records have not previously been taken in the East China Sea. The sea temperatures, as measured on the current meters, spar buoy, and on three thermistor chains, were examined to again provide a setting for the analysis of the effects of mesoscale cells and also to give an idea of the thermal response of the sea to the cold air outbreaks.

Surface cooling and evaporation during cold air outbreaks result in unstable conditions which cause surface waters to sink. Some aspects of this sinking process, particularly how the process was affected by the passage of mesoscale atmospheric cells, were studied.

II. PREVIOUS WORK

Heat Fluxes during Cold Air Outbreaks

Intense winter season outbreaks of cold continental air over the ocean have been studied in several areas of the northern hemisphere. Outbreaks are generally restricted to mid latitudes off the eastern edges of continents by the blocking action of the Aleutian and Icelandic lows (Worthington, 1972). These outbreaks are characterized by high sensible and latent heat fluxes from the ocean to the atmosphere. A variety of techniques have been used to estimate these fluxes and consequently the results are difficult to compare.

Manabe (1957) and Malkus (1962) discussed the atmospheric effects of an outbreak over the Sea of Japan. Estimates of heat exchanges were made by performing a heat balance on the air mass over the Sea of Japan using aerological data from surrounding land stations. They estimated a sensible heat transfer of 1030 cal/cm^{2}day and a latent heat transfer of 450 cal/cm^{2}day. Other terms in air-sea heat exchange budget were estimated to be minimal. They also felt that the oceanic heat source resulted in a synoptic scale convergence field which aided cyclonic development.

In the Atlantic off the Carolina coasts, Ichiye and Zipser (1967) reported very large heat transfer during six hours of an extreme

outbreak. Using data from three airplane flights along air flow trajectories a total mean heat flux of 8234 cal/cm^{2}day (3017 cal/cm^{2}day of sensible heat and 5217 cal/cm^{2}day of latent heat) was estimated. The estimate peaked over the Gulf Stream to a total of nearly 10,000 cal/cm^{2}day. The latent heat loss over the Gulf Stream required an evaporation rate of over five centimeters of water per day.

Off the Gulf Coast of Texas outbreaks are called "Northers." Using changes in sea temperature during a 15 day Norther, Nowlin and Parker (1974) estimated an average total heat loss rate of 400 cal/cm^{2}day within 50 kilometers of shore and 700-1500 cal/cm^{2}day farther offshore. At first thought one would expect the heat loss to be greatest near shore where the air has not been modified by the waters. Nowlin and Parker felt that the nearshore waters, being shallower, were cooled by the air mass more rapidly than the deeper offshore waters. As a result, over the 15 day period of the Norther, the average air-sea temperature difference was less nearshore, and therefore the heat exchanges were less.

In southern Europe winter season cold air flows are called "Mistrals." Bunker (1972), using aircraft data taken as part of the MEDOC study of a Mistral in the Mediterranean Sea off southern France, estimated a sensible heat flux of 383 cal/cm^{2}day and a latent heat flux of 970 cal/cm^{2}day.

The AMTEX program, which consisted of two experiments in successive years, studied cold air outbreaks in the East China Sea. The preliminary results from the first year, AMTEX '74, indicated sensible and latent heat fluxes during an outbreak of 690 and 860 cal/cm^{2}day respectively. The flux estimates were based on 12 hourly aerological and surface data sets from six stations. Preliminary estimates of the AMTEX '74 heat fluxes based on the bulk aerodynamic method were smaller than the above estimates. In spite of variances in estimates the total heat fluxes during a cold air outbreak in the AMTEX area in 1974 were from 1000 to 1500 cal/cm^{2}day.

In all the above mentioned studies latent and sensible heat fluxes were found to be the dominant terms in the air-sea heat exchange. The total cold air outbreak heat flux estimated ranged from 1000 to 10,000 cal/cm^{2}day, though most were around 1000 cal/cm^{2}day. In all cases but one (Manebe, 1957; Malkus, 1962) the latent heat flux was greater than the sensible heat flux.

Effects of Outbreaks on Ocean Waters

Due to large heat fluxes during outbreaks over oceans, the waters will become cooler and more saline causing surface density to increase. The surface waters will then become unstable and sink.

Nowlin and Parker (1974) found that during a Texas Norther the continental shelf waters showed a temperature drop and salinity increase and that the TS characteristics at the end of the outbreak were similar to those of a water type found beneath the Subtropical Underwater core in the Gulf of Mexico. They concluded that the modified shelf waters flowed off the shelf and acted as a source of deeper Gulf water.

The primary purpose of the MEDOC program off southern France was not to study a cold air outbreak, but to study the formation of Mediterranean Deep water during a Mistral. Stommel, Voorhis, and Webb (1971) found that the Mistral caused dramatic sinking of surface waters in localized regions. Within one of these regions before the Mistral there was a mixed layer about 200 meters thick and then 2000 meters of fairly stable water with a potential temperature change from 13.17°C at 200 meters to 12.72°C at 2200 meters. After the Mistral the water was well mixed at 12.80°C to 2200 meters. Using a vertical current meter it was found that the sinking process was one of intermittent convective downward plumes on a hierarchy of horizontal scales up to one to five kilometers alternating with upward flow of deeper water. After the Mistral the newly formed water spread out at a depth of about 900 meters.

In a larger scale hypothesis Worthington (1971) feels the late winter outbreaks off the east coasts of North America and Asia produce deep isothermal layers on the inside of the North Atlantic and North Pacific gyres and subsequently are in a large part responsible for the general circulation in these regions.

Sinking Processes of Modified Surface Waters

In a series of papers, T.D. Foster has tried to describe how surface water, upon having its density increased, mixes to depth. For the molecular case of pure water cooled from above by evaporation he proposes a cyclic process: a thermal boundary layer is formed by diffusion; this layer eventually becomes unstable and is destroyed by a localized convective downflow that drains the boundary layer, the convective element dies down at depth, and finally the surface boundary layer is reformed by diffusion (Foster, 1971). He has developed a linear model for this process that gives characteristic horizontal spacing and periodicity of this cycle and has found rough confirmation by laboratory experiments. In another paper Foster (1972) discusses a similar process in a salt driven regime. Here he discusses the Weddell Sea where the density of the surface waters is increased by the freezing of sea ice and subsequent release of salt. In this paper he extends his argument by hypothesizing that the molecular intermittent convective process does not mix to the

bottom, but rather forms a secondary boundary layer that will itself go through a similar cyclic process with a turbulent mixing viscosity forming larger secondary convective plumes.

Foster has presented no evidence that the above process takes place. He also has not looked at the more difficult problem of a system forced both by cooling and increasing salinity under a wind stressed turbulent regime. On a first approximation, if the mixing process is fully turbulent and dropping temperature and increasing salinity were combined into one density increasing term, then an analogous process could take place and large convective elements could periodically develop.

It is conceivable that convective plumes do not only transfer cooler, more saline water to depth, but that they also transfer momentum. Leetmaa and Welch (1972) consider the situation of a steady wind blowing over tropical waters. They propose that the wind imparts momentum only to the topmost homogeneous layer. They refer to a diurnal situation where daytime solar heating produces a stable surface wave-mixed layer about eight meters thick, and nighttime radiative cooling convectively mixes the water to about 100 meters. They feel, and have supporting evidence, that the wind stress will impart momentum just to the upper eight meters during daylight hours producing higher surface currents, and that this momentum will be diffused down to 100 meters at night resulting

in slower surface currents. If this idea is valid then the currents below eight meters must be greater at night than in the day.

Mesoscale Atmospheric Convective Cells

In the early 1960's satellite imagery revealed that over large areas of the ocean cumulus clouds were not scattered randomly, but organized into cell-like groupings from 30 to 80 kilometers in diameter. This discovery suggested a scale of free convective motion that is significant to air-sea exchange mechanisms in the planetary boundary layer (Agee, Chen, and Dowell, 1973). Hubert (1966) formulated a statistical model wherein organized cloud formations could usually be classified as "open" or "closed" cells (Fig. 1). In an open cell air rises on the edge of the cell and sinks in the center. Clouds will form in the rising air and therefore an open cell, in a satellite photo, appears as a polygonal clear area surrounded by cloudy walls. On the other hand, in a closed cell air rises in the center and descends on the edges and appears in satellite photos as polygonal cloudy areas surrounded by clear walls. In the laboratory convective cells usually form in regular hexagonal shapes with even horizontal scales. In the atmosphere the cells are not very regular and show a spread in horizontal scales. Also, in the atmosphere open and closed cells can occur simultaneously in a given area (e.g. Fig. 26).

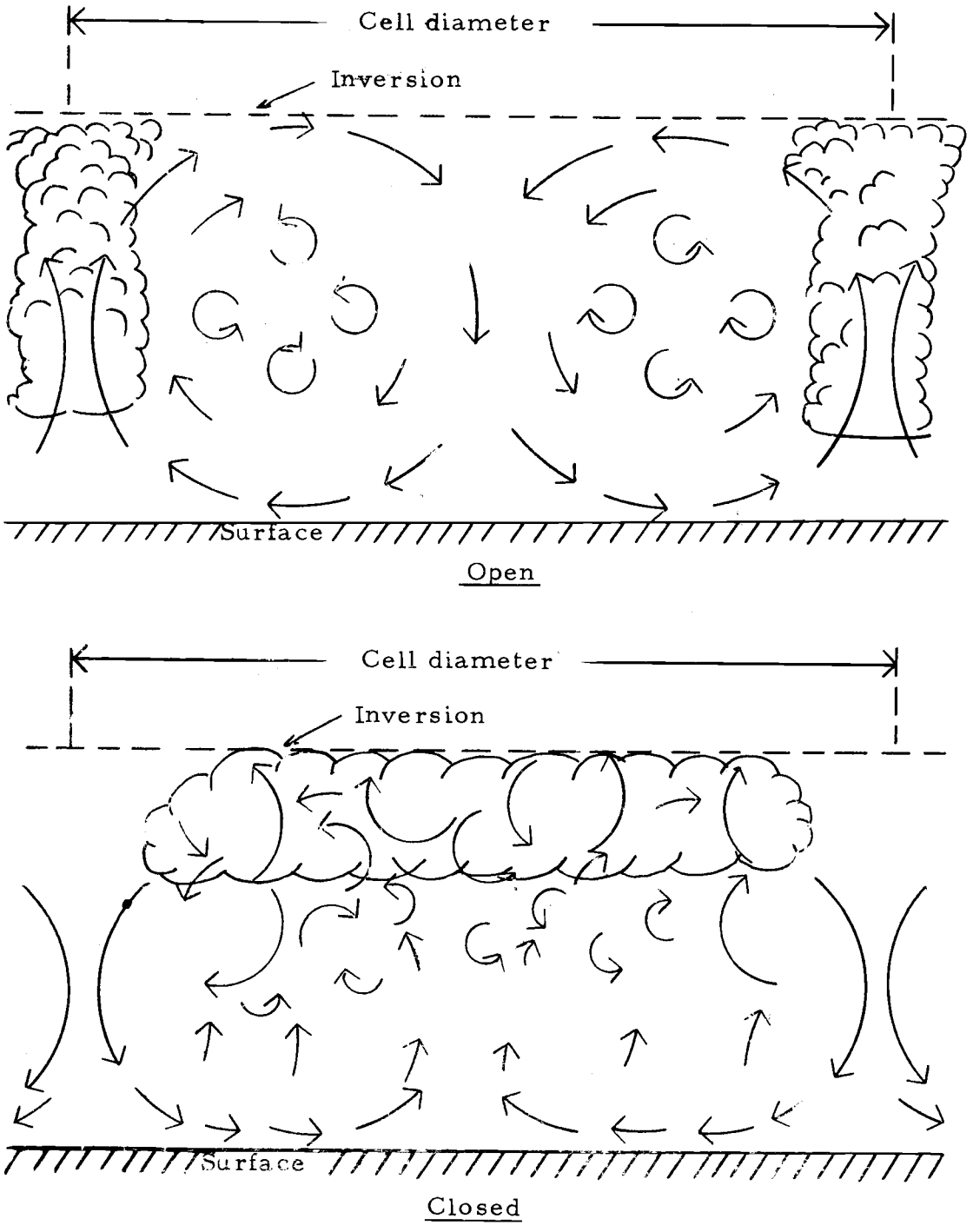

Figure 1. Cross-sectional model of open and closed cells (from Hubert, 1966).

The aspect ratio (ratio of diameter to depth) of the atmospheric cells usually ranges from 20:1 to 30:1. This compares with laboratory convective cell aspect ratios of around 3:1. Agee, Chen, and Dowell (1973) propose that this difference is due to the anisotropic eddy viscosity in the atmosphere versus the isotropic molecular viscosity in the laboratory. These authors also found that open cells were generally found over warm waters off the east coasts of continents and closed cells were generally found over cooler waters off the west coasts of continents.

Hubert (1966) concluded that the forcing mechanisms were surface heating at sea level and radiative cooling at the cloud tops. He generally felt that where surface heating dominated open cells would be formed, and where radiative cooling dominated closed cells would be formed. This is in line with his statistical conclusion that open cells are more likely to be found over warm waters and closed cells over cool waters. The key to the sense of circulation seemed to be whether the eddy viscosity decreases with height (open cells) or increases with height (closed cells).

Hubert (1966) also concluded that the cells are frequently confined to a shallow surface layer by an inversion. Formation of cells seemed to require quasi-steady state heating and a negligible vertical wind shear. The quasi-steady state heating requirement necessitates a certain set-up time when cold air flows off a land mass. Photos (e.g. Fig. 28) reveal clear areas adjacent to land where the air is too

dry to form clouds. Further offshore clouds begin to show organization either as streaks parallel to the air flow and/or cells. It should be noted here that although cloud formations act as indicators of cells, it is conceivable that a cellular pattern could exist without the presence of indicative cloud formations.

Effects of Mesoscale Atmospheric Convective Cells on Ocean Waters

Mesoscale cells imbedded in cold air outbreaks organize and modulate the transfer of oceanic energy to the atmosphere. This research was undertaken to see if this modulated heat extraction would cause a recognizable response in the water column. Unfortunately no references could be found that apply directly to this question or to the more general question of oceanic responses to atmospheric processes that occur on time scales on the order of one hour or space scales on the order of 20 kilometers.

East China Sea

The East China and Yellow Seas are situated over a large, flat, shallow shelf bounded on the west and north sides by China and Korea and on the southeast side by the Okinawa trench and Ryukyu island chain (Fig. 2a). The predominant current feature of this area is the Kuroshio, the core of which flows along the continental slope southeast

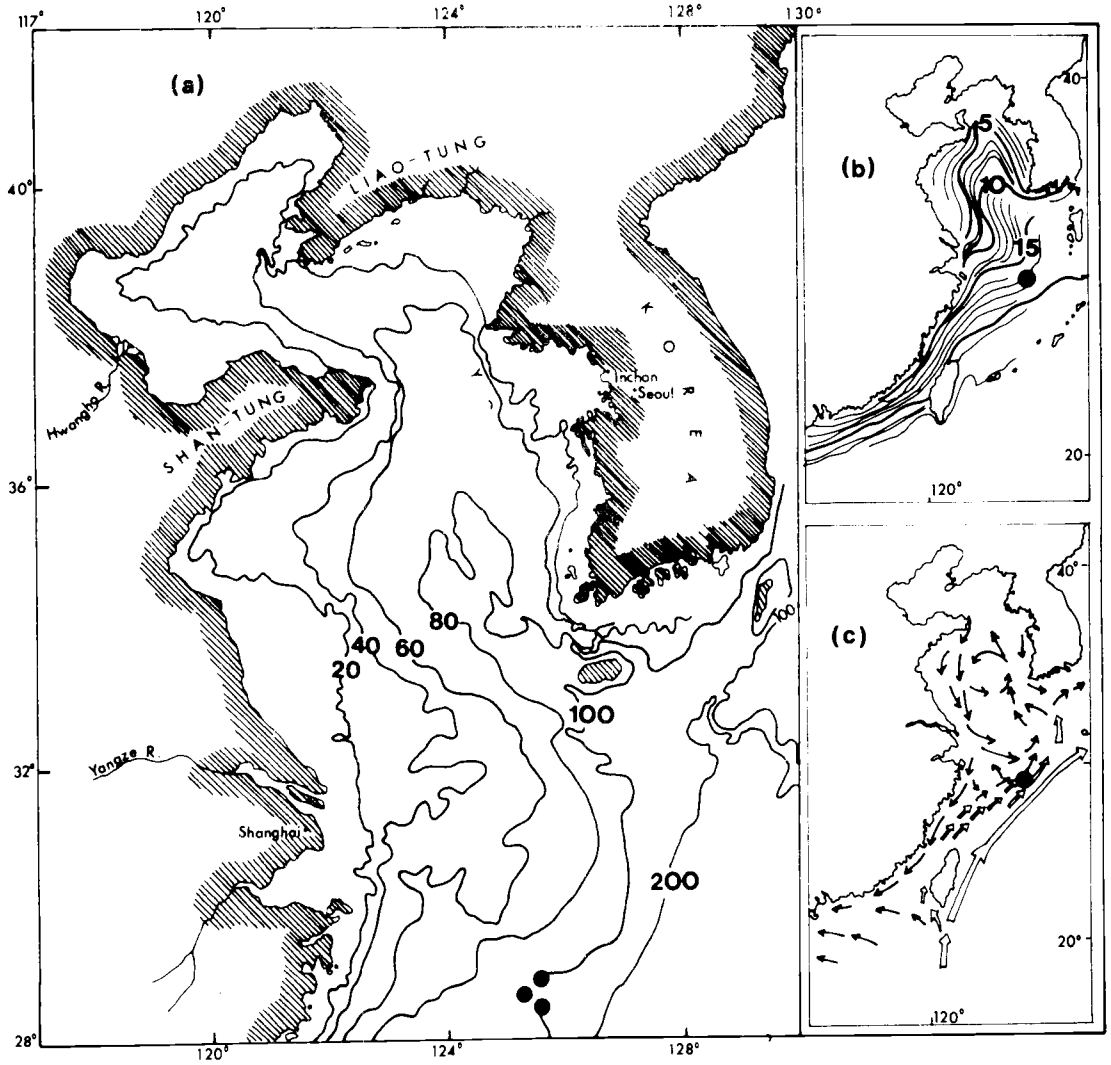

Figure 2. Maps of the East China Sea with current meter positions indicated. (a) bottom topography, (b) wintertime surface temperatures ($^{\circ}$C), and (c) wintertime currents (from Niino and Emery, 1961). Isobath depths in meters.

of the 200 meter isobath from southwest to northeast (Fig. 2c). The bulk of the Kuroshio flows to the east of Japan, some flows between Korea and Japan as the Tsushima Current, and a little flows into the Yellow Sea as a warm current (Niino and Emery, 1961; Ninomiya, 1972; Nitani, 1972). The Yellow Sea warm current is mainly inferred, during the winter, from surface temperature contours (Fig. 2b). A tongue of warm water protrudes up the east side of the Yellow Sea and a tongue of cold water protrudes down the west side and on into the center of the East China Sea. The general circulation in the East China and Yellow Seas, particularly in the winter, is inferred to consist of a counter-clockwise flow with warm Kuroshio water flowing to the north and cold Yellow Sea and river outflow waters (Yangtze and Hwang Ho rivers) flowing to the south. The general currents in the array area (Fig. 2c) would therefore be expected to flow towards the northeast, parallel to the Kuroshio.

No references were found concerning current meter records taken in this region or of more precise current descriptions than those based on sea surface temperatures.

The winter season horizontal temperature structure in the East China Sea (Fig. 2b) is basically a temperature gradient from cold waters (2^{o}C) in the northwest reaches to the warm waters (20^{o}C) of the Kuroshio Current).

III. DATA BASE

AMTEX and the East China Sea

The area chosen for the AMTEX experiments was the East China Sea in the vicinity of the Ryukyu island chain to the southwest of Japan (Fig. 2a). The AMTEX stations were mainly located on islands but some meteorological ships were used in the East China Sea to obtain data unaffected by the presence of land. This area was chosen for several reasons (Lenschow, 1972). The Kuroshio flowing to the northwest through the area keeps the sea surface temperature near 20°C in the winter, while it is also an area of cold air outbreaks from the Chinese mainland. The Kuroshio to the southeast and the cold Asian mainland to the northwest maintain a strong regular temperature gradient in the East China Sea (Fig. 2b). This gradient and the distance of the island recording stations from the Chinese mainland (about 700 kilometers) imply that the cold air mass will be extensively modified by the time it reaches the experimental area. The modified air was what the meteorologists wished to study. Also, satellite photos revealed this to be an area of mesoscale cellular activity.

The array of meteorological spar buoys was deployed in the East China Sea near latitude 28°30' N and longitude 125°20' E

(Fig. 2). This site was chosen for several reasons: (1) it was near one of the meteorological ships of the AMTEX program, the Keifu Maru, which supplied back-up data; (2) it was distant from any land so that there would be no land effects recorded; and (3) the water was shallow ($\approx$100 meters) which facilitated the mooring of these buoys. The bulk of the East China Sea, including the buoy area, lies above a broad, flat continental shelf so that bottom topographic effects should be minimal (Fig. 2a, and Niino and Emery, 1961).

Available Data

The main body of data available for this thesis was obtained from a triangular array of current meters and from one of the meteorological spar buoys moored with the current meters. The triangle was nearly equilateral, 24 kilometers per side, and all data on these meters were measured in five minute intervals. Hourly weather observations were available from the Japanese meteorological ship, Keifu Maru, which was stationed to the southwest of the array. In addition, periodic satellite cloud photos over the East China Sea and occasional STD's in the array area were available.

In addition to the above data records, three thermistor chains were deployed in a line running from northwest to southeast about 25 kilometers to the west of the current meters. Each of these chains measured the sea temperature every five meters from a depth of

20 meters to a depth of 70 meters. These data were recorded in 10 minute intervals.

The meter locations and running periods are summarized in Figures 3 and 4. The three current meters were all suspended 20 meters below the sea surface from subsurface floats. The spar buoy was a 60 foot ($\approx$20 meter) tubular metal shaft tethered to a subsurface float (Robinson, 1973). Current meter number 4 [CM4], located at latitude 28°34.2' N and longitude 125°13.5' E, ran from 1710 February 13, 1975 to 1635 February 24, 1975, and measured current speed [CS(4)], sea temperature [ST20(4)], and pressure, but no current direction. Current meter number 7 [CM7], located at latitude 28°38.8' N and longitude 125°27.2' E, ran from 1520 February 13, 1975 to 1610 March 1, 1975, and measured current speed [CS(7)], current direction [CD(7)] and sea temperature [ST20(7)]. Current meter number 10 [CM10], located at latitude 28°26.6' N, and longitude 125°25.3' E, ran from 1255 February 14, 1975 to 1045 March 1, 1975 and measured current speed [CS(10)], current direction [CD(10)], and sea temperature [ST20(10)]. The spar buoy [SB10] was set at the same location as CM10 (Fig. 5). It ran from 1240 February 14, 1975 to 1025 February 20, 1975 and measured wind speed [WS], wind direction [WD], dry-bulb air temperature [DB], and wet-bulb air temperature [WB], all at a height of four meters above the sea surface. For a shorter period, up to 1110

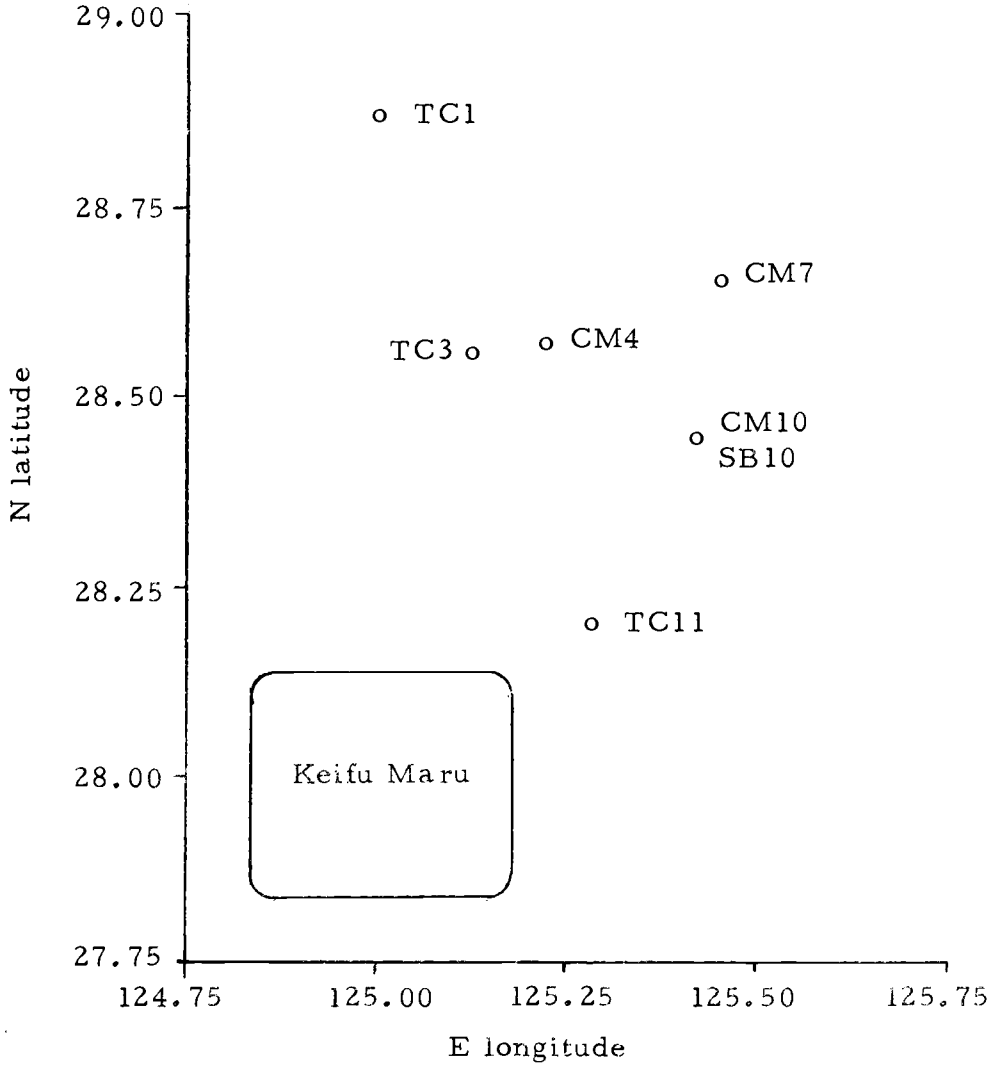

Figure 3. Positions of current meters, thermistor chains, spar buoy, and area of operation for the Japanese meteorological ship, Keifu Maru.

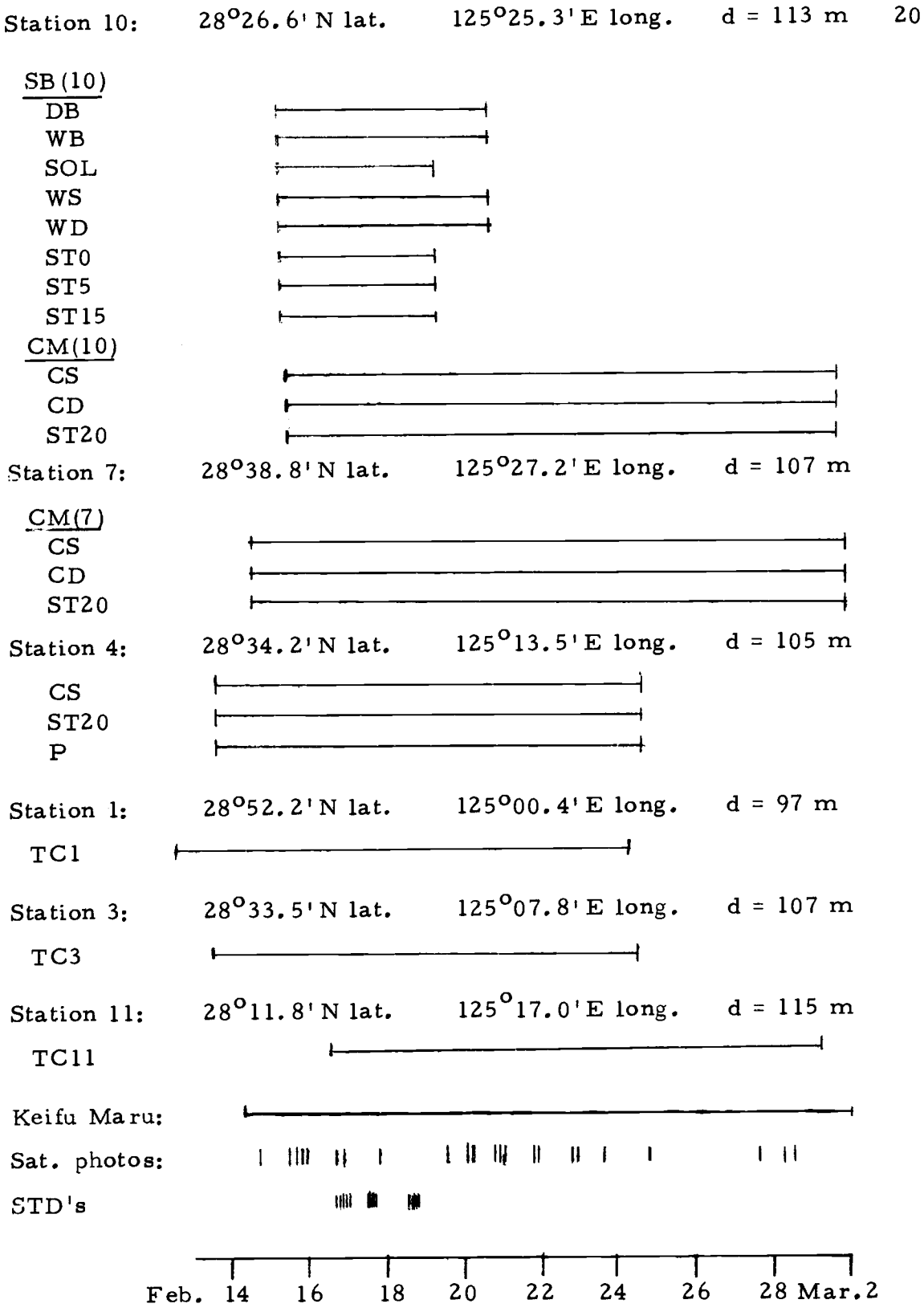

Figure 4. Positions and running periods of data records used.

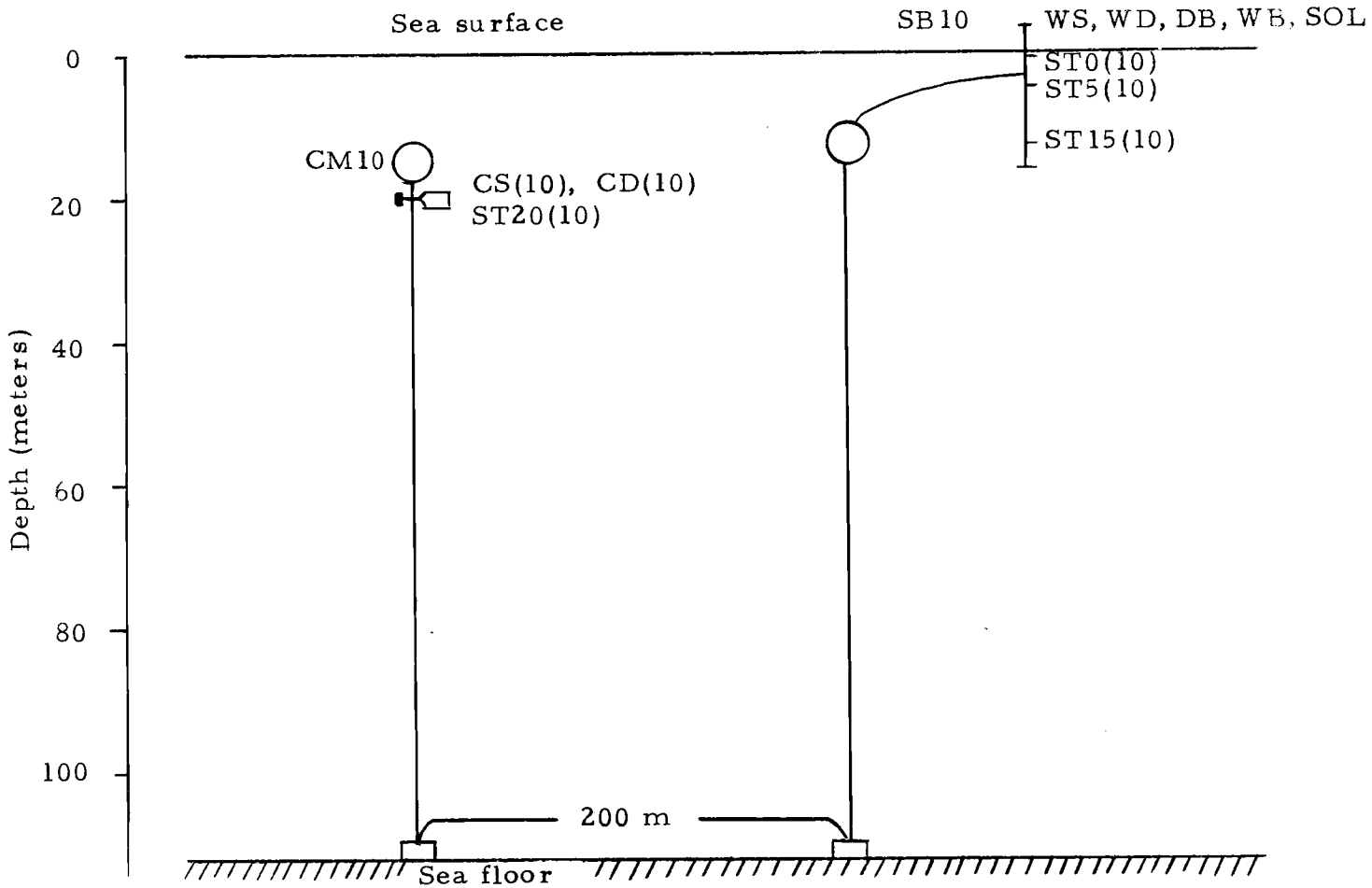

Figure 5. Deployment schematic for current meter and spar buoy at AMTEX station 10.

February 18, 1975, the spar buoy also measured incoming solar radiation [SOL] and sea temperatures at the sea surface, 5, and 15 meters [ST0(10), ST5(10), ST15(10)].

The current meters, wind speed sensor, wind direction sensor, meteorological data recorder, and thermistor chain data recorders were Anderraa types with the time intervals governed by quartz crystal clocks. The direction compasses in the wind direction sensor were calibrated before and after the experiment to $\pm 1^{o}$ while the manufacturer's specifications state that they are accurate to $\pm 5^{o}$ in field conditions.

The wind speeds and current speeds were recorded by integrating the revolutions of the anemometer cups and current rotors over the specified time interval. The manufacturer states that the wind speeds are accurate to $\pm$ 2% above a threshold speed of .2-.3 m/sec. The manufacturer also states that the current speeds are accurate to $\pm$ 2% or 1 cm/sec, whichever is greater, above a threshold speed of 2.5 cm/sec.

The solarimeter (Science Associates, No. 615-1) employed 80 junction copper constant thermopile elements similar to the Epply sensor. The dry-bulb and wet-bulb air temperatures were measured, to $\pm$ .01^{o}C, by dry and wick-wetted thermistors imbedded in a radiation shield.

The signal levels were significantly greater than the instrument noise for all sensors except possibly for the sea temperature sensors. Sea temperatures, on the current meters, spar buoy, and thermistor chains, which were also calibrated before and after the experiment, were measured by thermistors and limited in resolution by the digitizing process in the Anderraa recorders to $\pm$ .01^{o}C.

In the body of this thesis sea temperature fluctuations, with ranges of approximately .03^{o}C, were studied. The sea temperature fluctuation records were formed by applying a band pass filter. Each data point in the fluctuation record was a weighted sum of 145, 5 minute, sea temperature readings interpolated to a precision of .001^{o}C. The increased precision assumed in the filtering process was justified by the consistent results found by using these fluctuation records in the remainder of this thesis. For example, the four sea temperature fluctuation records on February 16 at station 10, displayed in Figure 42, all show the same fluctuating pattern. Temperature measurements with greater resolution would have been preferable, but the measurements used were sufficient.

The atmospheric parameters measured on the spar buoy are the main source of information as to when mesoscale cells are present over the array. This fact and the shortness of the spar buoy record made it necessary to restrict the main data analysis to the period from 1255 February 14, 1975 to 1025 February 20, 1975.

Fortunately this six day period encompassed a major cold air outbreak.

IV. GENERAL RESULTS

Currents

Basic Data Description

The raw data from CM10 (Fig. 6) indicate that the semi-diurnal tidal current dominated the record, with the fortnightly tide evident as a modulation of the semi-diurnal tidal current.

About one-half of the current record is clean and about one-half noisy. The noisiest period was from February 19, 1975 to February 23, 1975. There were four periods of cold air outbreaks during the current meter record, and these four periods coincided with the noisy portions of the current record (Fig. 6). The increase in wind speeds and surface instability during outbreaks indicates that the apparent noise in the current record was real.

The V component record (N-S) is noisier than the U component (E-W) record. Later in this section it will be shown that the current fluctuations are aligned approximately 25^{o} to the right of the wind. During outbreaks the winds are generally out of the north and during the outbreak of February 21 the winds were from the north-northwest. Therefore any outbreak-induced fluctuations would show up in the V component.

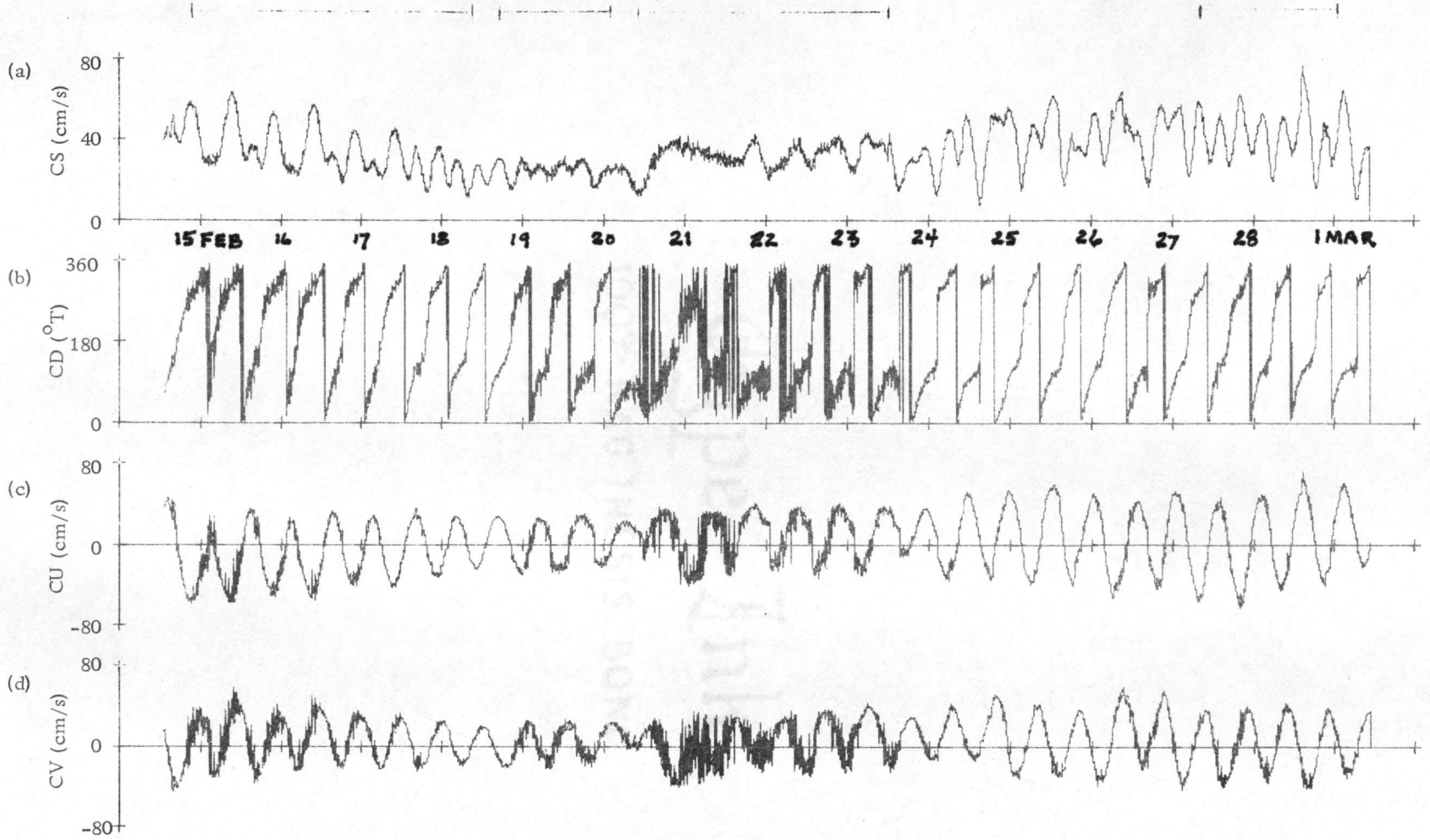

Figure 6. Raw current meter data from AMTEX station 10 [CM10]; (a) current speed [CS(10)] in cm/sec, (b) current direction [CD(10)] in degrees, true, (c) current U component [CU(10)] in cm/sec, and (d) current V component [CV(10)] in cm/sec. Bars denote periods of cold air outbreaks.

Progressive Vector Diagrams

Progressive Vector Diagrams (P.V.D.) made of simultaneous CM7 and CM10 records (Fig. 7) reaffirm the semi-diurnal dominance both since they both show definite loops, and since they yield mean velocities of $V_{(7)} = 8.94$ cm/sec towards 55^{o} true and $V_{(10)} = 7.26$ cm/sec towards 30^{o} true, compared to average speeds of CS(7) = 33.70 cm/sec, and CS(10) = 34.93 cm/sec. The P.V.D.'s also show general mean flow to the northeast except for a four day period at CM10 when the flow was to the northwest, and a four day period when the flow at CM7 was south of east. These periods of anomalous flow imply at least two periods of curved mean flow near the two current meters, which will be discussed later.

Current Roses

In each 10^{o} direction interval the percentage of total water movement and the average speed of the movement, along with the mean current velocity vector are displayed as current roses (Fig. 8). Since there is no predominant flow direction the currents are again inferred to be rotational. Under the assumption that the currents are mainly semi-diurnal tidal the two average speed roses were considered representative of the semi-diurnal tidal elipse. The tidal elipse was then estimated to have its major axis running from

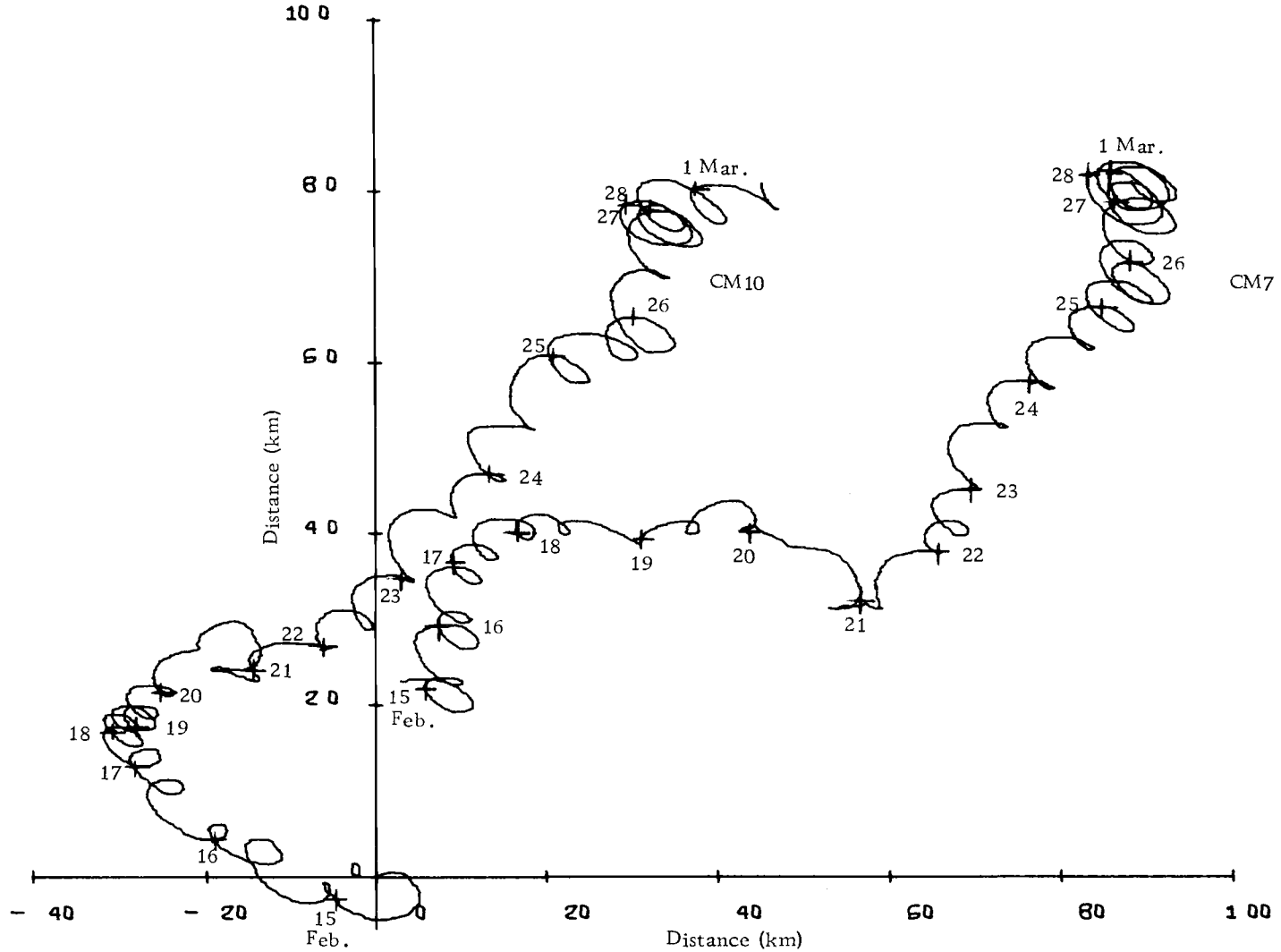

Figure 7. Progressive vector diatrams for simultaneous current meter records from AMTEX stations 7 and 10. Starting point for station 7 diagram offset to represent station separation. Data period was from 1255 February 14 to 1045 March 1. 0000 hour of each day marked by +.

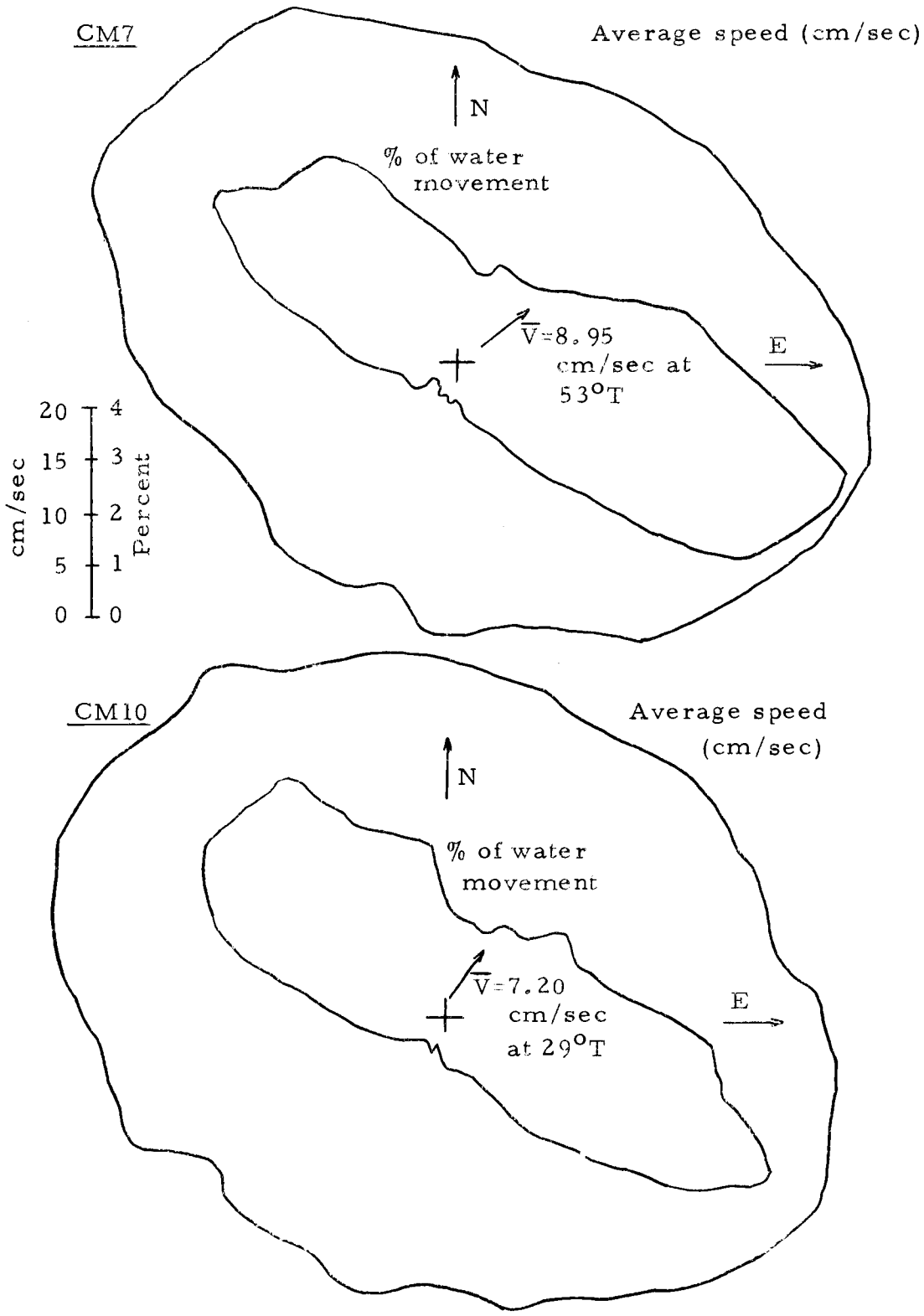

Figure 8. Current roses for AMTEX stations 7 and 10. Average speed and percentage of total water movement given for each 10° interval. Mean current velocity vectors also indicated.

northwest to southeast and had an eccentricity of 0.74 (based on CM7 data) or 0.80 (based on CM10 data).

Spectral Analyses

Rotary spectra[1] of the current records at stations 7 and 10 are presented in Figure 9. In both records the two dominant peaks were at the negative and positive semi-diurnal tidal frequencies (0.081 c/hr). The negative peak, implying clockwise rotation, dominated in both records. The less dominant positive semi-diurnal spectral peak implies that the motion was elliptical at that frequency. According to Mooers (1973) the eccentricity of a rotational ellipse is given by $2(S_- S_+)^{1/2} / (S_-+S_+)$ where S_- and S_+ refer to the spectral energy density at the negative and positive values of the frequency of interest. At the semi-diurnal frequency station 7 had $S_- = 275.7$ cm^2/sec and $S_+ = 29.0$ cm^2/sec which gives an eccentricity of 0.59 and station 10 had $S_- = 29.0$ cm^2/sec and $S_+ = 31.0$ cm^2/sec for an eccentricity of 0.61. Both of these eccentricities are smaller than the approximate values calculated from the average speed per 10^o interval in Figure 8, but the values are close. The dominance of the semi-diurnal tide in the current record is best shown in Figure 10, a plot of the spectral energy density times frequency versus the logarithm of the frequency

[1] For a discussion of the derivation and use of rotary spectra, see Gonella (1972) and Mooers (1973).

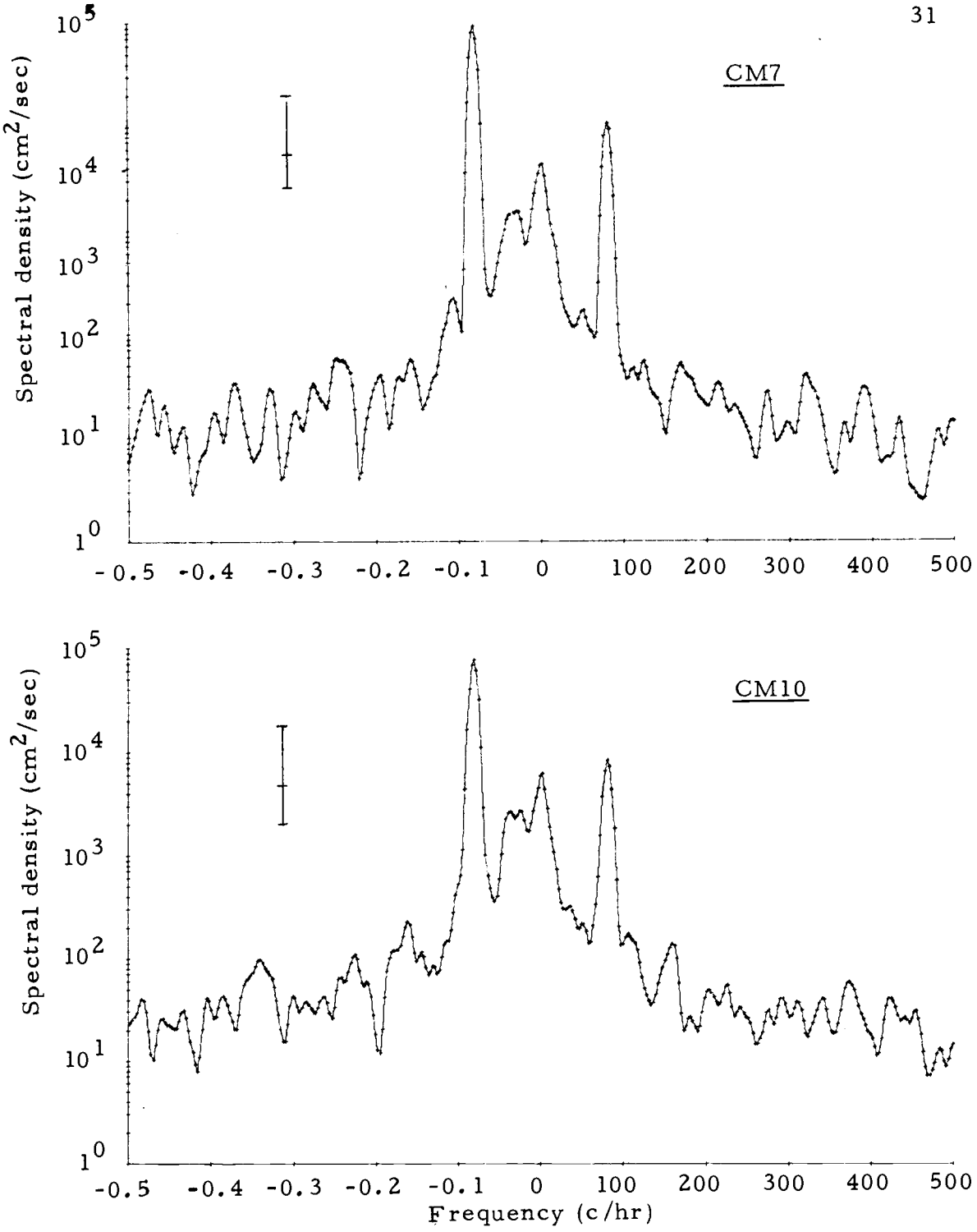

Figure 9. Rotary spectra of currents at AMTEX stations 7 and 10. 95% confidence interval bars are indicated.

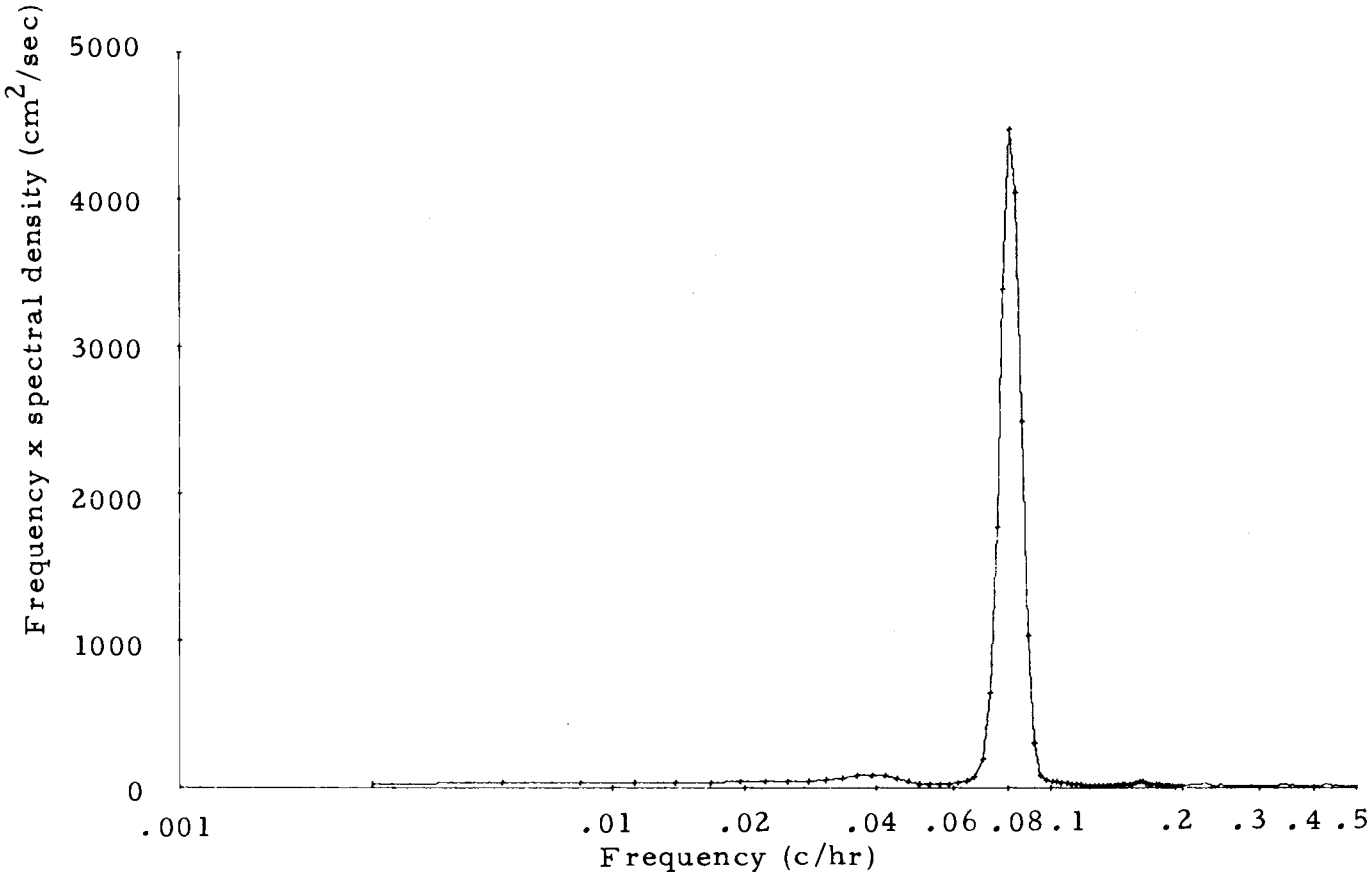

Figure 10. Spectrum of U current component at AMTEX station 10. Plot is frequency times spectral density versus the logarithm of frequency. In this plot the area under a segment of the curve is proportional to the energy in that frequency band.

for one current component (U at station 10). In this plot energy is proportional to area under the curve. It is evident that well over 90% of the energy was in the semi-diurnal tidal frequency band.

The rotary spectra indicate a few other significant peaks. At station 7 the 0.0 frequency peak (mean flow) is the next largest peak below the semi-diurnal. Then there is a peak at F = -0.036 c/hr (T = 27.5 hours). This peak implies clockwise rotation and there is no apparent matching positive peak. The inertial period at station 7 is 25.04 hours. The band width of this spectrum is about 0.01 c/hr so the -0.036 c/hr peak probably represents the inertial peak. At station 10 the 0.0 c/hr frequency (mean flow) is again the largest below the semi-diurnal, but then there is a double peak near the inertial frequency. The two peaks are the same size. One is at f = 0.036 c/hr and probably represents inertial oscillations. The other is a f = 0.022 c/hr (T = 44.7 hours). Even though the heights of these peaks are not relatively significant, the separation in frequency is greater than the band width, so they could represent two different oscillations. Station 10 is located about 100 kilometers from the shelf break. Longuet-Higgins (1968) discusses the trapping of waves along a depth discontinuity. He concluded that these waves would have periods greater than the inertial and amplitudes that drop off exponentially with distance from the discontinuity. This type of wave provides a possible explanation for the f = 0.022 c/hr peak at

station 10. Not only is the period basically correct, but a similar doublet is not apparent, or at most is represented as a widening of the inertial peak, at station 7 which is located an additional 20 kilometers away from the shelf break.

Using cross-spectral analysis it was evident that at the semi-diurnal frequencies both the U and V components at station 7 were highly coherent with those at station 10 and lagged them by about 10 minutes, indicating the tidal wave progressed from south to north. Cross-spectral analyses on the speeds at stations 4, 7 and 10 indicate that at twice the semi-diurnal frequency the three stations were highly coherent and that station 4 led both stations 7 and 10 by about seven minutes, and that station 10 led station 7 by about three minutes. It was concluded that the tidal wave moved from southwest to northeast.

Large Scale Features in the Mean Flow

Since the current records were so heavily dominated by the semi-diurnal tide, mean currents were extracted by taking the average velocity over successive tidal periods and smoothing them for the entire data record. The results, presented as progressive vector diagrams in Figure 11, again show strongly curved mean currents flowing about the two meters particularly from February 15 to

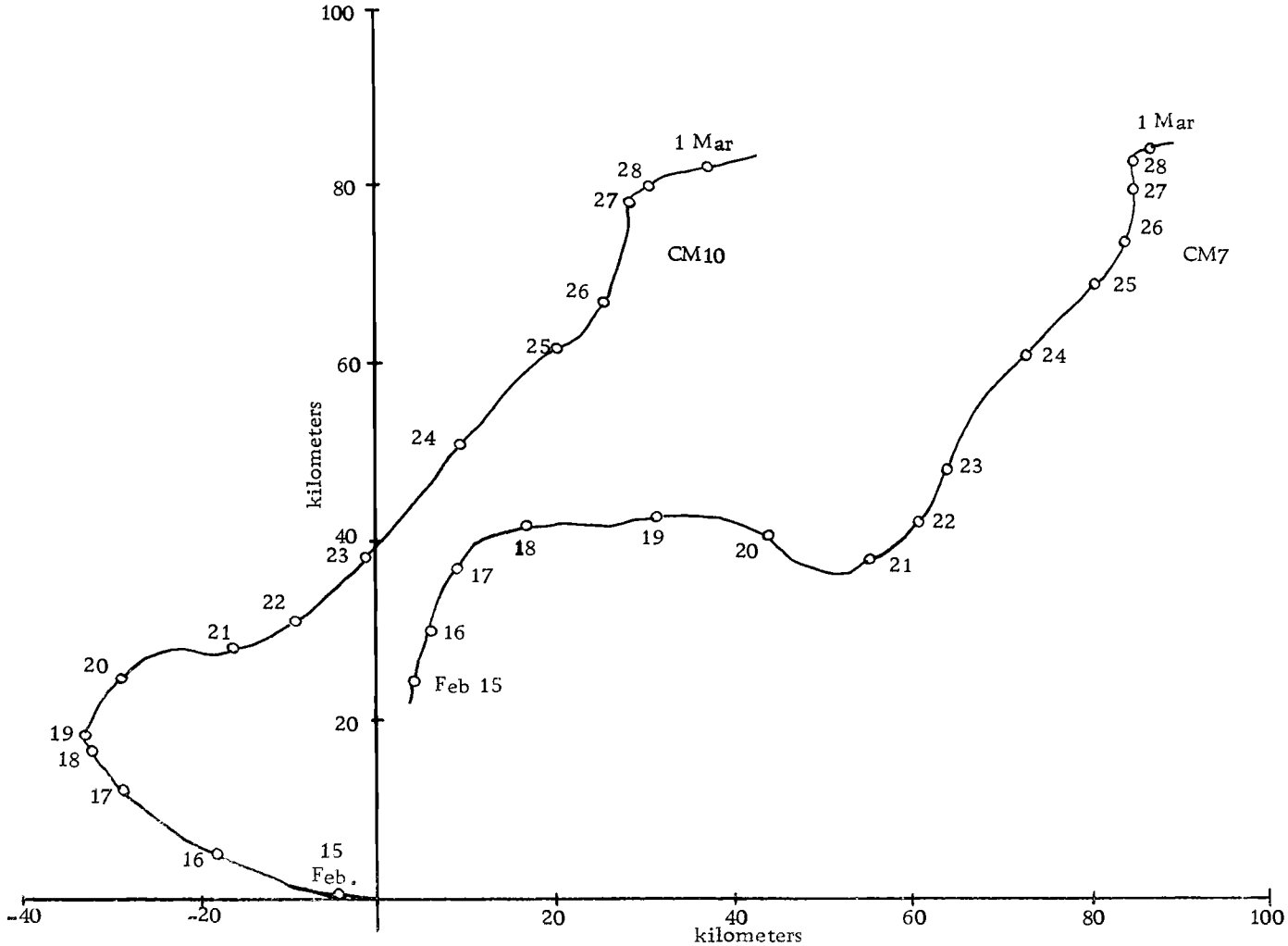

Figure 11. Progressive vector diagrams for simultaneous mean currents at AMTEX stations 7 and 10. Starting point for station 7 diagram is offset to represent station separation. Data period was from 1255 February 14 to 1045 March 1. 0000 hour of each day marked by a circle.

February 18, when the two mean currents were at nearly right angles to each other.

The first impression is that some sort of loop current was flowing around the two meters. A technique was developed to examine the possibility of loop currents. Perpendiculars were constructed for each pair of simultaneous current vectors and their intersection points were calculated. If the currents were circular this would yield the center of rotation. Then speeds and the distances of the meters from this calculated center of rotation were used to obtain two estimates of the rotational period.

A section of the data record was considered to fit this "loop" model if: (1) the sense of rotation of the two currents about the calculated center position was the same; (2) the distance from the two current meters to the calculated center position was less than 200 kilometers; and (3) the two calculated rotational periods were both less than 2000 hours and agreed with each other within a factor of two. There were four segments of the data record that met these criteria (Figs. 12 and 13). The first was the most dramatic. For 100 hours the two mean currents differed in direction from 45^{o} to 90^{o}, the estimated rotational periods ran from 100 hours to 430 hours (4 to 18 days), and the center position moved steadily from within five kilometers of station 7 to within six kilometers of station 10. If any of these segments could be considered a loop current it would

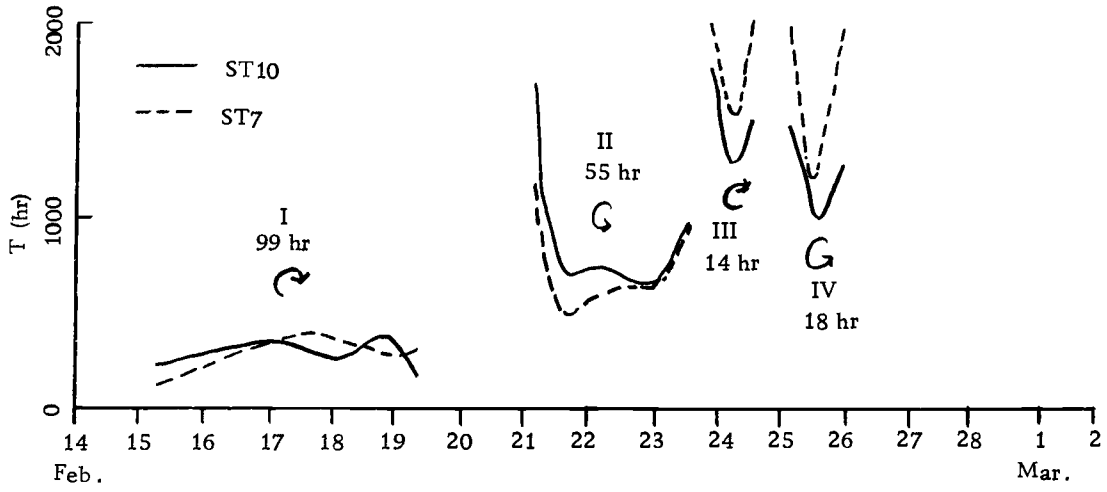

Figure 12. Loop model periods calculated from mean currents at AMTEX stations 7 and 10.

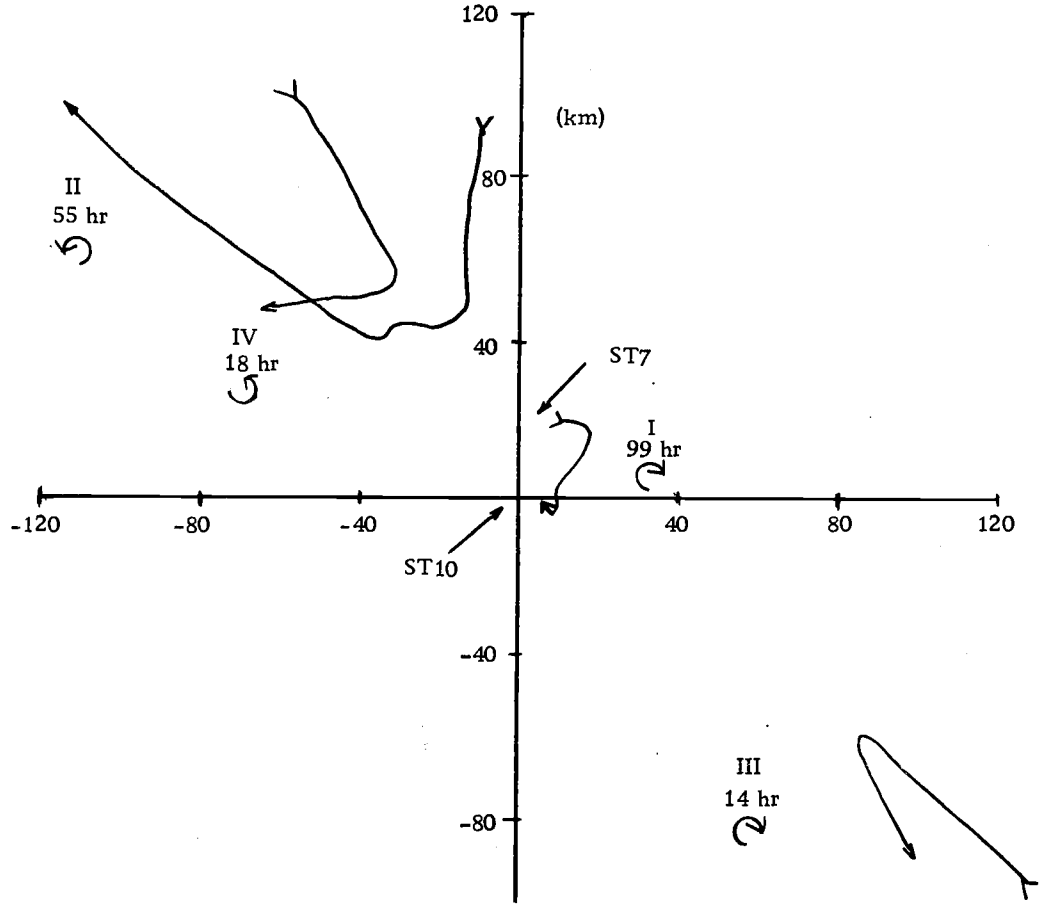

Figure 13. Loop model center positions calculated from mean currents at AMTEX stations 7 and 10. Positions given with respect to station 10 and location of station 7 indicated.

be this one. But, when all four segments were examined together, another pattern developed. The sense of rotation alternated between successive segments (clockwise, counterclockwise, clockwise, counterclockwise) and the location of the center points also alternated with the two clockwise rotations having center points to the east and south of the current meters and the counterclockwise rotations having their center points to the north and west of the meters (Fig. 13). The center positions within each segment generally moved from north to south, opposite to the general current flow. For segments II, III, and IV the center positions seemed to start far from the meters, move in close, and then move away again, indicating regular changes in the curvature of the rotational flow.

These observations could be explained by alternate closed loops of opposite rotations, embedded in the mean flow and moving from north to south and fortuitously passing on opposite sides of the current meters. The apparent changes in mean flow curvature and the large values of the calculated periods (up to 80 days) have led the author to reject the idea of closed loops and to conclude instead that there is a quasi-sinusoidal meander in the mean flow. This idea better accounts for the large apparent rotation periods and the movement of the center position. These meanders can become quite pronounced, approaching closed loop currents, as in segment I. There were two other segments of the data record that fit all the criteria except that their

calculated periods were greater than 2000 hours (up to 7000 hours). These two segments also showed opposite rotation and the same movements of their center positions reflecting changing curvature, but the motion of these center positions was generally from south to north.

Horizontal Temperature Gradients

The temperature records from the three current meters were combined to estimate the horizontal temperature gradient in the buoy array area. Based on average wintertime conditions (Fig. 2b) the horizontal temperature gradient was expected to be positive towards the southeast, but the calculated gradients during the experiment were generally positive towards the northwest (Fig. 14). The author cannot judge whether this is a regular feature of this part of the East China Sea or a temporary abnormality brought about by the meandering mean current flow.

Ekman Veering

In the body of this thesis the author wished to study phenomena concerning mesoscale atmospheric cells on a time scale less than five hours. To accomplish this the current meter data were filtered with a band-pass filter that would isolate oscillations from 0.5 hours

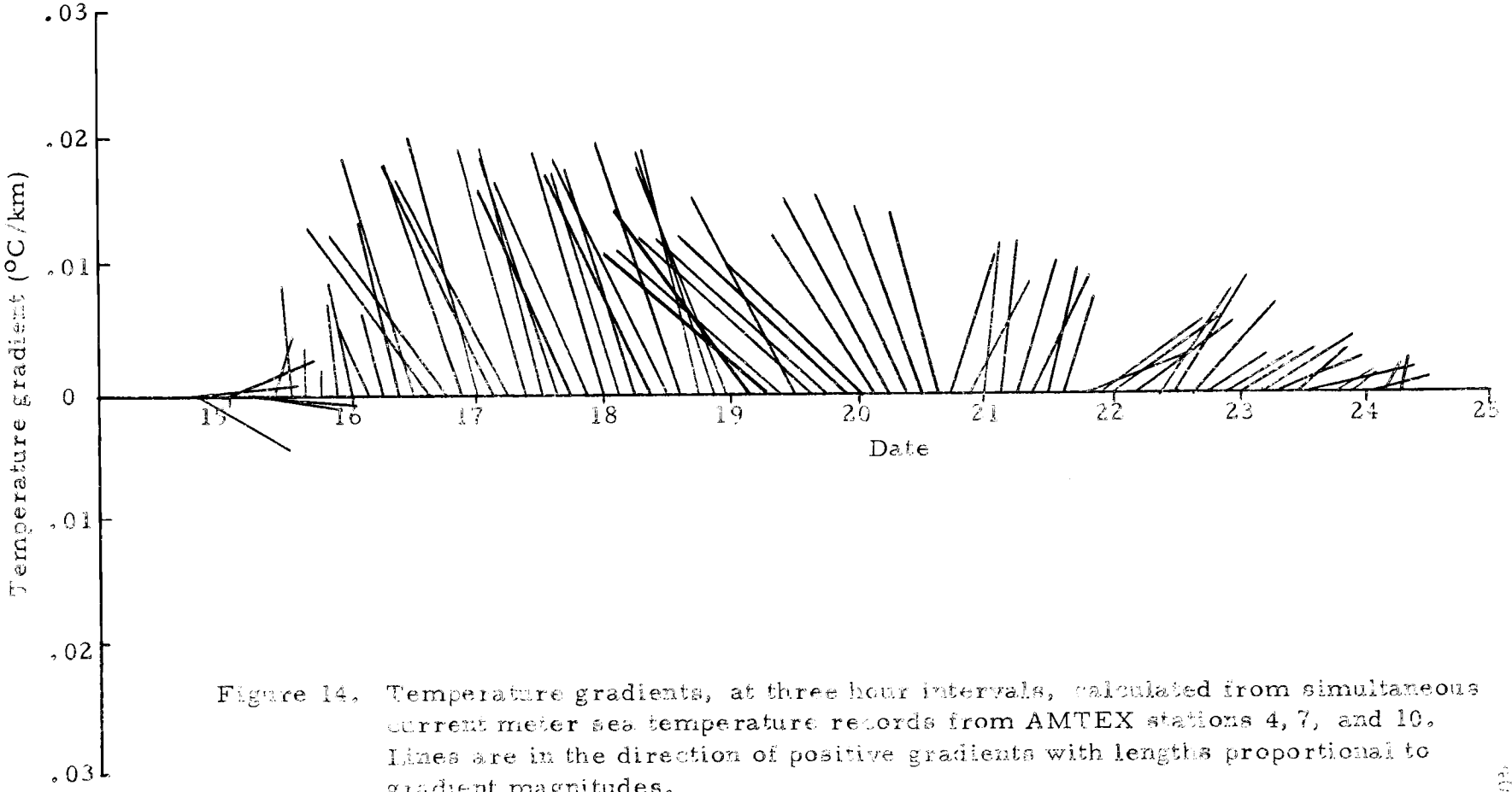

Figure 14. Temperature gradients, at three hour intervals, calculated from simultaneous current meter sea temperature records from AMTEX stations 4, 7, and 10. Lines are in the direction of positive gradients with lengths proportional to gradient magnitudes.

to five hours. A current rose showing the percentage of the total water flow in each 10^{o} interval was formed for the filtered data from 1855 February 14 to 0425 February 20 (Fig. 15). It was expected that the rose would be fairly circular representing isotropic turbulence, but the rose was definitely elongated in a direction NNE to SSW. In attempting to explain this anomaly it was noted that the wind direction during this period was predominantly to the south. The elongation of the rose was roughly 30^{o} to the right of the wind. Ekman veering was considered as a possible cause of the elongation. To test this idea the coordinates were rotated with respect to a smoothed wind direction record so that one component was always downwind and the other component was always to the right of the wind. The geographical orientation of this coordinate system varied throughout the data record as it followed the mean wind flow. The current rose formed for the band-passed current data in this coordinate system (Fig. 16) was elongated in a direction 25^{o} to 30^{o} to the right of the wind flow. Had there been a vertical line of current meters it might have been possible to display the Ekman spiral in this manner.

Summary

The current meter records at stations 4, 7, and 10 indicated that the flow in the East China Sea is heavily dominated by the semi-diurnal tide that progresses as a wave from the southwest to the

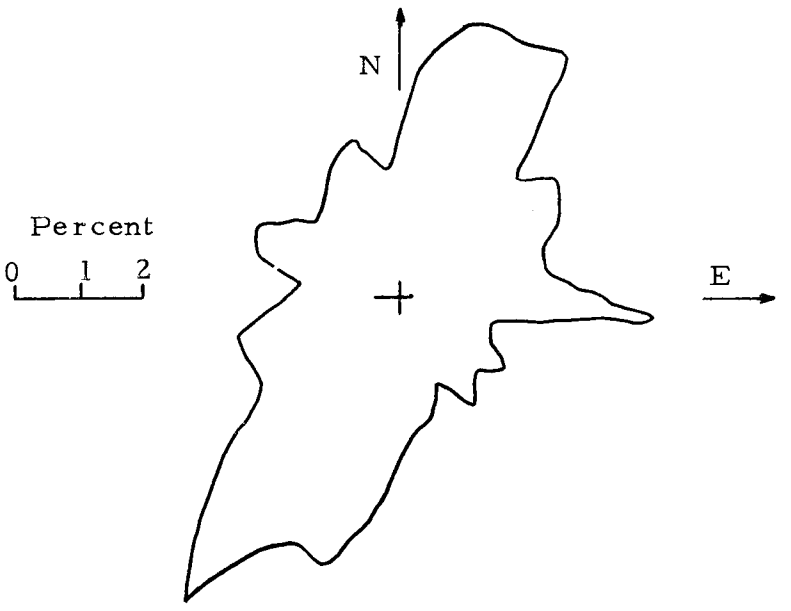

Figure 15. Current rose for band-passed (.5 hr to 5 hr) current fluctuations at AMTEX station 10. Plot gives the percentage of total water movement per 10^{o} interval.

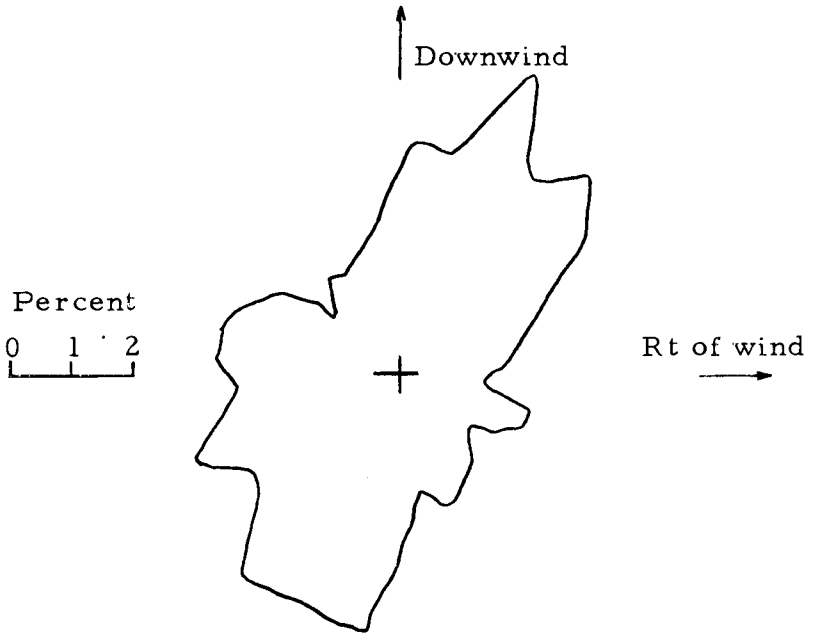

Figure 16. Current rose for band-passed (.5 hr to 5 hr) current fluctuations at AMTEX station 10 with coordinates rotated so that one component was always downwind and the other was always to the right of the wind. Plot gives the percentage of total water movement per 10^{o} interval.

northeast. The mean flow is generally to the northeast, but meanders are present which can approach closed loop currents. There is some inertial energy present and there appears to be some indication of waves with periods greater than the inertial trapped along the shelf break to the southeast of the array. The horizontal temperature gradients during a portion of the data record were contrary to expectations. Strong evidence for Ekman veering was found in the current data. The data records appeared noisier during cold air outbreaks, probably reflecting higher winds and greater instability present during outbreaks. Later in this thesis evidence will be presented that some of these fluctuations were forced by the passage of mesoscale atmospheric cells.

Cold Air Outbreaks

General Features

Spar buoy data indicate that on February 14, 1975, just after the buoy was placed in the water, the winds shifted from out of the west to out of the north (Fig. 17). At the same time the air temperature and absolute humidity began to drop. Keifu Maru data show that the air pressure rose dramatically during this period. In the 24 hour period from 1300 February 14 to 1300 February 15 the air temperature dropped 4.6^{o}C, the absolute humidity dropped 5.4 g/kg (50%), and

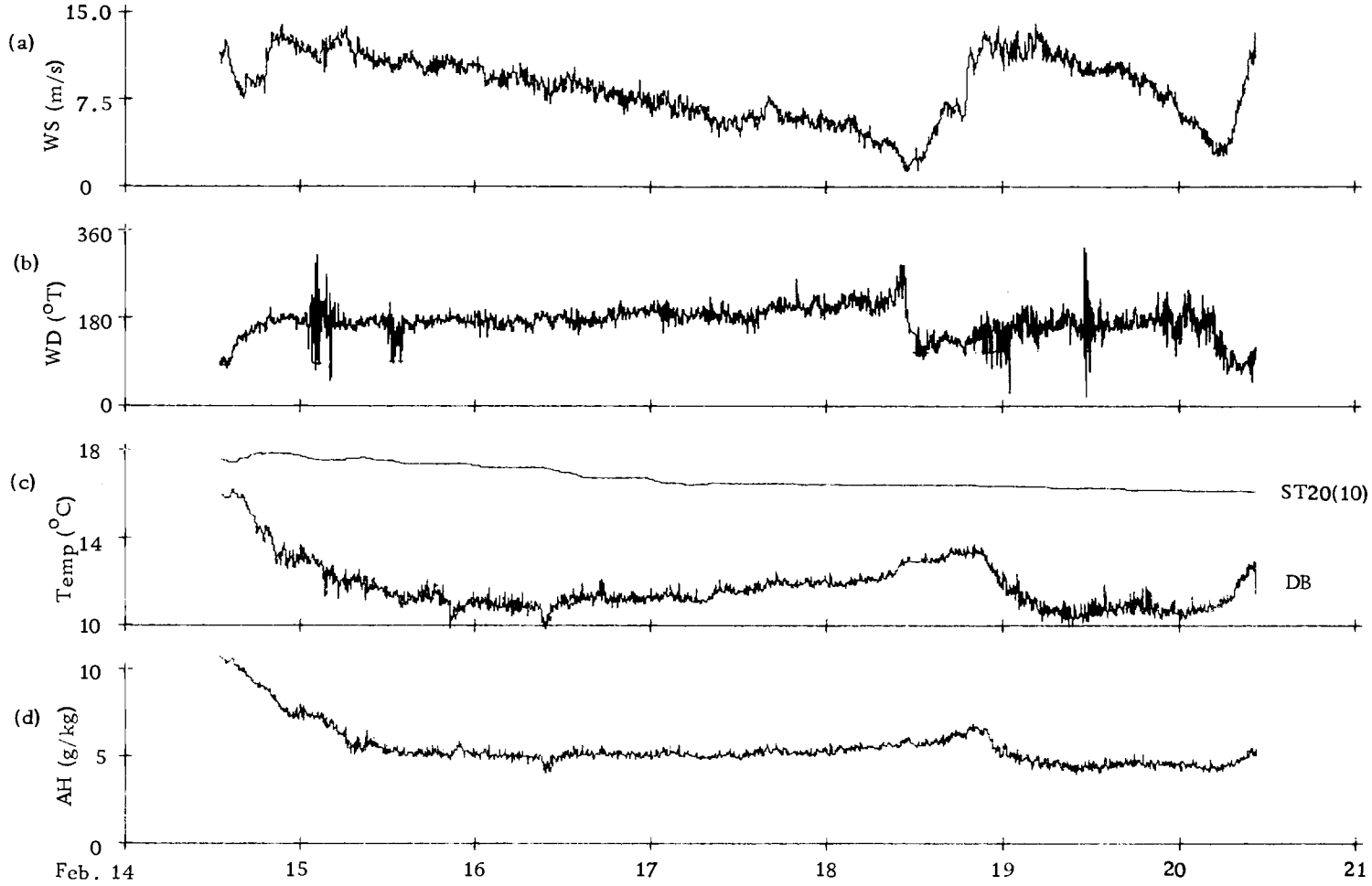

Figure 17. Raw spar buoy data from AMTEX station 10 [SB10] ; (a) wind speed [WS] in m/sec, (b) wind direction [WD] in degrees true, (c) dry bulb air temperature [DB] and sea temperature [ST20(10)] in degrees Centigrade, and (d) absolute humidity [AH] in g/kg.

the pressure rose 15.3 millibars. A low pressure disturbance moved through the area on February 14 and cold dry air flowed out behind it. For the next three days the wind speed decreased steadily while the wind direction shifted from west of north to east of north. The air temperature and absolute humidity reached a minimum on February 16, and then slowly rose. This outbreak appears to end on February 18, when the wind speed reached a minimum and the wind direction shifted back to southwest. Late on the 18th another, shorter outbreak (32 hours) began which ended early on the 20th. This outbreak is marked by an increase in wind speed, a shifting of wind direction back to northerly, and decreases in the air temperature and absolute humidity. Air pressure data from the Keifu Maru indicate an additional rise at the start of this ourbreak though without a preliminary dip in pressure. It is difficult to judge if the second outbreak is a separate event or just a resurgence of the first outbreak.

Cooling of the Water Column

The current meter temperature record at station 10 [ST20(10)] showed a definite cooling trend during this period. ST20(10) peaked at 17.92°C at 2000 February 14, 1975. At the end of the first outbreak (1100 February 18) ST20(10) was 16.39°C, representing a temperature change of 1.53°C in 87 hours. During the second outbreak (2100 February 18 to 0500 February 20), ST20(10) dropped

from 16.36°C to 16.19°C for a temperature change of 0.17°C in 32 hours. Eighteen STD's were taken in the array area on February 16, 17, and 18 (e.g. Fig. 18). These showed that the upper 75 meters were well mixed with a second well-mixed layer underneath that was about 0.7°C cooler and 0.1‰ less saline. There are no data indicating whether or not this 75 meter mixed depth was constant throughout the period. Under the assumption that it was, and neglecting advective and lateral diffusive heat transport terms a first approximation of heat lost by the water column was 3230 cal/cm^{2}day for the first outbreak and 975 cal/cm^{2}day for the second outbreak.

Scalar products were formed between the current vectors from station 10 [V (10)] and the temperature gradient vectors calculated from the three current meter temperature records to estimate the advective heat change of the water column. When the first estimate of the water column heat loss was corrected by the advective estimate, the average heat losses were 2720 cal/cm^{2}day for the first outbreak and 320 cal/cm^{2}day for the second outbreak.

Heat Flux Estimates

The bulk aerodynamic method was used to estimate the turbulent heat fluxes from the meteorological data (see Appendix). The results (Fig. 19) clearly delineate the two outbreaks. The heat loss was mainly due to evaporation. Bowens Ratio [BR], the ratio of

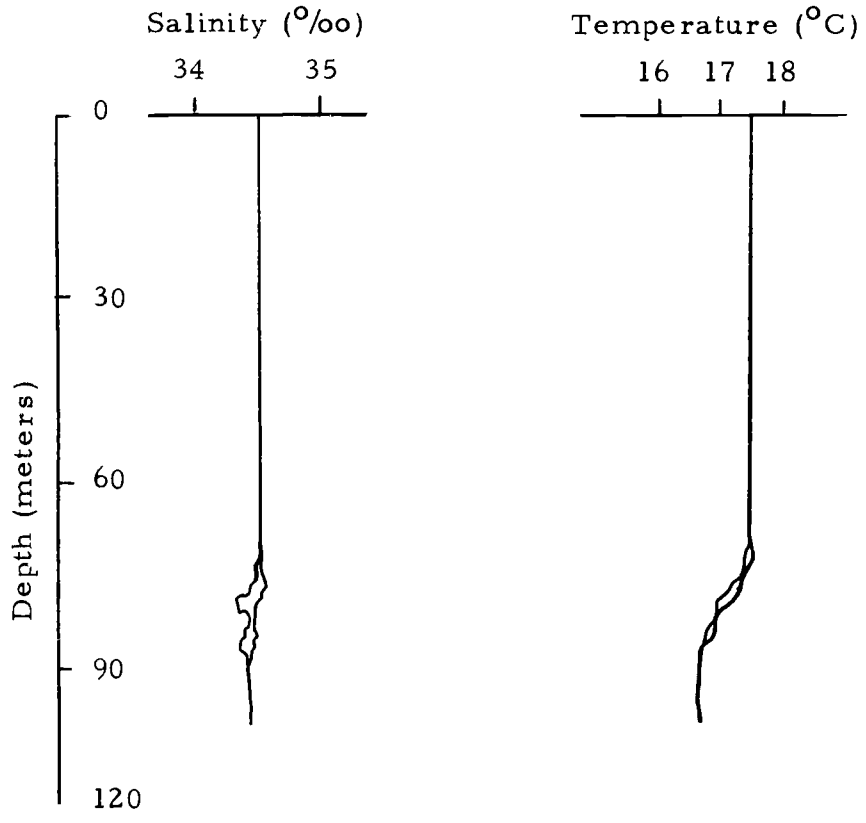

Figure 18. STD trace from near AMTEX station 10.

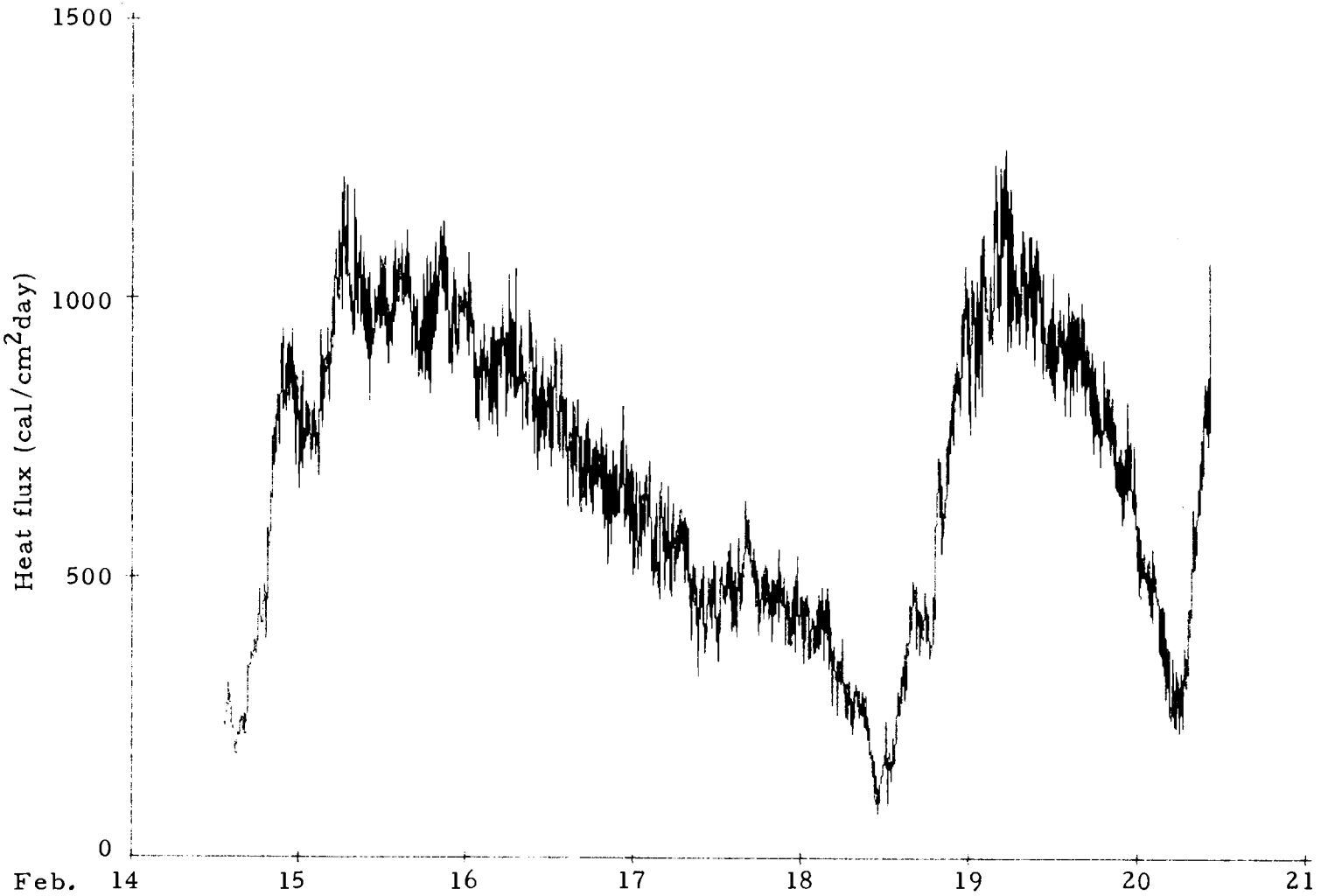

Figure 19. Turbulent heat fluxes, sensible plus latent, calculated from meteorological data at AMTEX station 10 by the bulk aerodynamic method.

sensible heat loss [HS] to latent heat loss [HL] averaged less than 0.4. Sensible heat fluxes were more important during the outbreaks as indicated by the higher values of Bowens Ratio (Fig. 20). In comparing the heat fluxes with the wind speeds (Figs. 17 and 19) it is evident that the wind speed was the dominant factor in the heat flux calculations. The total turbulent heat fluxes averaged 700 cal/cm^{2}day during the first outbreak with a peak value of 1220 cal/cm^{2}day at 0630 February 15, and 820 cal/cm^{2}day for the second outbreak with a peak value of 1270 cal/cm^{2}day at 0515 February 19. These values do not agree very well with the estimates based on water temperature changes and advection. The semi-diurnal dominance of the currents and the shallowness of the East China Sea suggest that lateral mixing would be important. Unfortunately there was insufficient spatial temperature data to estimate the lateral mixing term. The turbulent flux estimates calculated by the bulk aerodynamic method appear to provide the best picture of the heat exchange occurring in the vicinity of the spar buoy.

Thermistor Chain Data

The thermistor chains, located to the west of the current meter array (Fig. 4) provided temperature data at five meter intervals from depths of 20 meters to 70 meters measured every 10 minutes. These data were examined to ascertain whether the

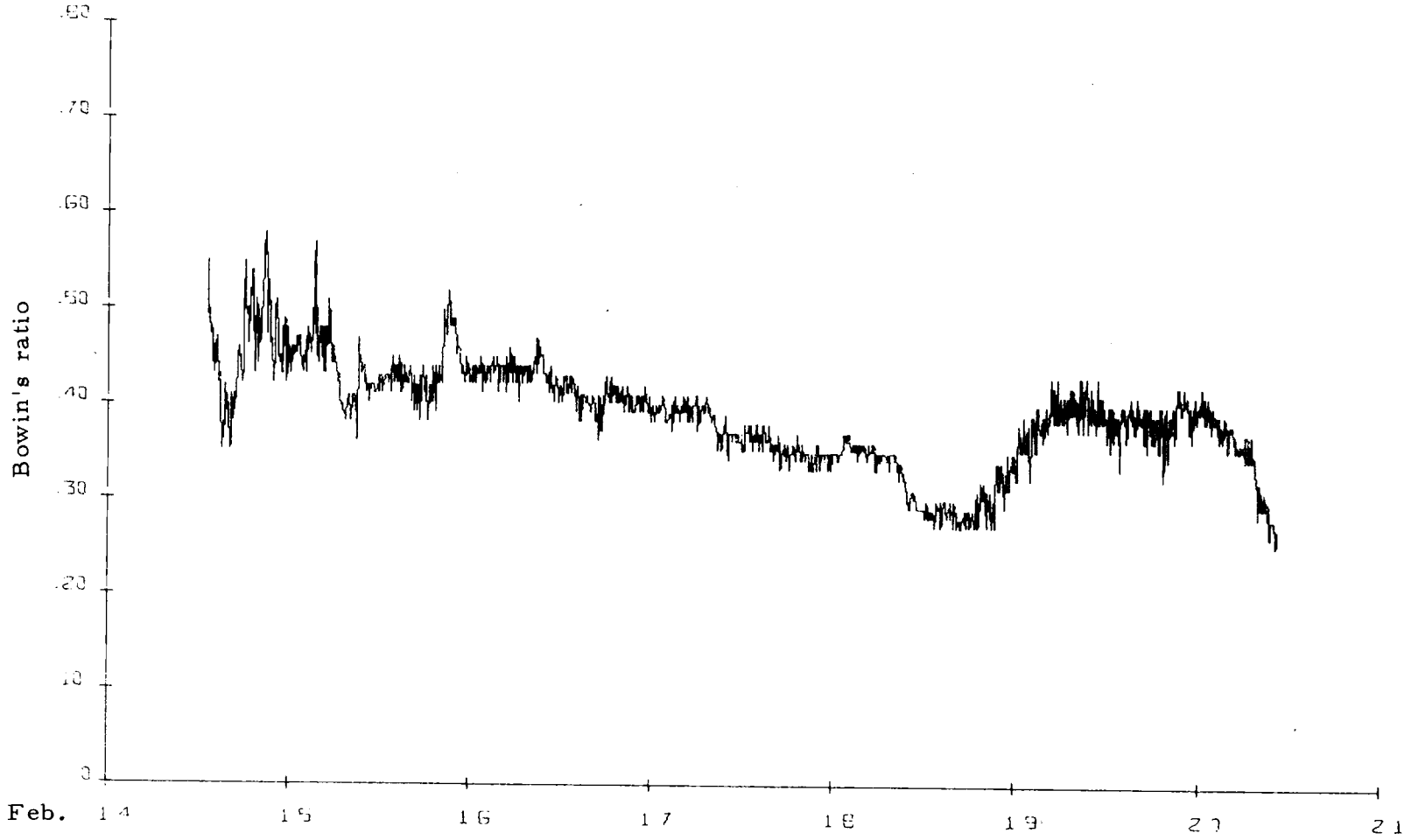

Figure 20. Bowens Ratio [BR] of the calculated sensible [HS] and latent [HL] heat fluxes at AMTEX station 10. BR = HS/HL

temperature records at a depth of 20 meters were representative of the sea temperatures at all levels above a depth of 75 meters. During the examination of these data some features of the vertical thermal structure of the East China Sea became evident. Although they were not directly related to the main thrust of this research, these thermal features were unique and important enough to warrant presentation.

Only the thermistor chain data from station 1 [TC1] can be considered completely reliable. The thermistor chains were suspended below a subsurface float and taped to the float's anchor cable. Sometime during the experiment the thermistor chains at station 3 [TC3] and at station 11 [TC11] became untaped and hung freely below the subsurface float. The chains were heavier than water and probably hung vertically so the TC3 and TC11 data are probably reliable, but the TC1 data are definitely reliable.

Features of Hourly Averaged Temperature Records

Plots of the hourly average temperatures at all depths for each station (Figs. 21, 22, 23) exhibit alternating periods of warming and cooling and also alternating periods of vertical gradients and no vertical gradients. The periodic appearance of vertical gradients was completely unexpected and is poorly understood. When present

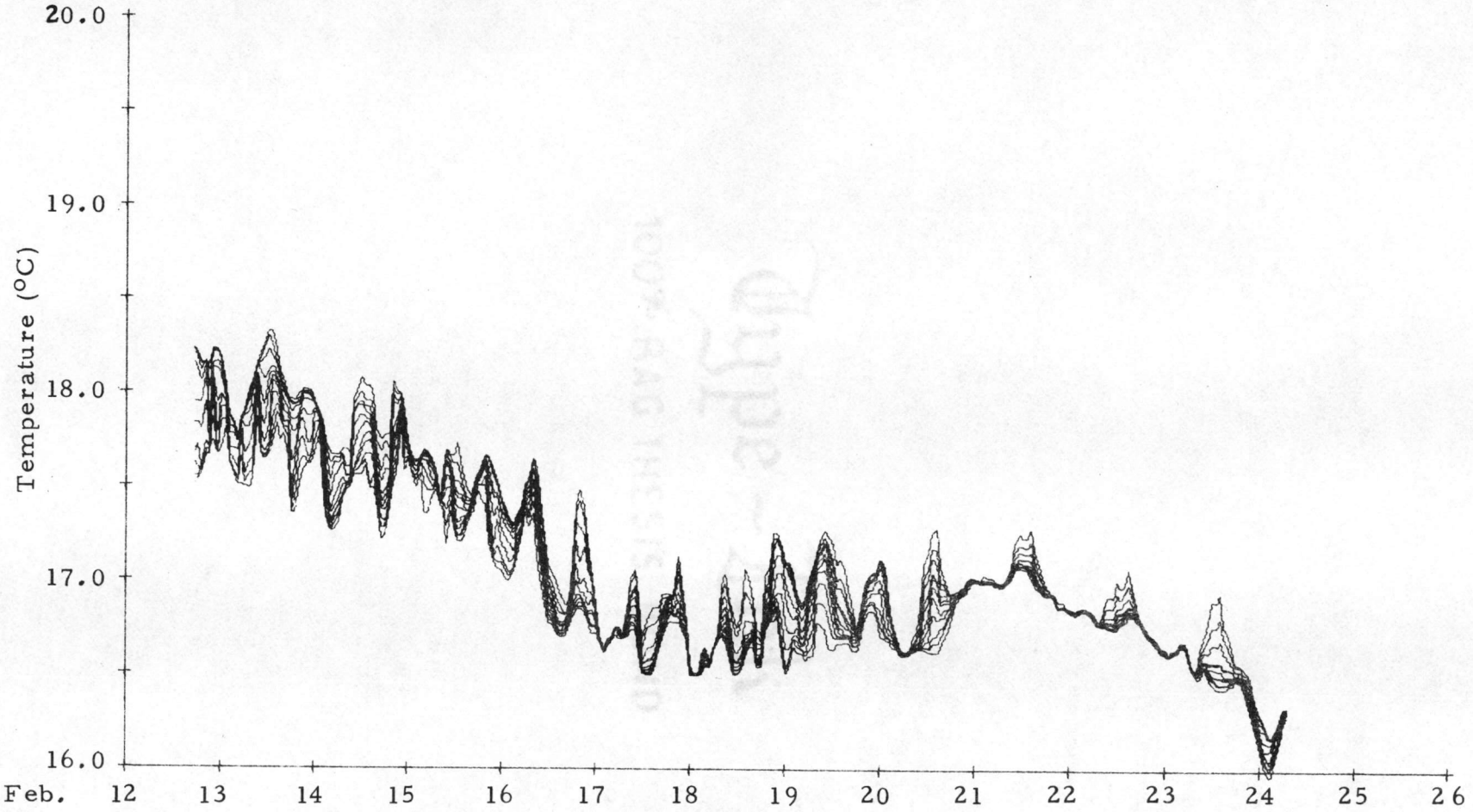

Figure 21. Hourly thermistor chain data from AMTEX station 1.

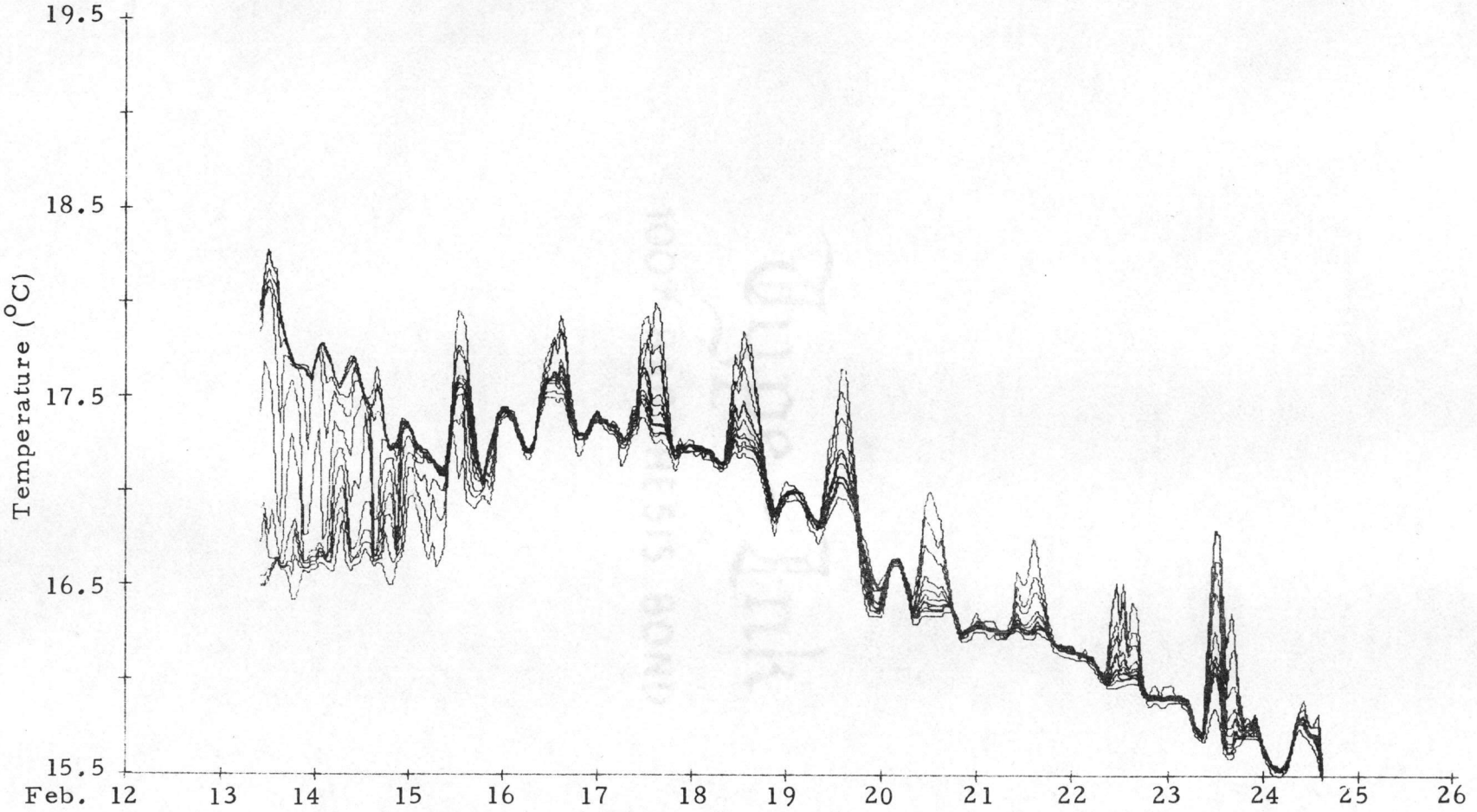

Figure 22. Hourly thermistor chain data from AMTEX station 3.

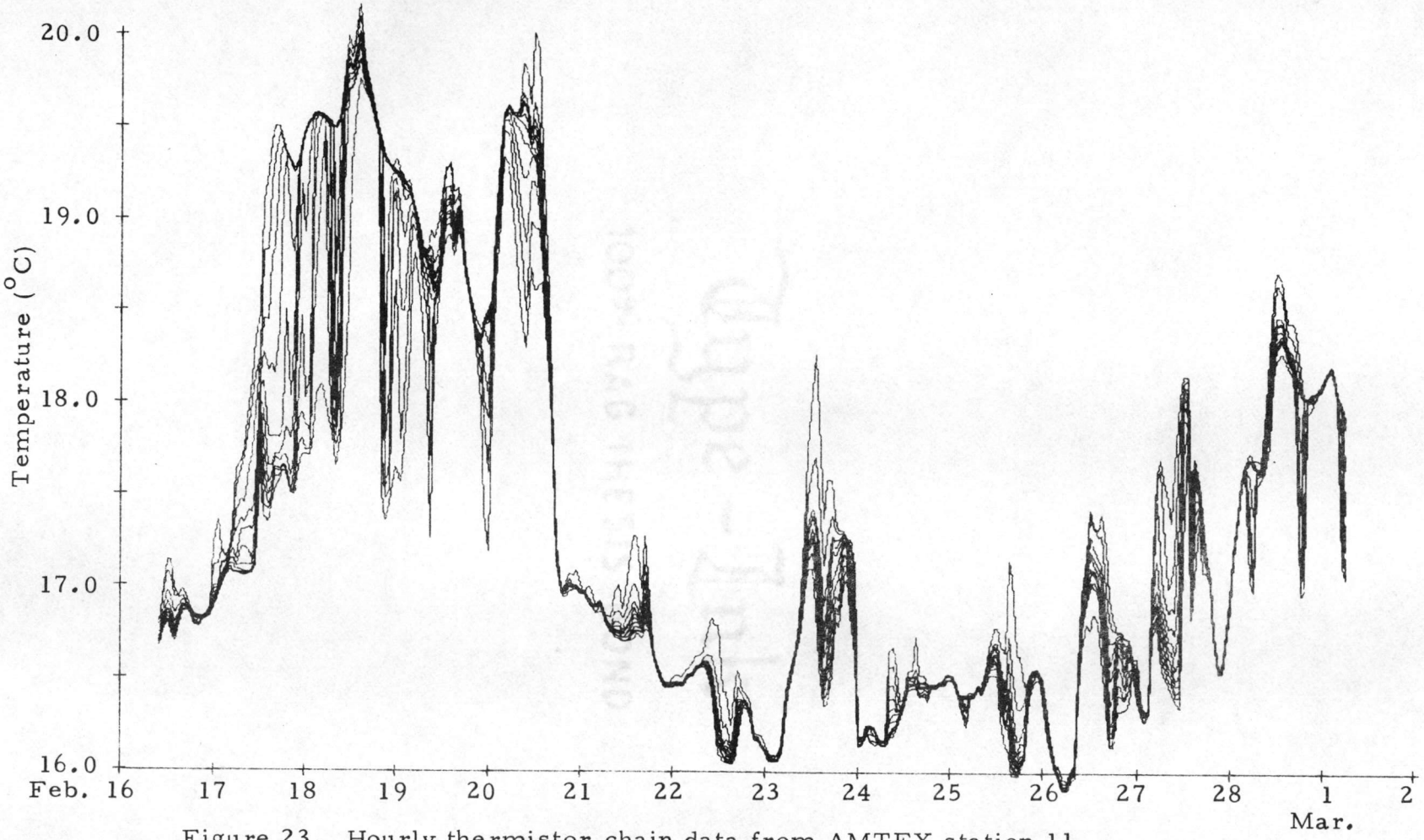

Figure 23. Hourly thermistor chain data from AMTEX station 11.

the gradients appear consistent with depth and on the order of $0.01^{\circ}C/m$. The records of TC1 and TC3 were similar. The record of TC11 was somewhat different, possibly a result of TC11 coming loose from the anchor cable or because TC11 was the southernmost station and different water conditions possibly were present. The rest of the discussion will concentrate on TC1 and TC3 data.

Spectral Analyses

Ten parameters were examined with spectral and cross-spectral techniques. The shallowest temperature on the three thermistor chains [TC1(20), TC3(20), and TC11(20)] represented the basic temperature field. The difference between the shallowest and deepest records on each thermistor chain [TC1(20) - TC1(70), TC3(20) - TC3(70), and TC11(20) - TC11(70)] represented the vertical temperature gradients. The current components at CM7 and CM10 [CU(7), CV(7), CU(10), CV(10)] represented the current fields. Spectra of the six thermistor chain parameters and the current components from station 10 are displayed in Figure 24. The four spectra from TC1 and TC3 all show dominant peaks at periods near 24 and 12.4 hours. There are also peaks present near eight and six hours. The two parameters at TC11 indicated energy at 24 and 12.4 hours, but these peaks are not significant. The current components show a

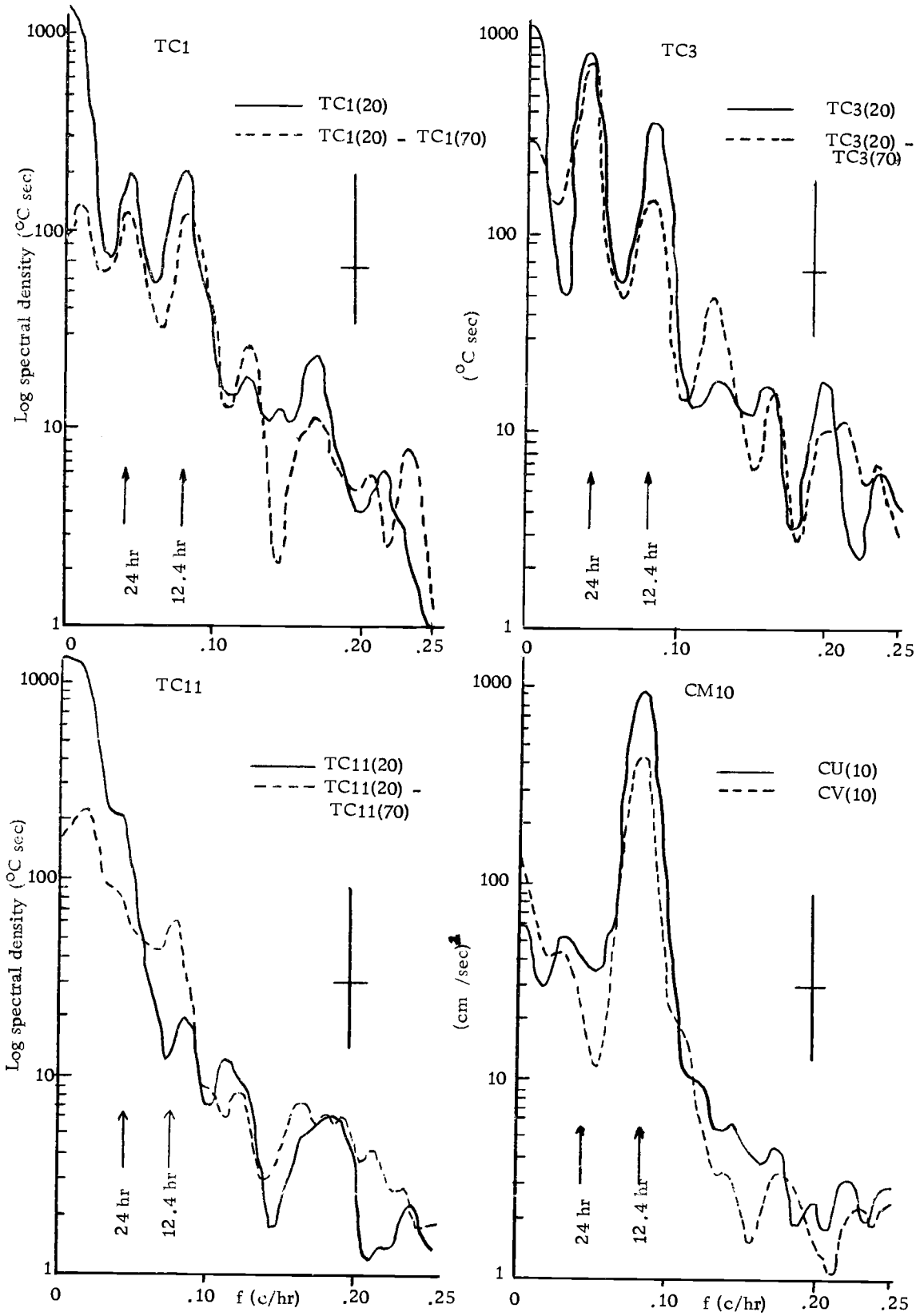

Figure 24. Spectra of thermistor chain parameters and AMTEX station 10 current components. 95% confidence interval bars are indicated.

dominant peak at 12.4 hours (semi-diurnal tidal) and much smaller, not quite significant, peaks at 27.5 hours (inertial).

The semi-diurnal tidal currents were probably related to the 12.4 hour peaks in the thermistor chain spectra. The thermistor chain spectra peaks near 24 hours could be a result of inertial currents (inertial periods 25 hours) or a result of diurnal solar heating. Since there is so little energy in the current spectra near 24 hours, the 24 hour thermistor chain spectral peaks probably resulted from the solar heating cycle. No explanation for the eight hour and six hour spectral peaks is known, except for possible harmonic interaction of the 24 and 12.4 hour cycles.

Cross-spectral analysis between TC1(20) and [TC1(20) - TC1(70)] indicated significant coherence at 12.4 and 24 hours. TC1(20) led [TC1(20) - TC1(70)] slightly at 24 hours and lagged [TC1(20) - TC1(70)] slightly at 12.4 hours. TC3(20) and [TC3(20) - TC3(70)] were also significantly coherent at 12.4 and 24 hours, but the phase relations were reversed from those at TC1. The phase shifts were all on the order of one hour and barely significant.

Cross-spectral analyses between the thermistor chain parameters at station 1 and the current components at station 7 (located 51 kilometers to the ESE of station 1) showed no coherences at 24 hours but significant coherences at 12.4 hours. The phases indicated that the U component led the maximum temperatures and maximum

temperature gradients by approximately five hours and the V component led the maximum temperatures and maximum temperature gradients by approximately nine hours. The currents rotate clockwise and the above results indicate that warmer sea temperatures and vertical temperature gradients occurred after the currents had been flowing from the northwest. When cross-spectral analyses were performed between the TC3 parameters and the current components at station 10 (located 30 kilometers to the east of station 3) results similar to the above were found, but were not statistically significant.

Discussion of Hourly Thermistor Chain Data

From the above results it would seem that solar heating and semi-diurnal tidal advection cause the periodic changes in water temperature and vertical temperature gradients. Solar heating is hard to accept as a cause of these changes for several reasons: (1) the dominant heat transfer during cold air outbreaks is from the waters to the atmosphere; (2) solar heating is not felt to penetrate deeper than eight meters (Reed and Halprin, 1973); and (3) if the solar heat wave is being mixed downward the heat waves at depth should lag the shallower heat waves much more than is evident (Hoeber, 1972).

The apparent tidal advection is also difficult to acdept as a cause of these changes. If the three thermistor chains had been

coincidentally placed along an oceanic front then the cross-spectral results would indicate that the warmer, thermally stratified water lay to the west of the thermistor chain line and the cooler, isothermal water lay to the east. This would generally fit with the result from the three current meter temperature records that indicated the temperature gradient was positive to the northwest. But it is highly improbable that the thermistor chains were placed along a front. Another possibility would be to hypothesize that the normal temperature configuration was one of no vertical gradients but a definite horizontal gradient. If the tidal currents had some vertical shear, with faster currents at the surface than at depth, then the tidal current flowing from the warmer waters would cause warm surface waters to flow farther than the subsurface waters, resulting in a vertical temperature gradient. When the tidal currents reverse the gradients will be removed. Unstable vertical temperature gradients that would also form by this method would destroy themselves as they formed.

This last possibility seems to the author the best explanation for the 12.4 hour cycles in the temperature and temperature difference record, but it does not explain sections of the record where stratification was associated with a cooling trend in the total record (e.g. early hours of February 16, 1975 at station 1).

Fine Scale Features of the Thermistor Chain Data

The 10 minute thermistor chain data are noisy. Figure 25 shows the difference between the thermistor records at all depths on TC1 and a mean value of TC1(70). Spikes in the record often appear simultaneously with depth. This is probably a result of the general instability of the water column and indicates that short time scale temperature variations penetrate rapidly through the water column.

Summary

The main significance of the thermistor chain data to this thesis is that the temperature records at a depth of 20 meters were representative of the temperature structure to at least 70 meters. The water column above 70 meters can be considered a single layer in that it is often isothermal. Thermal stratification, when present, is seemingly the result of large scale processes unrelated to cold air outbreaks and mesoscale cells. Most important, spiking in the temperature records appears simultaneously with depth indicating rapid penetration of temperature fluctuations.

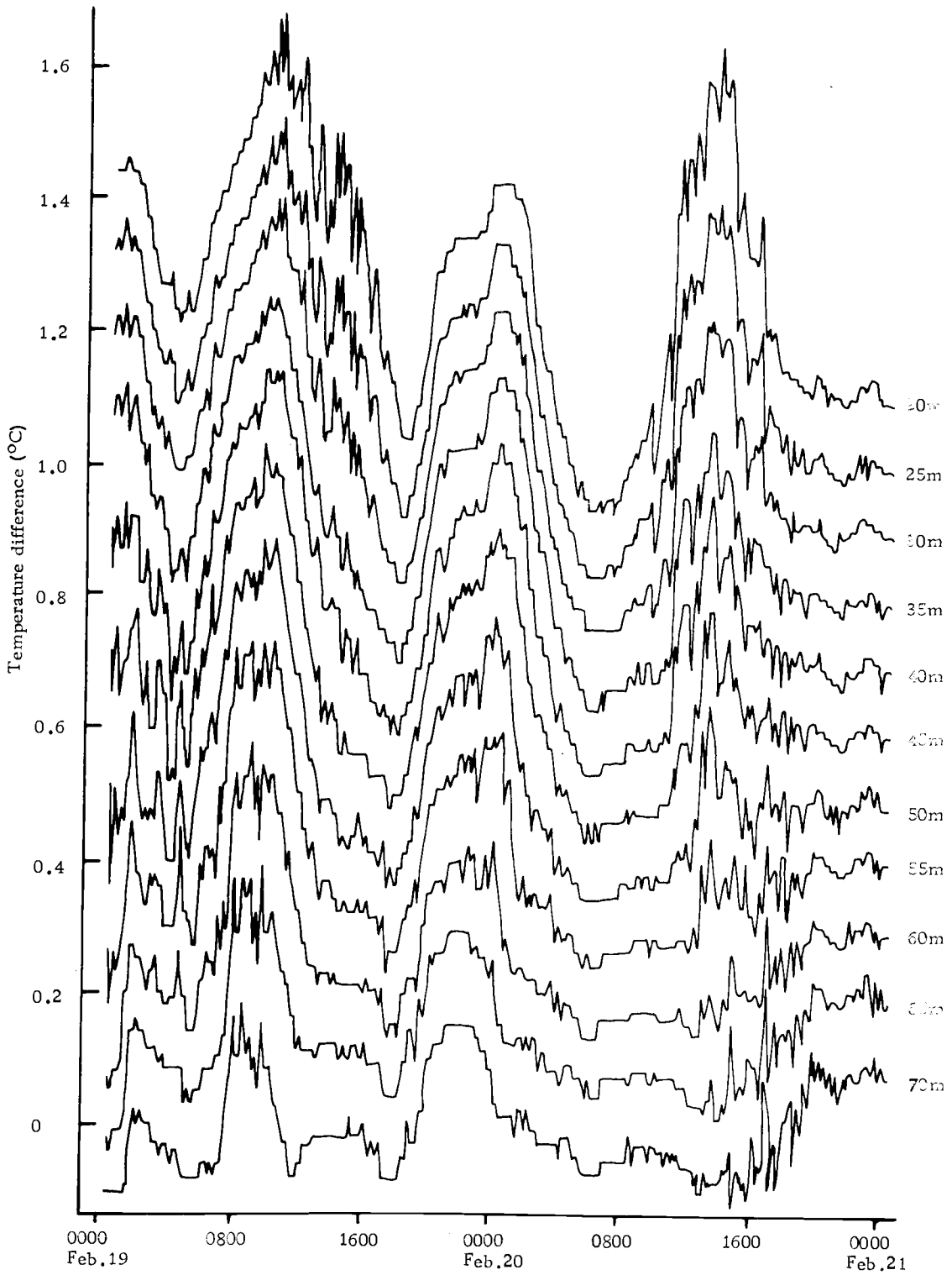

Figure 25. Forty-eight hours of 10 minute thermistor chain data from AMTEX station 1. Temperature records successively offset by 0.1°C.

V. MESOSCALE ATMOSPHERIC CONVECTIVE CELLS

Satellite Imagery

The presence of cloud rings in satellite photos has been up to now the main indicator of mesoscale cells. A series of such photos were taken during AMTEX '75 and some are represented in Figures 26-29. On the morning of February 14, 1975 two and one-half hours before SB 10 was deployed, a general cloud cover associated with the low pressure disturbance mentioned previously existed over the area. By noon on February 15, about 24 hours after the start of the outbreak, cumulus clouds were present and apparently organized (Fig. 26). On the north edge of the cloud pack small cumuli are scattered in a random manner. As one moves south in the photo the cumuli are organized first into lines parallel to the flow and then into open cells. Further south the cells are closed. The character of the transition zone between the areas of open and closed cells is difficult to determine. It appears that as cells moved through a transition zone the cloudy cell walls in the open cells thickened and eventually broke up into closed cells.

Figure 27 depicts the situation on February 16, 1975 when the mesoscale cells seemed, from this and later evidence, to be the best formed. Here the same north to south pattern of scattered cumuli,

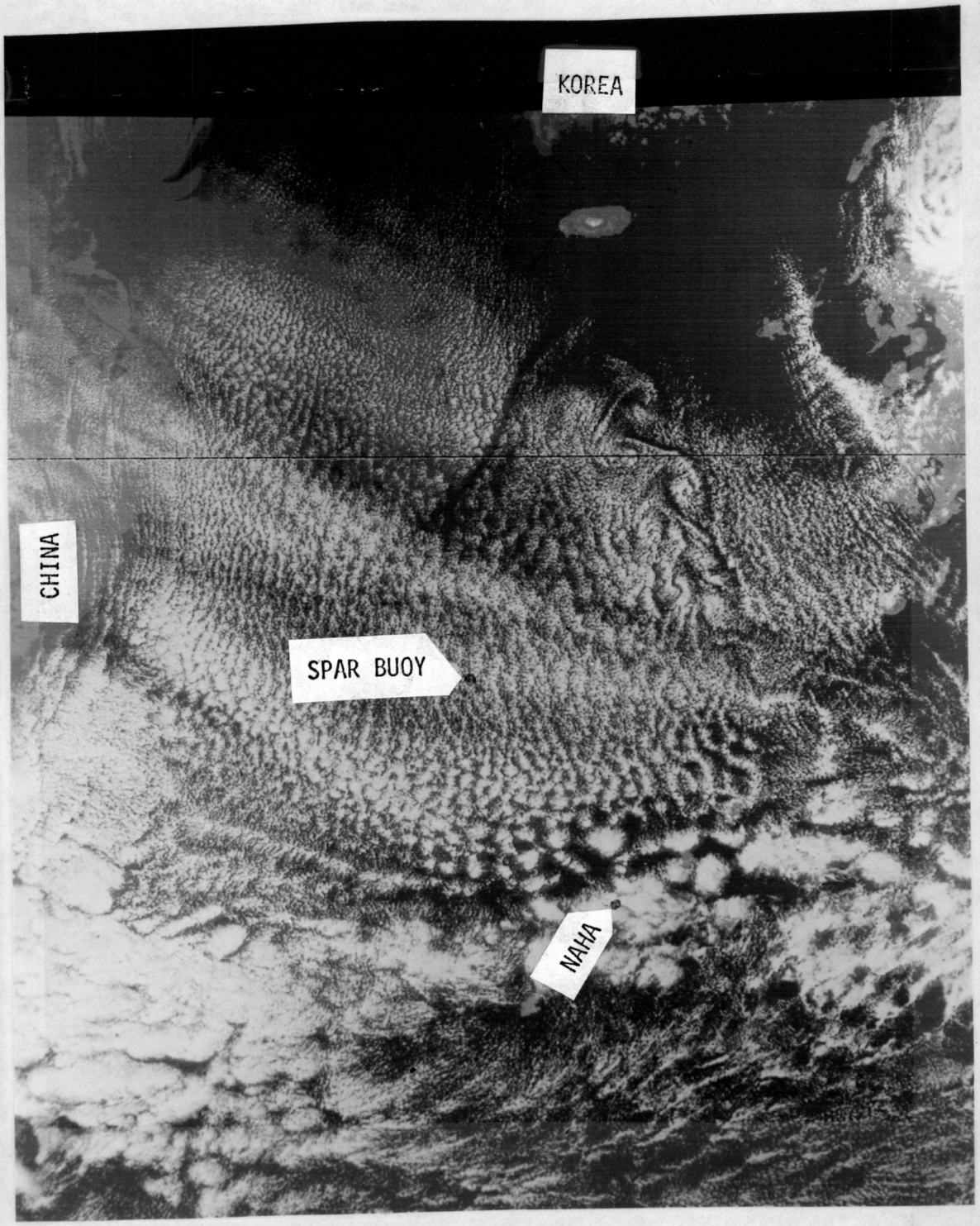

Figure 26. Satellite cloud photograph taken over East China Sea at 1213 February 15, 1975. Spar buoy, Naha separation = 315 km.

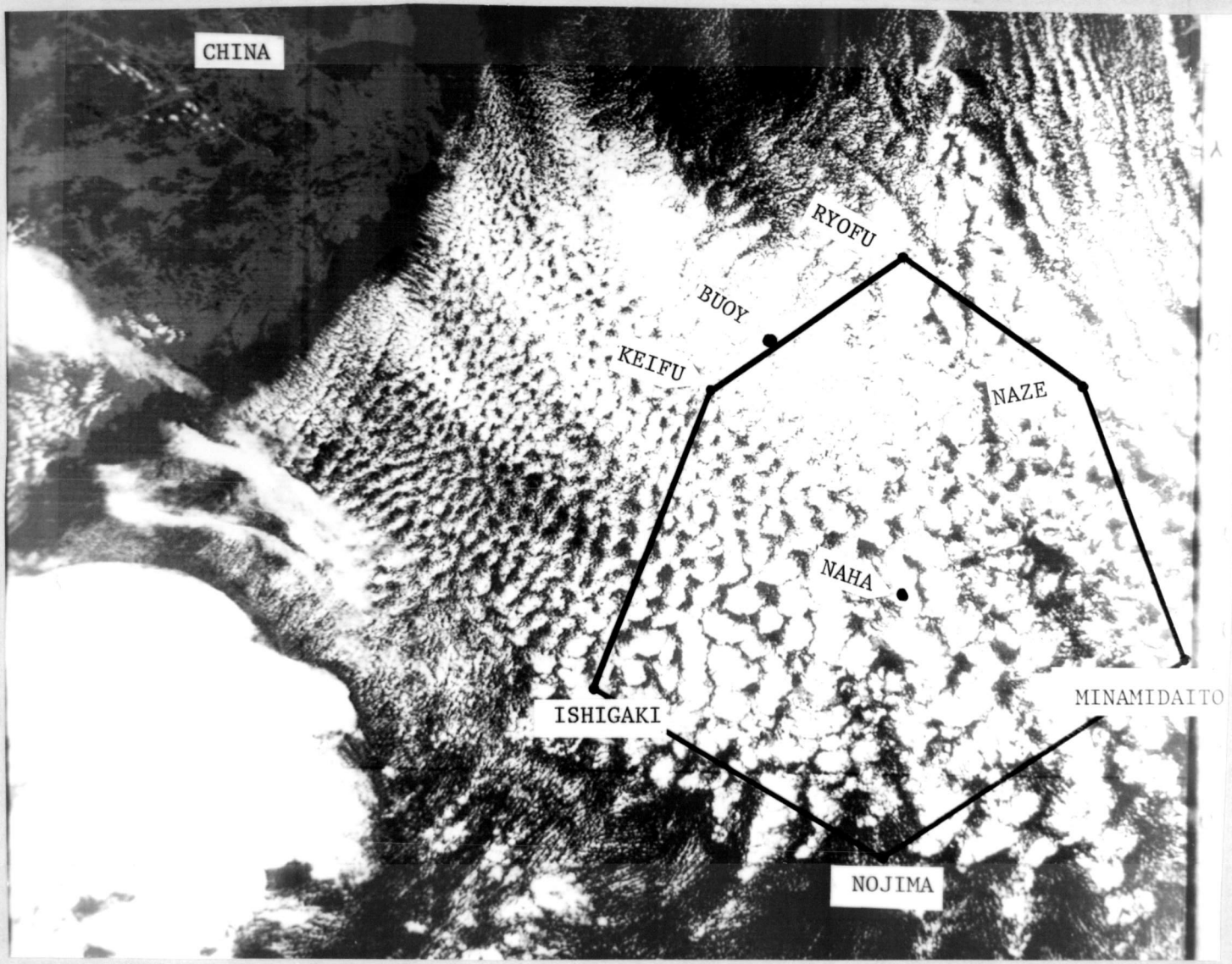

Figure 27. Satellite cloud photograph taken over East China Sea at 1115 February 16, 1975. Spar buoy, Naha separation = 315 km.

streamlines, open cells, and closed cells is apparent, though there is more of a closed cell dominance. In this photo the transition from open to closed cells is best seen on a west to east line perpendicular to the flow, south of the buoy. The cells are not regular. They seem to be elongated and aligned in the direction of flow. This is particularly evident in the area to the southwest of the spar buoy. There is also an apparent increase in cell size as they move downwind.

On February 17, 1975 (Fig. 28) the amount of cloud cover has decreased. The cells are mainly of the closed type and are aligned parallel to the flow. Some open cells are apparently present on the periphery of the cloud pack. There is no photo for the 18th when the first outbreak apparently ended. On the 19th at 1200 the photo (Fig. 29) shows the buoy area covered by an open cellular pattern. On February 20 the general cloud cover dissipated though some cellular organization was still present.

Referring to Figure 27, it is apparent that a characteristic cell size is difficult to determine, but over the buoy area it was between 20 and 30 kilometers. The marked presence of closed cells was surprising. Hubert (1966) concluded that closed cells would mainly be found over cold waters. Over a region like the AMTEX area, with very warm Kuroshio waters underneath, open cells were expected. It is also evident in all these photos that there was a clear area upstream of the organized cloud pack. This supports the idea that the

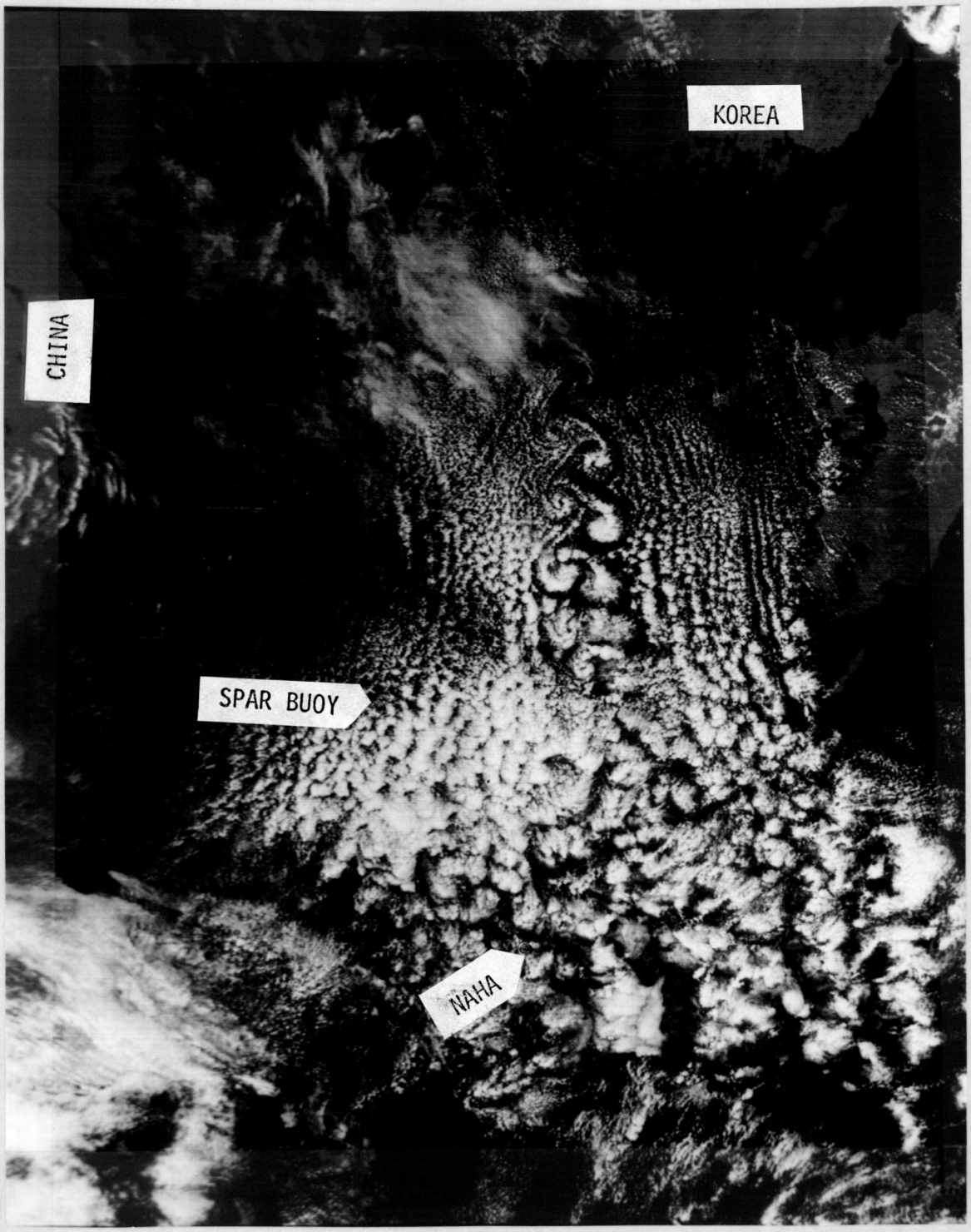

Figure 28. Satellite cloud photograph taken over East China Sea at 1136 February 17, 1975. Spar buoy, Naha separation = 315 km.

Figure 29. Satellite cloud photograph taken over East China Sea at 1740 February 19, 1975. Spar buoy, Naha separation = 315 km.

cold, dry air needs time to pick up enough moisture to form clouds. From the lack of cellular structure in cumuli on the northern edge of the cloud pack it was evident that the mesoscale cells, as well as the cloud signatures took some time to be set up.

Incoming Solar Radiation Data

To get a more precise idea of the passage of cells over the buoy, buoy data must be used. A solarimeter, which measured incoming solar radiation, operated from 1240 February 14, 1975 to 1110 February 18 (Fig. 30). Spiking is evident in this record that can be related to the passage of cells. The general semicircular pattern for each day reflects the amount of solar radiation present during daylight hours. The high peaks represent times when there were no clouds between the meter and the sun and the low peaks represent times when the buoy was in the shadow of a cloud. This does not tell when clouds were directly overhead. At this latitude and at this time of year the maximum noontime solar elevation from the horizon is only 49^{o}. At other times it is less. Therefore when the solarimeter was in the shadow of a cloud, the surface point underneath the cloud was at least as far away from the spar buoy as the cloud was high ($\approx$2000 meters).

Other problems of using a single point data source should be discussed here. Satellite photos show that the cells are irregular in

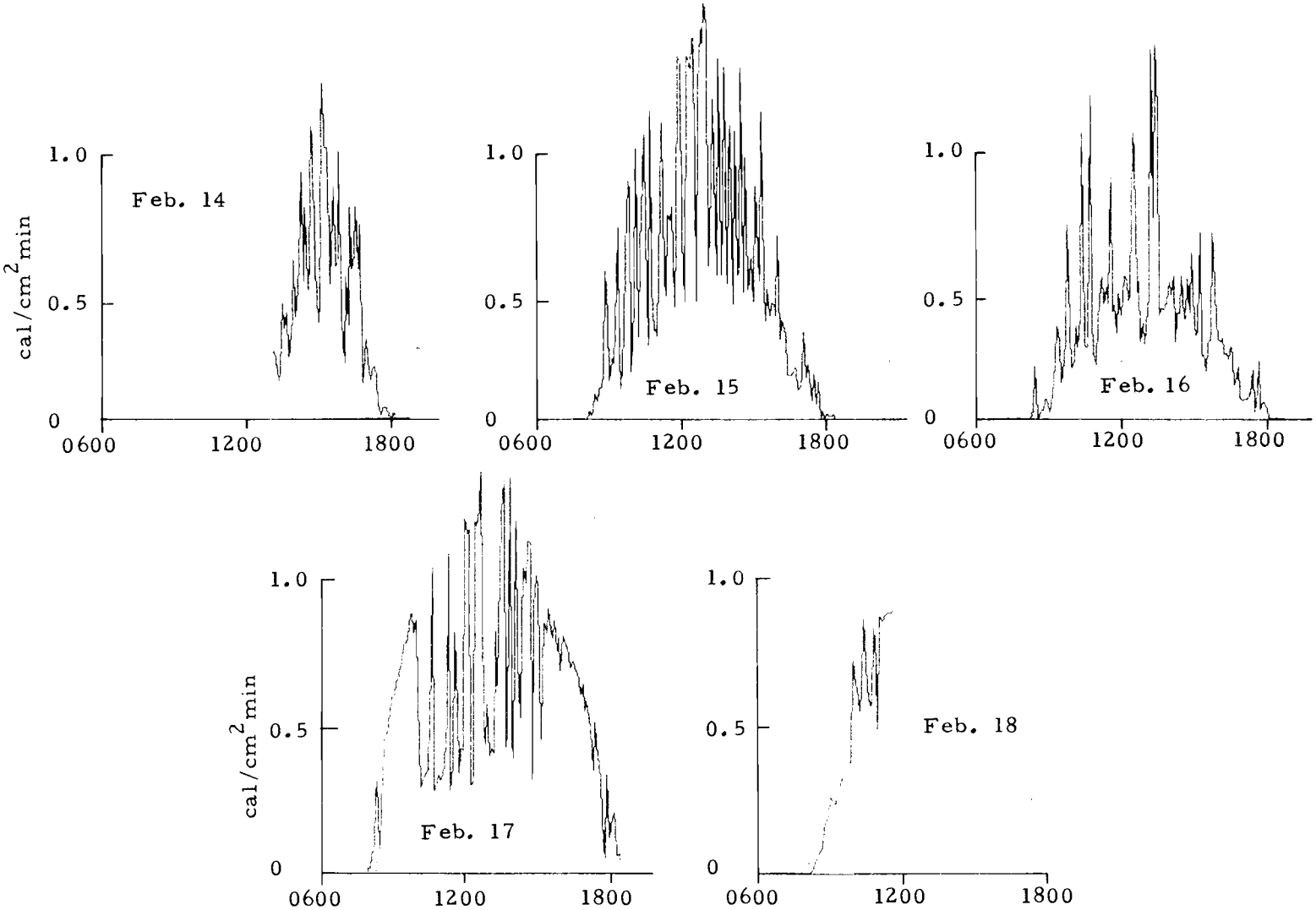

Figure 30. Incoming solar radiation measured at AMTEX station 10.

size and shape. Even if they were regular their centers would not necessarily pass over the buoy, so the spacing between solarimeter peaks will tend to be less than the cell size would imply. Also, a point source cannot always distinguish between open and closed cells. In the extreme case of open versus closed cells, the open cells have thin, cloudy walls and a large, open center, and the closed cells have thin, open walls and a large, cloudy center. Solarimeter data would reflect this difference by having broad, high peaks alternating with narrow, low valleys for open cells (e.g. February 15, 1975 in Fig. 30), and broad, low valleys alternating with narrow, high peaks for closed cells (e.g. February 16, 1975 in Fig. 30). If the cell walls are thick or if the edges of the cells pass over the meter rather than the centers then this distinction may become weak.

The solarimeter data for the 15th and 16th of February indicate a periodicity of about 50 minutes. With an average wind speed during these two days of about 8 to 10 m/s this gives an average cell diameter of roughly 24-30 kilometers.

Air Temperature and Absolute Humidity Fluctuations

The author's main concern was the response of the water column at the spar buoy to the presence of mesoscale cells. Because of the problem discussed above concerning the angle of the sun and because the solarimeter can only give data during daylight hours, fluctuations

in the air temperature and absolute humidity records were used to describe the passage of cells over the buoy in addition to the solarimeter data. Hubert's model (1966) of mesoscale atmospheric cells calls for cool, dry air to descend to the surface under clear areas and for warm, moist air to ascend from the surface under clouds, therefore in the presence of cells air temperature and absolute humidity fluctuations should be highly correlated.

The temperature and absolute humidity records were band-pass filtered to isolate fluctuations between one-half and five hours. These two band-passed records were then correlated in 12 hour segments offset every two hours. The plot of these correlations with time (Fig. 31) indicates that there was significant, but not very great, correlation on the 14th and 15th. On the 16th the correlations jumped to greater than 0.8 then decreased but never dropped below 0.5 for the rest of the record. From this result it is concluded that on the 15th, when satellite photos (Fig. 26) showed some open cellular organization over the buoy, the cells were not very well developed, and by the 16th, when the satellite photos (Fig. 27) revealed strong closed patterns, the cells were well-developed. The cells appeared to be particularly well-developed for 30 hours from 2300 February 15 to 0500 February 17, then the organization seems to drop off with short resurgences late on the 17th and on the 20th. There may be a maturing process for mesoscale cells. In this case it took roughly

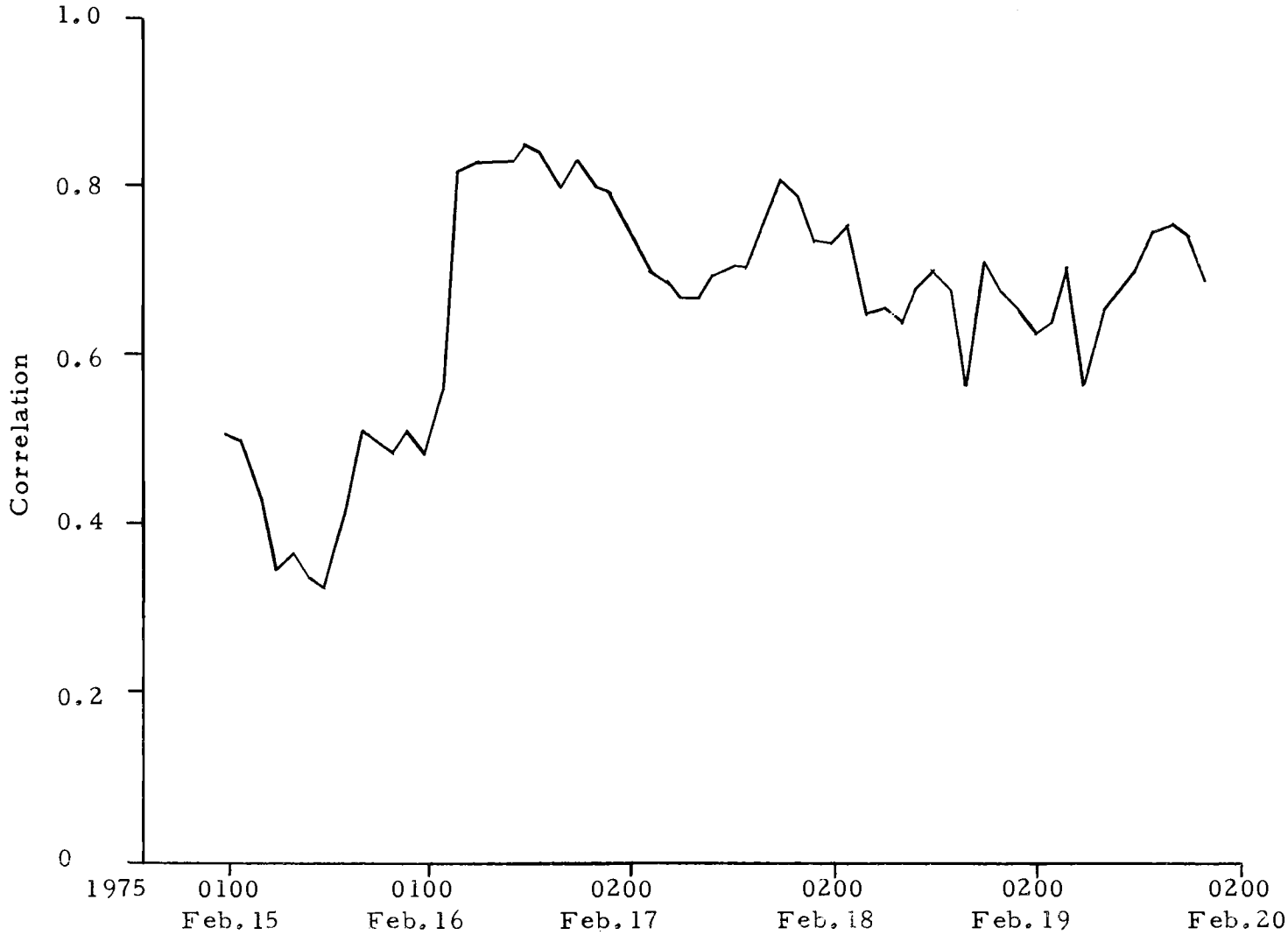

Figure 31. Correlations of 12 hour segments of air temperature and absolute humidity fluctuations at AMTEX station 10.

35 hours after the cold air outbreak commenced for well-developed mesoscale cells to be formed. Then they are quite persistent as evidenced by the result that on the 18th, when the outbreak essentially ceased, the air temperature and absolute humidity fluctuations still correlated well.

The fact that high correlations occur with closed cells, while low correlations occur with open cells could indicate that closed cells are the more mature and better developed form of mesoscale cellular convection. This is contrary to the conclusion of Hubert (1966) and Agee et al. (1973) that the sense of cellular convection is dependent on the magnitude of surface heat fluxes.

Mesoscale Index [MSI]

In order to have one set of numbers that would indicate the presence of cells the author constructed a non-dimensional index [MSI] from the band-passed air temperature and absolute humidity records. The band-passed air temperature and absolute humidity values were divided by their respective standard deviations over the entire record and then summed.

$$MSI(t) = \frac{\text{Band-passed DB}(t)}{\text{St. Dev. of band-passed DB}(t)} + \frac{\text{Band-passed AH}(t)}{\text{St. Dev. of band-passed AH}(t)}$$

Since Hubert's cell description (Fig. 1) calls for cooler and dryer air to be present under open portions and warmer, moister air to be present under cloudy portions, MSI will be least under open portions and greatest under cloudy portions. It is informative to compare MSI with solarimeter data on February 16, 1975 (Fig. 32). It is apparent that the index does act as predicted. This index [MSI] was then used as the input for studying the character of the cells, and more importantly, the oceanic response to cells.

Winds and Fluxes within Mesoscale Cells

The cell model, as described by Hubert (1966), implies a fluctuation in the surface wind speed superimposed on the mean flow. A maximum in the wind speed should occur in front of an open area where the cellular flow is added to the mean flow and a minimum should occur behind an open section where the cellular flow will be subtracted from the mean flow. To test this idea the wind speed record was filtered with the same band-passed filter that was used on the air temperature and absolute humidity records. Then this record was compared with the MSI record using a lag-correlation analysis that will be described later. It was found that the wind speed reached a maximum about 15 minutes in front of an MSI minimum and a minimum about 10 minutes behind an MSI minimum.

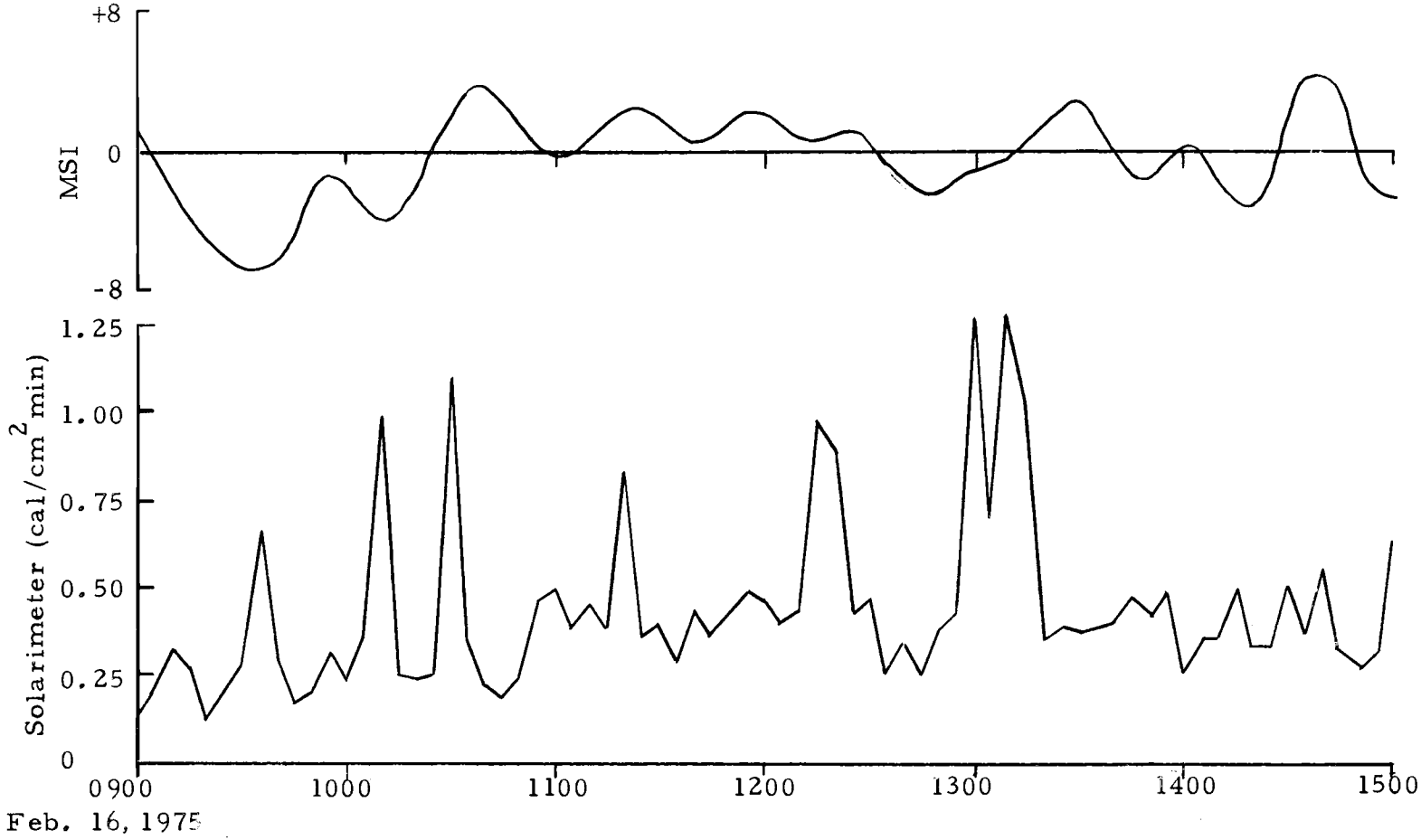

Figure 32. Incoming solar radiation and MSI on February 16, 1975 at AMTEX station 10.

The wind speed fluctuations are very important because the heat fluxes are proportional to the products of wind speed and air-sea temperature differences, and wind speed and air-sea vapor density differences. In this situation the wind speed dominates and statistically the fluxes are greatest about 5 to 10 minutes before the passage of an MSI minimum. The wind speed fluctuation, and hence the heat flux fluctuations, do not correlate as well with MSI as the air temperature and absolute humidity fluctuations correlate with each other. The lower atmosphere is very unstable under outbreak conditions and consequently there are significant turbulent fluctuations also present in the wind speed record.

Cell Model for February 16, 1975

The sizes of the fluctuations associated with cells during the 30 hour period of strong cellular development on February 16 are examined (Fig. 33). An average period for cell passage is 45 minutes, and with an average wind speed of 8 m/s this yields an average diameter of about 22 kilometers. The air temperature fluctuation was about $0.4^{\circ}C$ and the absolute humidity fluctuation was about 0.4 g/kg. The wind speed fluctuation was about 1 m/s. The heat fluxes remained high throughout this period at about 800 $cal/cm^2 day$; the fluctuations in the fluxes are about 100 $cal/cm^2 day$ or about 12.5%. So a description of a representative cell on

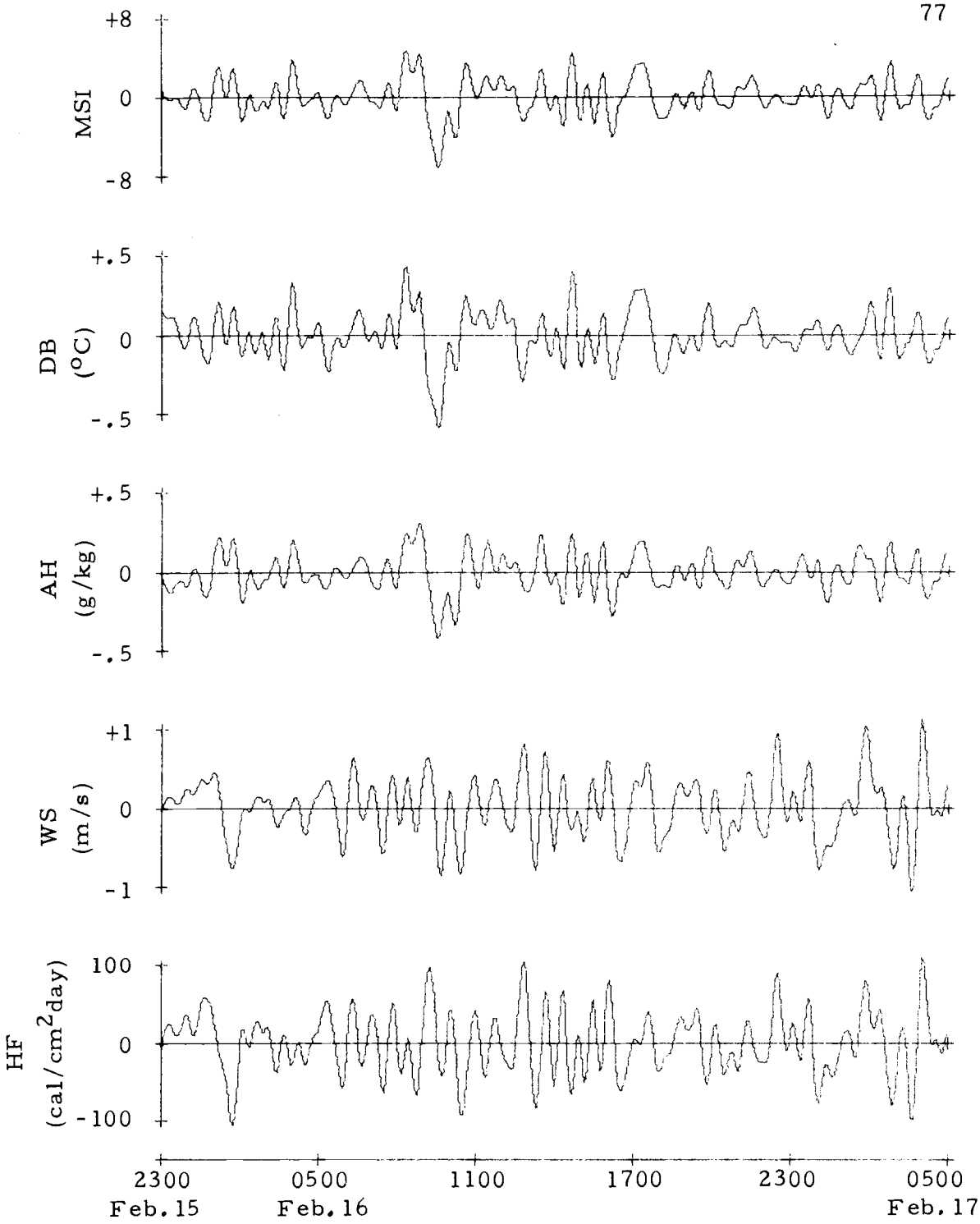

Figure 33. MSI and band-passed wind speed (WS), air temperature (DB), absolute humidity (AH), and heat flux (HS+HL) for 30 hours of prime cellular development from 2300 February 15, 1975 to 0500 February 17, 1975.

February 16 (Fig. 34) is a closed cell, 22 kilometers in diameter moving at 8 m/s, and taking about 45 minutes to pass overhead. Under the open cell walls the air is 0.4^{o}C cooler and 0.4 g/kg dryer than under the cloudy cell center. The wind speed is greatest (8.5 m/s) about seven kilometers in front of the following cell wall and least (7.5 m/s) about five kilometers behind the leading cell wall. The upward heat flux has a maximum value about three to four kilometers in front of the trailing cell wall and a minimum value (12.5% less) about six kilometers behind the leading cell wall.

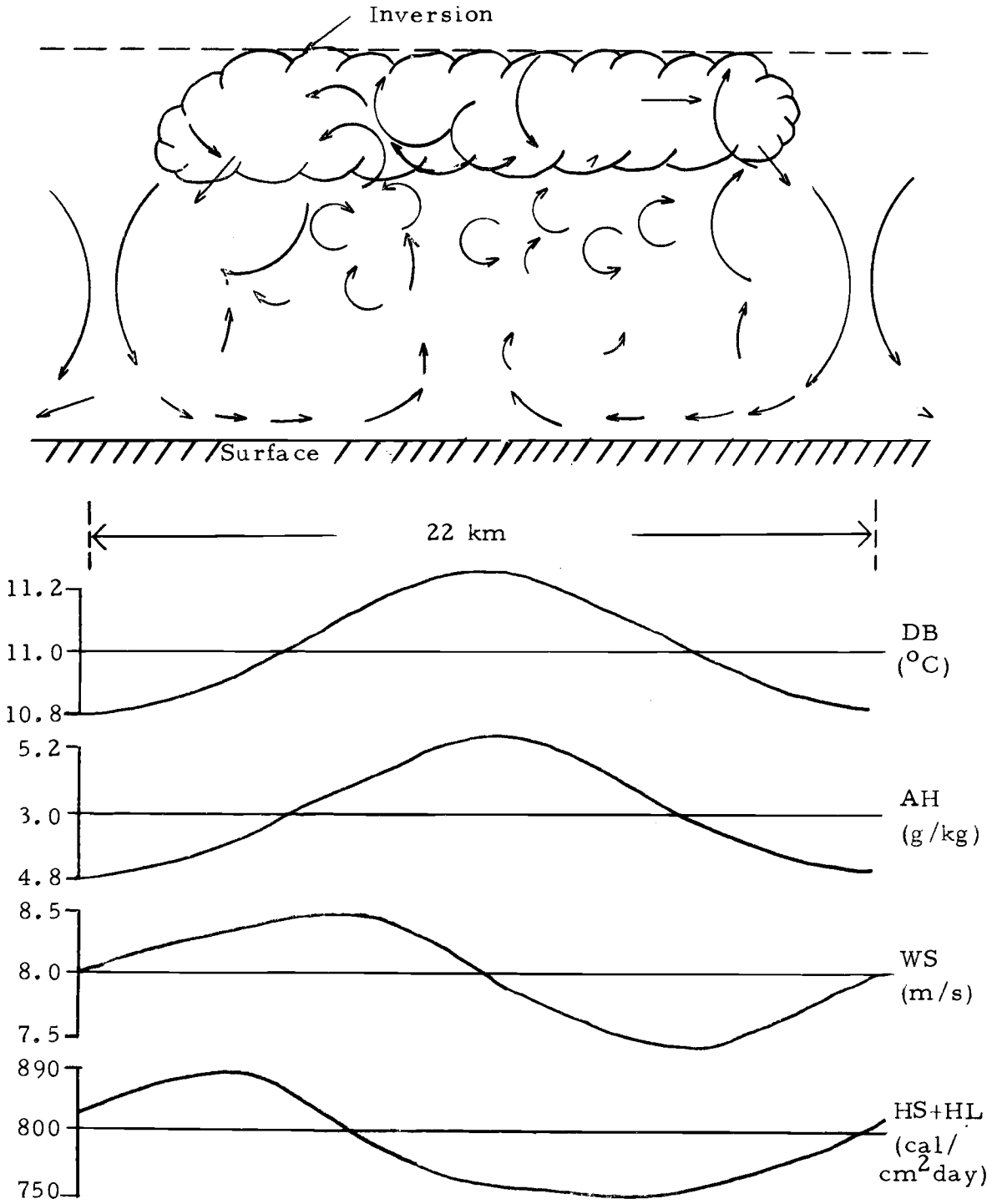

Figure 34. Cross-sectional schematic of a representative closed mesoscale atmospheric cell on February 16, 1975 at AMTEX station 10.

VI. OCEANIC RESPONSE TO MESOSCALE ATMOSPHERIC CELLS

Lag Correlation Analysis

In analyzing the oceanic response to the presence of mesoscale cells the MSI record was used as the input and the fluctuations of oceanic measurements (temperatures and currents) were examined for indications of a response. The oceanic fluctuation records were formed by using the same band-passed filter on ocean temperature and current component data as was used on the air temperature and absolute humidity records to form MSI. Ideally cross-spectral analysis could be used, but the author felt that this could not be done for the entire record for two reasons: (1) the presence and state of development of the mesoscale cells was not consistent throughout the record so any spectral analysis would be severely limited by non-stationarity in the data records; and (2) the cells were not regularly shaped, and their centers did not all pass perfectly over the spar buoy, so sharp peaks in the MSI spectrum could not be expected.

Therefore, the author decided to use a technique in which shorter sections of the MSI record would be compared directly with sections of the oceanic parameter fluctuations record to see if patterns in the oceanic parameter fluctuations reflected the MSI record in some significant manner.

The technique used was one of repeated calculation of lag correlations involving successive 12 hour sections of the data record. The first 12 hour section of MSI was correlated with 20, 12 hour sections of the oceanic parameter fluctuations, each successively lagged by five minutes. Then this process was repeated for the entire record with successive 12 hour sections of the MSI record offset from previous 12 hour MSI record sections by two hours.

The output of this analysis was an array of correlations with each row corresponding to a particular 12 hour section of the MSI record and each column corresponding to the lag of the oceanic parameter fluctation record. The author went through this array and recorded the highest correlation and its lag for each 12 hour MSI section. These numbers were then plotted and analyzed.

In order to analyze the results of this lag correlation analysis, some criteria of significance must be used. Snedecor and Cochran (1967) show that when the calculated correlation between 144 independent number pairs (12 hours of 5 minute data) has an absolute value greater than 0.2 then it can be concluded, to a highly significant extent ($p > .99$), that there exists some relationship between the number pairs.

The correlations calculated in the lag correlation analysis are not of independent number pairs but rather of number pairs from

two time series. Box and Jenkins (1970) describe a significance test procedure for lagged cross correlations. The method involves estimating the standard deviation for each calculated lag correlation, assuming a normal distribution, and comparing the calculated lag correlation to the estimated standard deviation of the correlation.

The estimate of the standard deviations of the calculated correlations is inversely proportional to the square root of the number of number pairs and proportional to a function (eq. 11.1.7, Box and Jenkins, 1970) of the autocorrelations, and cross-correlations of the two time series summed over an appropriate number of lag intervals.

It will be shown by example in the next section that the lack of independence of the number pairs does not appreciably affect the confidence levels described by Snedecor and Cochran (1967). Throughout the discussion of lag correlation results it will be assumed that a correlation of 0.2 implies that some relationship between the two records exists and that a correlation of 0.4 implies a strong relationship.

Correlations of 0.2 or 0.4 are small and only explain a small portion of the fluctuations studied, but it is a significant portion.

MSI versus ST20(10)

As an example of the above process, MSI was compared with the sea temperature fluctuations as recorded by the current meter at station 10 [ST20(10)]. Figure 35 shows the output correlation array with the selected correlations marked. Some subjective decisions had to be made in selecting the correlations, but generally it was a straightforward process. Figure 36 then shows the plot of the selected correlations and their lags with time. Also included in this figure is a plot of the correlations (0-lag) between the band-passed air temperature and absolute humidity records that act as an indicator of mesoscale cellular development.

There are three periods during which the lag correlations are greater than 0.2 and one is as high as 0.46. These periods coincide with periods of strong mesoscale cellular development. The period of prime interest is that encompassing February 16, 1975. This was in the middle of a cold air outbreak when the air temperature and absolute humidity fluctuations had the highest correlations. The lags during this period were in the 30 to 45 minute range. This indicates that air temperature fluctuations (as indicated by MSI) show up as water temperature fluctuations at 20 meters about 45 minutes later. By itself this cannot be considered a conclusive result. A 0.4 correlation though significant, is small, and the sea temperature

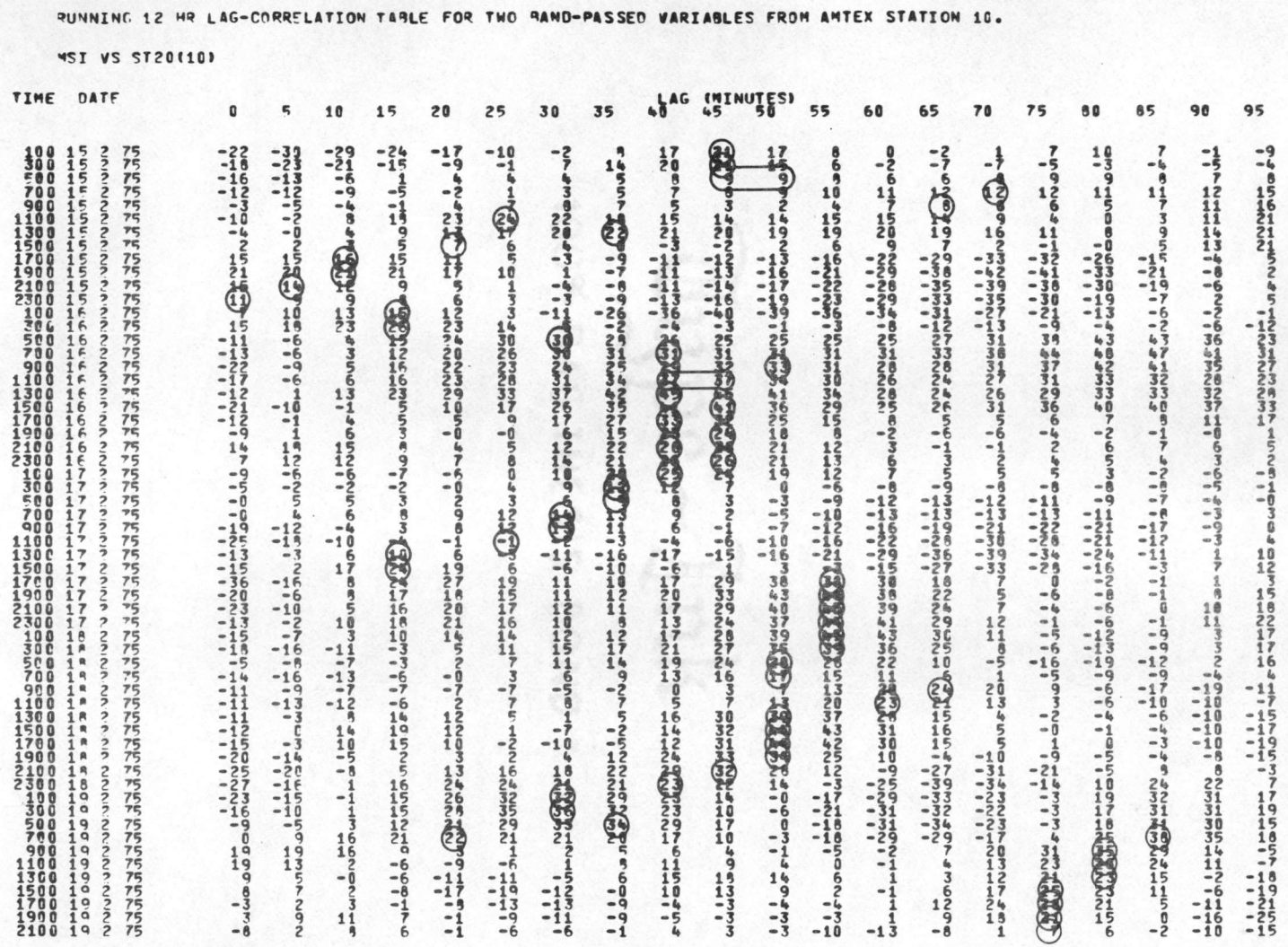

Figure 35. Array of correlations from lag correlation analysis of MSI versus ST20(10), with selected correlations marked. Numbers in array are correlations times 100.

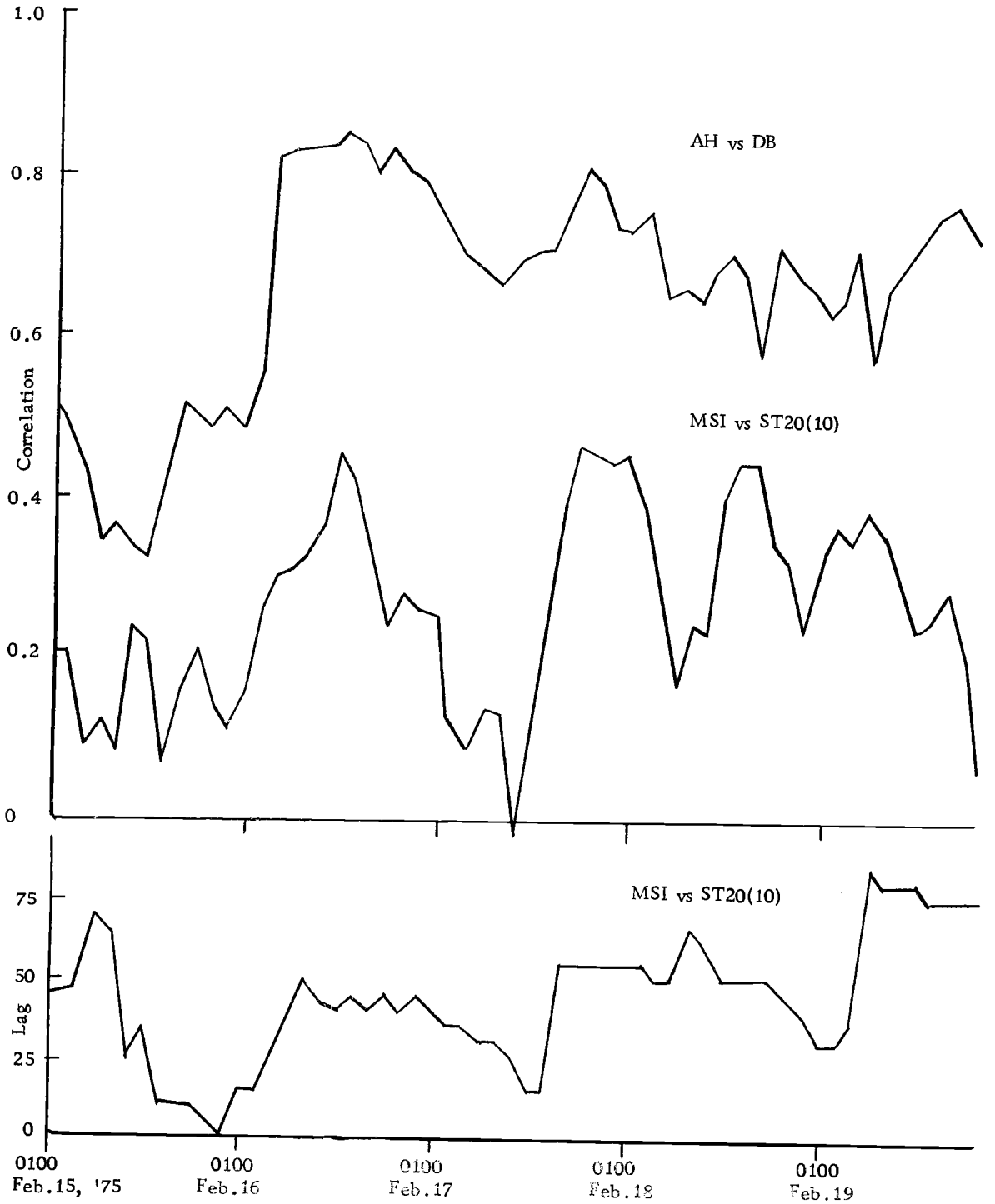

Figure 36. Selected correlations and lags from lag correlation analysis of MSI versus ST20(10). The correlations between 12 hour segments of air temperature and absolute humidity fluctuations are included for reference.

fluctuations are very small, close to the resolution of the temperature sensor.

Applying eq. 11.1.7 of Box and Jenkins (1970) to the calculated lag correlation of 0.45 found at a lag of 40 minutes during the 12 hour segment centered on 1300 February 16, an estimate of the standard deviation of this correlation was found to be 0.12. The calculated correlation was 3.75 times the estimated standard deviation and was concluded to be highly significant.

MSI versus ST0(10), ST5(10), ST15(10)

There were three other sea temperature records at the spar buoy station [ST0(10), ST5(10), ST15(10)] at shallower depths than the current meter record (0, 5, and 15 meters). These records were shorter than the other buoy records. Figure 37 shows the plots of selected correlations between MSI and these four sea temperatures [ST0(10), ST5(10), ST15(10), and ST20(10)]. The curves are offset for ease of observation. It is evident that the four plots are extremely similar. During the 30 hour period centered on February 16, 1975, when the mesoscale cell development was greatest, the correlations with all four temperature records were significant and all peaked at values > 0.4.

The plots of the lags of the selected correlations between MSI and the four sea temperature records discussed above are not as

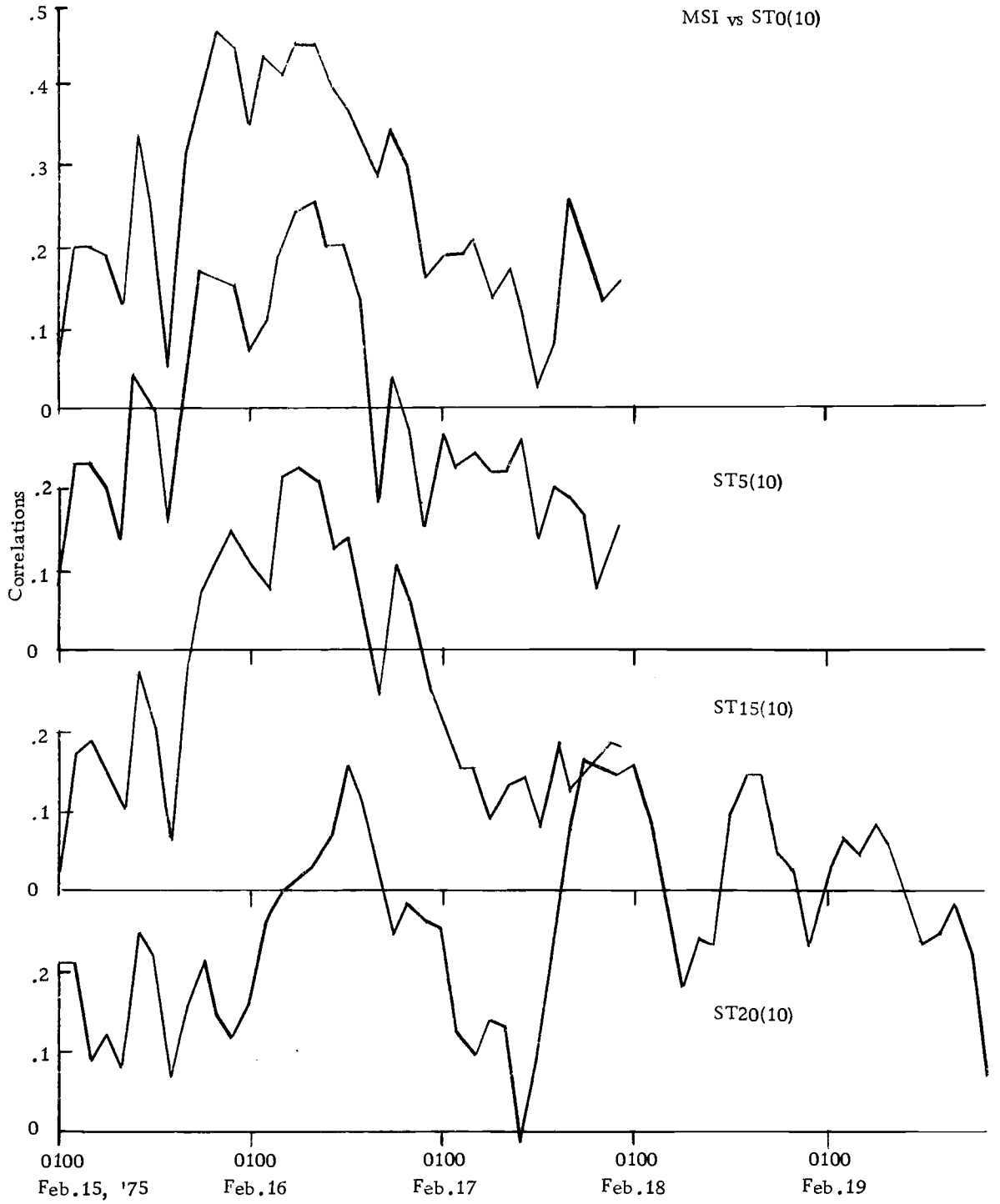

Figure 37. Selected correlations from lag correlation analyses of MSI versus ST0(10), ST5(10), ST15(10), and ST20(10).

consistent as the correlations themselves (Fig. 38). Here the lags for the three sea temperature records on the spar buoy are basically identical, but different from the lags for the sea temperatures measured on the current meter. For seven points around 0000 February 16, the four lags are similar but before and after this the three spar buoy records indicate an unexplained shifting mode behavior. The shifts in the lags are about 50 minutes which is the average periodicity of the cells and could represent a 360^{o} phase shift. There was a definite horizontal distance between the spar buoy and the current meter (Fig. 5). This distance was quite small with respect to the horizontal scale of the mesoscale cells, but it might not be small with respect to the norizontal scale of the oceanic response to the cells. Also, there was some evidence that the metal spar buoy itself acted as a heat conductor. When the air temperature and four sea temperature records were filtered with a high-pass filter, the five minute air temperature fluctuations correlated excellently with the three spar buoy sea temperature fluctuations, but very poorly with the current meter sea temperature fluctuations.

One hypothesis the lag record does not support is the idea that the sea temperature fluctuations are steadily mixed downward. The three spar buoy temperature lags are all basically the same and are similar to portions of the current meter sea temperature lag record. The sea temperature fluctuations appear to occur

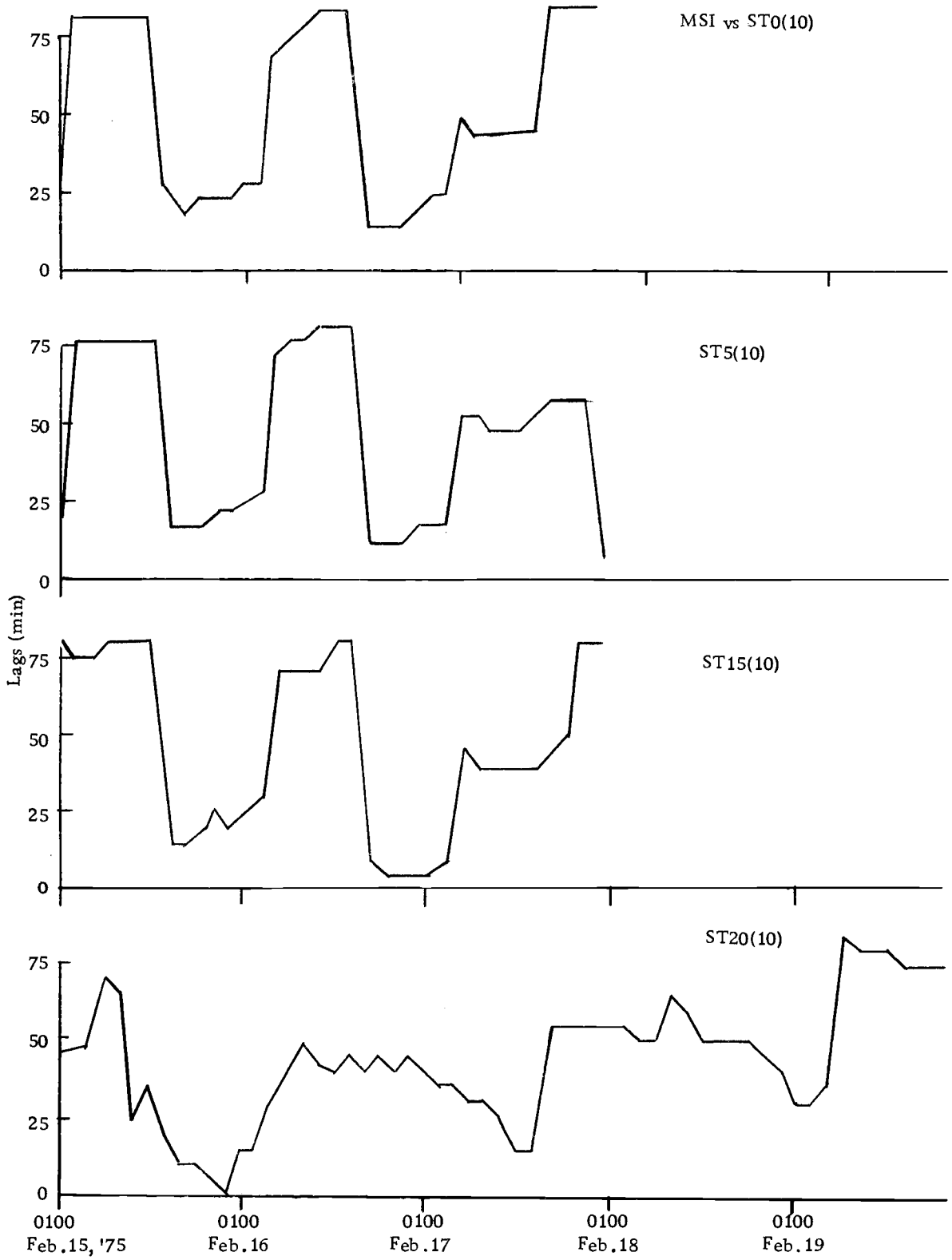

Figure 38. Lags of selected correlations from lag correlation analyses of MSI versus ST0(10), ST5(10), ST15(10), and ST20(10).

simultaneously at the four depths about 30 to 45 minutes after the passage of the air temperature fluctuations (as indicated by MSI). This idea is supported by the thermistor chain data (Fig. 24) which show nearly simultaneous temperature fluctuations at depths from 20 to 70 meters.

MSI versus Current Components at AMTEX Station 10

The next step was to analyze possible motion responses in the water column. Several problems arose. Current motions are vector processes and care is needed in choosing an interesting coordinate orientation. Also, there is no particular reason why positive or negative correlations should be expected. With temperature records one expects that the oceanic response to a dip in air temperature would be a dip in sea temperature (positive correlation), but with currents the type of response is not predictable.

In the section entitled "Ekman Veering" of this paper it was noted that the band-passed current fluctuations were generally oriented about 25^{o} to 30^{o} to the right of the mean wind. It was decided that a coordinate system aligned 25^{o} to the right of the mean wind would be examined. The band-passed current fluctuations were rotated so that the positive V component [CVE(10)] was 25^{o} to the right of the smoothed wind direction, and the positive U component

[CUE(10)] was 115° to the right of the smoothed wind direction. This is a coordinate system that changes its geographical orientation with time, but not its orientation with respect to the wind.

When these band-passed current components were compared to MSI by lag correlation analysis both the best positive and negative correlations were examined and the one that gave the most consistent and interesting results was analyzed.

Figure 39 presents the results of the lag correlation analyses of MSI versus ST20(10), CVE(10), and CUE(10). Negative correlations are reported for both current components. The open parts of the mesoscale cells represented by minimum values of MSI are the parts in which fluxes and wind speeds are greater. Therefore negative current correlations imply responses to the greater heat fluxes and wind speeds in the positive V components (25° to the right of downwind) and positive U components (90° to the right of positive V component). Most of the correlations reported indicate a significant relationship between MSI and the current fluctuations. The V component correlations are consistently better than the U component correlations which was expected from the orientation of the components.

The correlation pattern for the current fluctuations does not follow the cell development as well as the sea temperature fluctuation correlations, but there are similarities. For both current

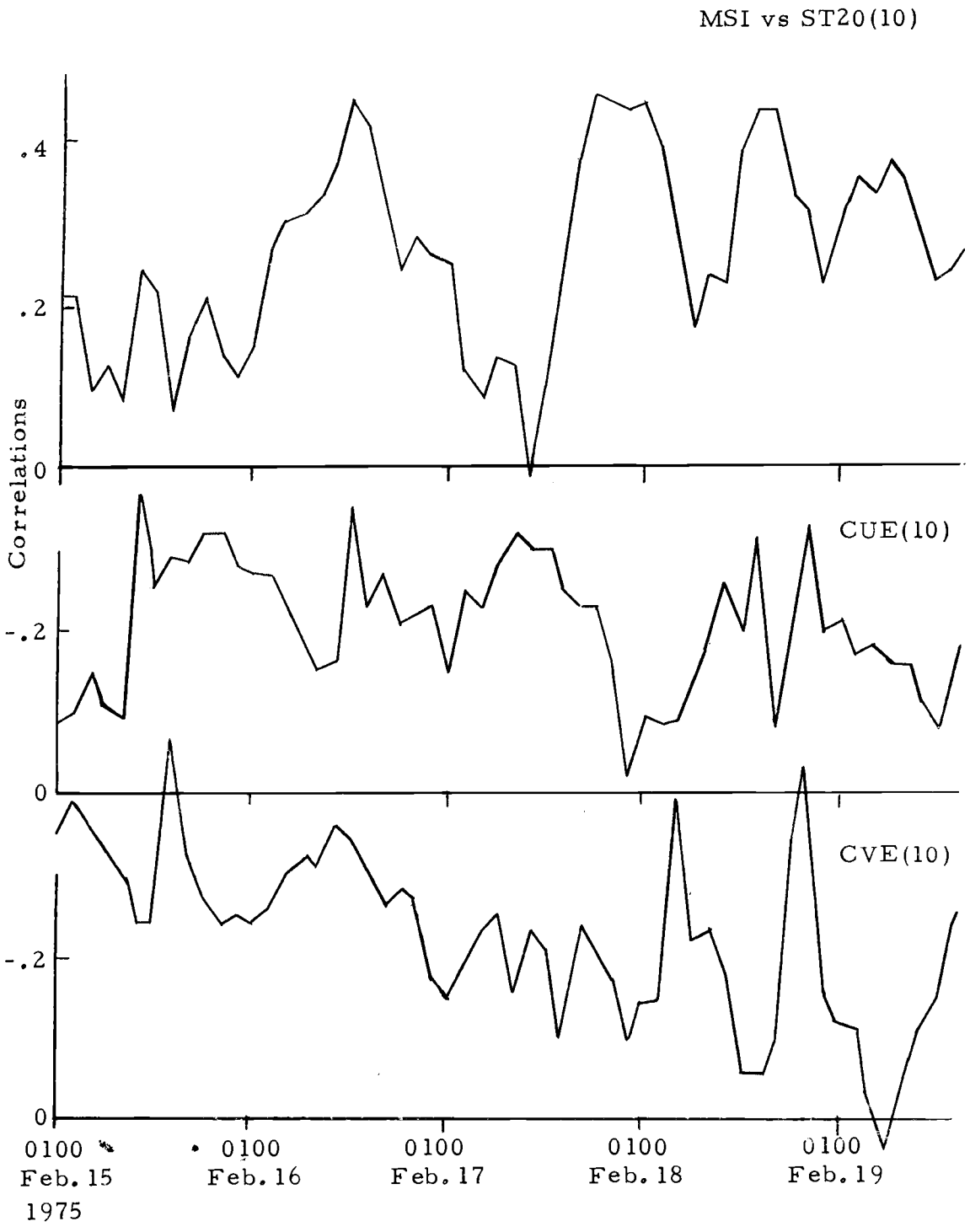

Figure 39. Selected correlations from lag correlation analyses of MSI versus ST20(10), CUE(10), and CVE(10).

components there were significant correlations around the prime period of cellular development on February 16, but unlike the sea temperature results the current components were also significantly correlated on the day before the prime period. Apparently the currents responded to the open cells on the 15th as well as to the closed, better developed cells on the 16th. After the 16th the current component and sea temperature fluctuation correlations all had related peaks that coincided with apparent cellular development.

The lags for the current component fluctuation correlations (Fig. 40) showed consistent results for the prime period on the 16th. Here the CUE(10) fluctuation lags were nearly identical to the ST20(10) fluctiation lags ($\approx$40 minutes) and the CVE(10) fluctuation lags were 15 to 20 minutes longer. Before and after the prime period on the 16th the three lag sets did not agree. On the 15th, under the open cells, the current responses seem to occur more rapidly. This is particularly so for the CVE(10) fluctuations that have lags of less than 10 minutes, which shifts dramatically to 60 minutes at the start of the prime period on the 16th. There are similarities in the lags during the entire record, but the best agreement does occur during the prime period when the cellular development was apparently greatest.

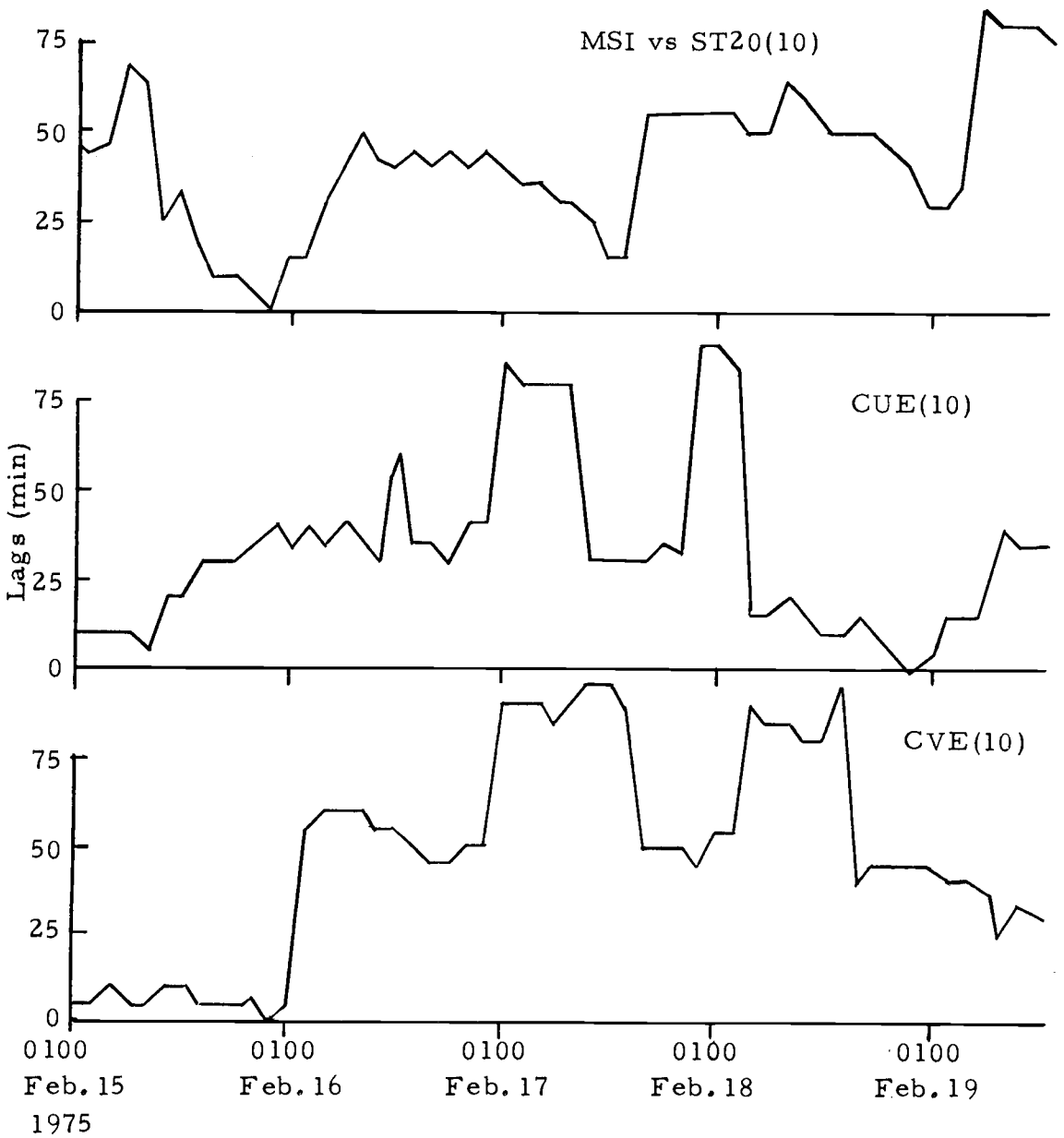

Figure 40. Lags of selected correlations from lag correlation analyses of MSI versus ST20(10), CUE(10), and CVE(10).

MSI versus Ocean Parameters
from Other Stations

MSI represents the cellular structure over station 10 and the previous sections discuss the ocean response at this station. There were also ocean measurements made at stations 4 and 7 (Fig. 4). Since station 7 lies to the north of station 10 the cells that pass over station 10 should have previously passed over station 7 and similar cells should have passed over station 4. The connection is tenuous, but perhaps the oceanic parameters at stations 4 and 7 would show correlations with MSI at station 10 which would increase the confidence in the results at station 10.

The lag correlations between MSI and the band-passed sea temperature record at station 4 [ST20(4)] were not supportive of the station 10 results. There was no period of high positive correlations, but there was a period in and around the prime period of February 16 where strong negative correlations exist. Station 4 is to the west of station 10 so the same cells will not pass over both stations. For MSI versus ST20(7) results are obtained that do support the station 10 results. On February 16 the positive correlations are actually higher than those between MSI versus ST20(10). For over 20 hours on the 16th the correlations are greater than 0.5, all at the same lag of 50 minutes. The lag is surprising since it implies that the temperature fluctuations at station 7 show up 50 minutes after the

cells pass over station 10, or about 95 minutes after they pass over station 7. Station 7 has the only other current record and MSI was compared with the station 7 component fluctuations parallel to CUE(10) and CVE(10). There were significant positive correlations on the 16th between MSI and the U component [CUE(7)] lagged about 15 minutes in front of MSI (about 30 minutes after cells pass over station 7). The sign of these correlations is opposite to those recorded for the U component at station 10. Station 7 is located about three kilometers to the east of the north-south line through station 10 and this could be responsible. The V component fluctuations had high negative correlations with MSI, particularly on the 16th when they peaked at 0.51. The rotated V component lags on the 16th were about 10 minutes (about 55 minutes after the cells passed over station 7). On the 16th the wind-rotated V component fluctuations at station 10 had significant negative correlations lagged 55 minutes behind MSI and the wind-rotated V component fluctuations at station 7 had strong negative correlations lagged 10 minutes behind MSI, which is equivalent to the 55 minute lag at station 10.

In summary, this lag correlation analysis indicated that the ocean parameters fluctuated in a pattern that consistently correlated well with the MSI fluctuations, particularly for the 30 hour period centered on February 16, 1975, when the air temperature and absolute humidity fluctuations correlated highly indicating well-developed

mesoscale cellular activity. The best responses were in the sea temperature fluctuation records and in the current fluctuations aligned 25^{o} to the right of the mean wind.

Prime Period Data Summary

The air temperature and absolute humidity fluctuation correlations and the lag correlation analyses results indicated that the 30 hours of data from 2300 February to 0500 February 17 represented the prime period of mesoscale atmospheric cellular development and the prime period of oceanic response to the cells. During this period the surface fluxes were high, though below maximum values (Fig. 19), satellite imagery indicated well-formed, closed mesoscale cells, and the air temperature and absolute humidity fluctuations correlated with each other with values greater than 0.8. The lag correlation analysis results, summarized in Figure 41, all indicate that the waters responded to the passage of mesoscale atmospheric cells in a significant manner. The oceanic responses were particularly evident as sea temperature fluctuations and current fluctuations aligned 25^{o} to the right of the mean wind, approximately 50 minutes after the passage of cells.

Figure 42 shows the data fluctuation records during the prime period. The average passage time of mesoscale cells over the spar buoy was estimated from the MSI record by counting the number of

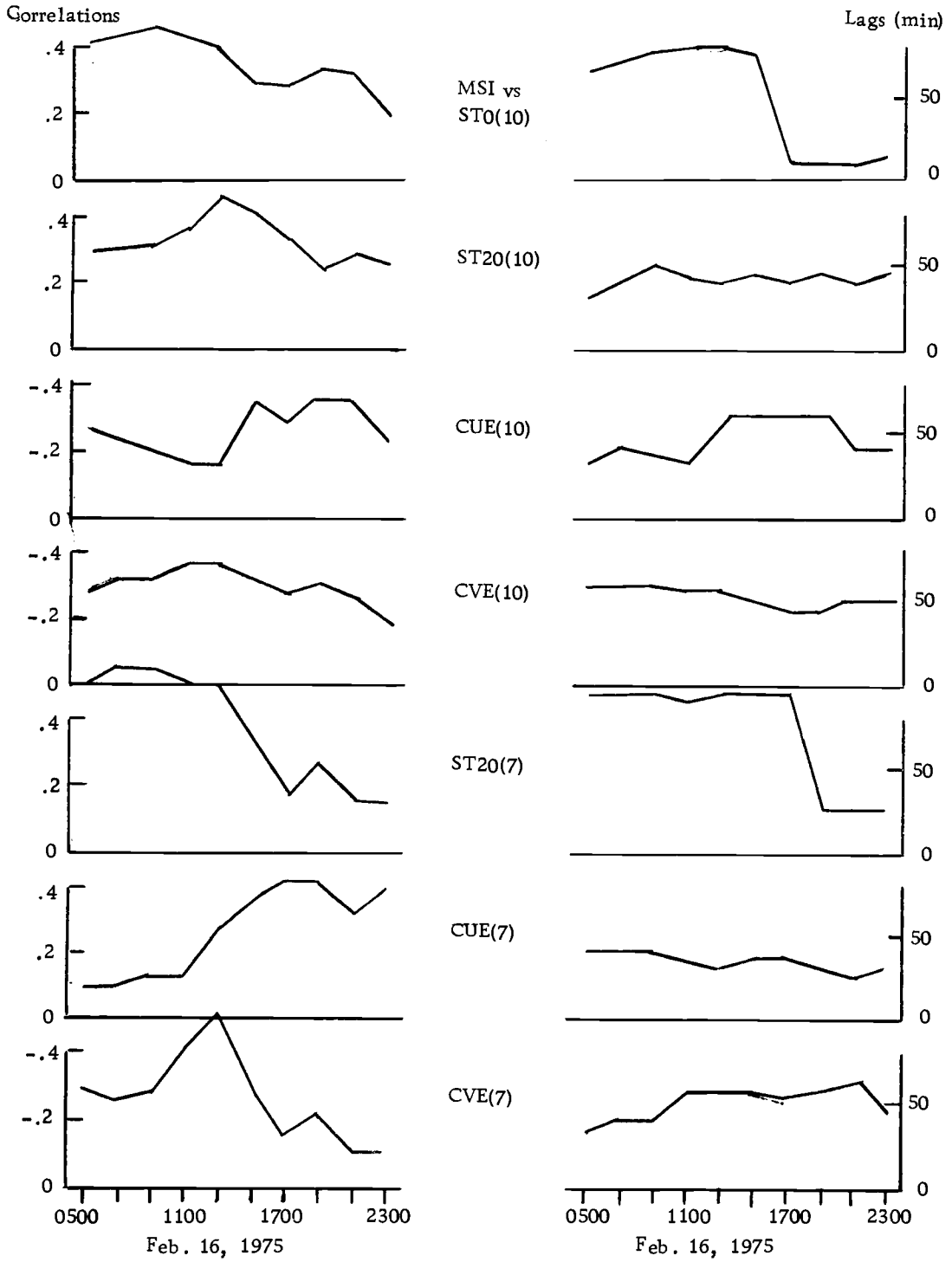

Figure 41. Summary of selected correlations and their lags from lag correlation analyses of MSI versus ST0(10), ST20(10), CUE(10), CVE(10), ST20(7), CUE(7), and CVE(7) during 30 hours of prime interest from 2300 February 15, 1975 to 0500 February 17, 1975.

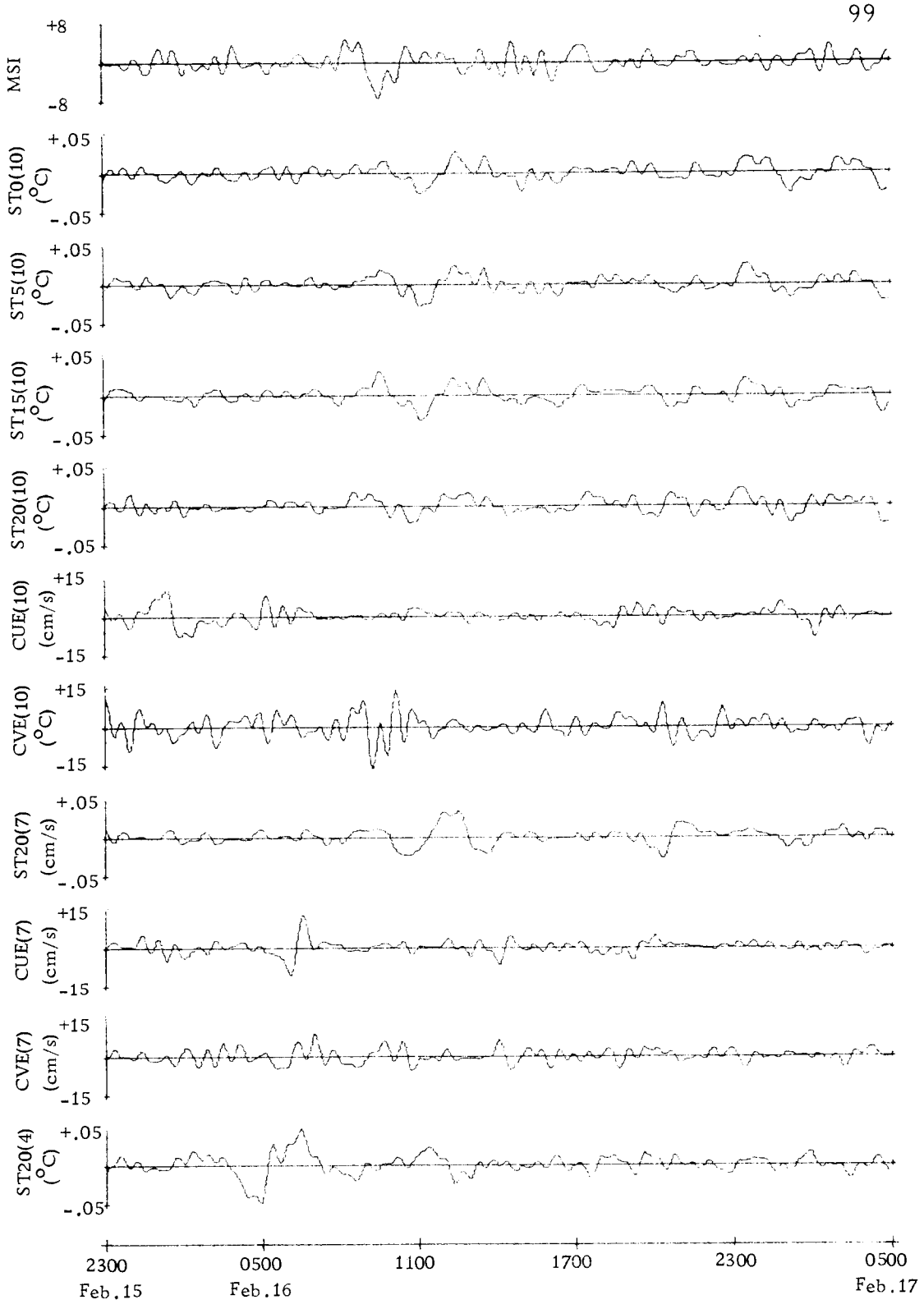

Figure 42. Plots of MSI and band-passed (.5 hr to 5 hr) ST0(10), ST5(10), ST15(10), ST20(10), CUE(10), CVE(10), ST20(7), CUE(7), CVE(7), and ST20(4) during 30 hours of prime interest from 2300 February 15, 1975 to 0500 February 17, 1975.

peaks and dividing the total into 1800 minutes (30 hours). This yielded the previously reported estimate of 50 minutes. If the number of positive zero crossings is used instead, then an estimate of 75 minutes is found. Based on satellite imagery and solarimeter data it was concluded that the 50 minute estimate was correct. The significance of the 75 minute estimate found here and also found in spectral analysis to be reported in the next section is unclear.

Spectral Analysis of Prime Period Data

If any portion of the data record is amenable to spectral analysis it would be the prime period of 30 hours from 2300 February to 0500 February 17. The spectrum of MSI during this period (Fig. 43) indicates significant energy was present at periods of 164, 75 and 34.6 minutes. There was a peak at 50 minutes that was only significant at the 80% level. No explanation is known for the 164 and 34.6 period peaks and for the relatively small amount of energy in the 50 minute period peak.

Figure 44 displays the spectra calculated for the three band-passed current meter temperature records [ST20(10), ST20(7) and ST20(4)]. Peaks are not evident here at 164 or 34.6 minutes though peaks are present near these periods (at $\approx$200 minutes and $\approx$38 minutes). There are peaks for the temperature records at stations 10 and 4 at 50 and 75 minutes but not at station 7.

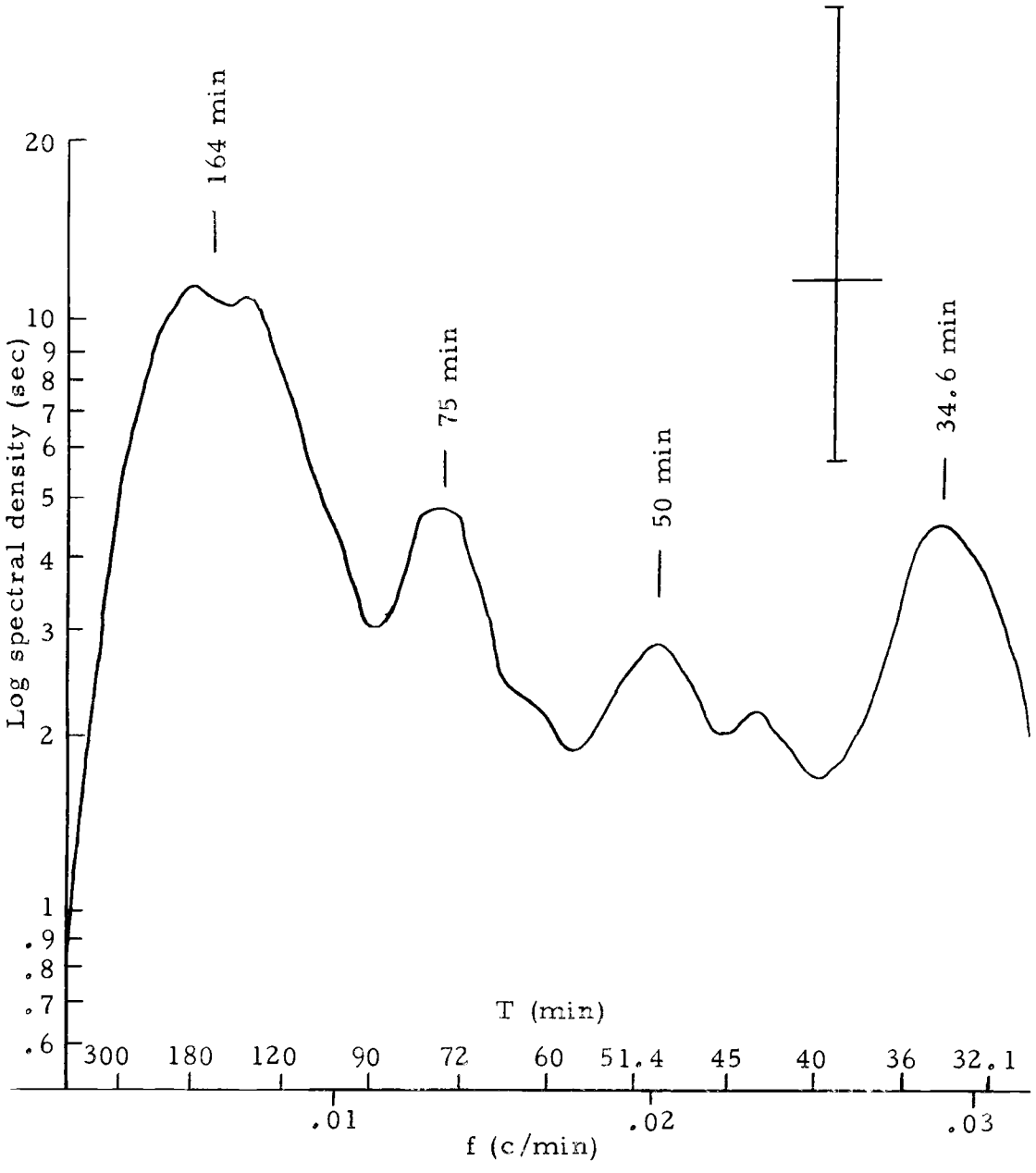

Figure 43. Spectrum of MSI record during 30 hours of prime interest from 2300 February 15, 1975 to 0500 February 17, 1975. 95% confidence interval bars indicated.

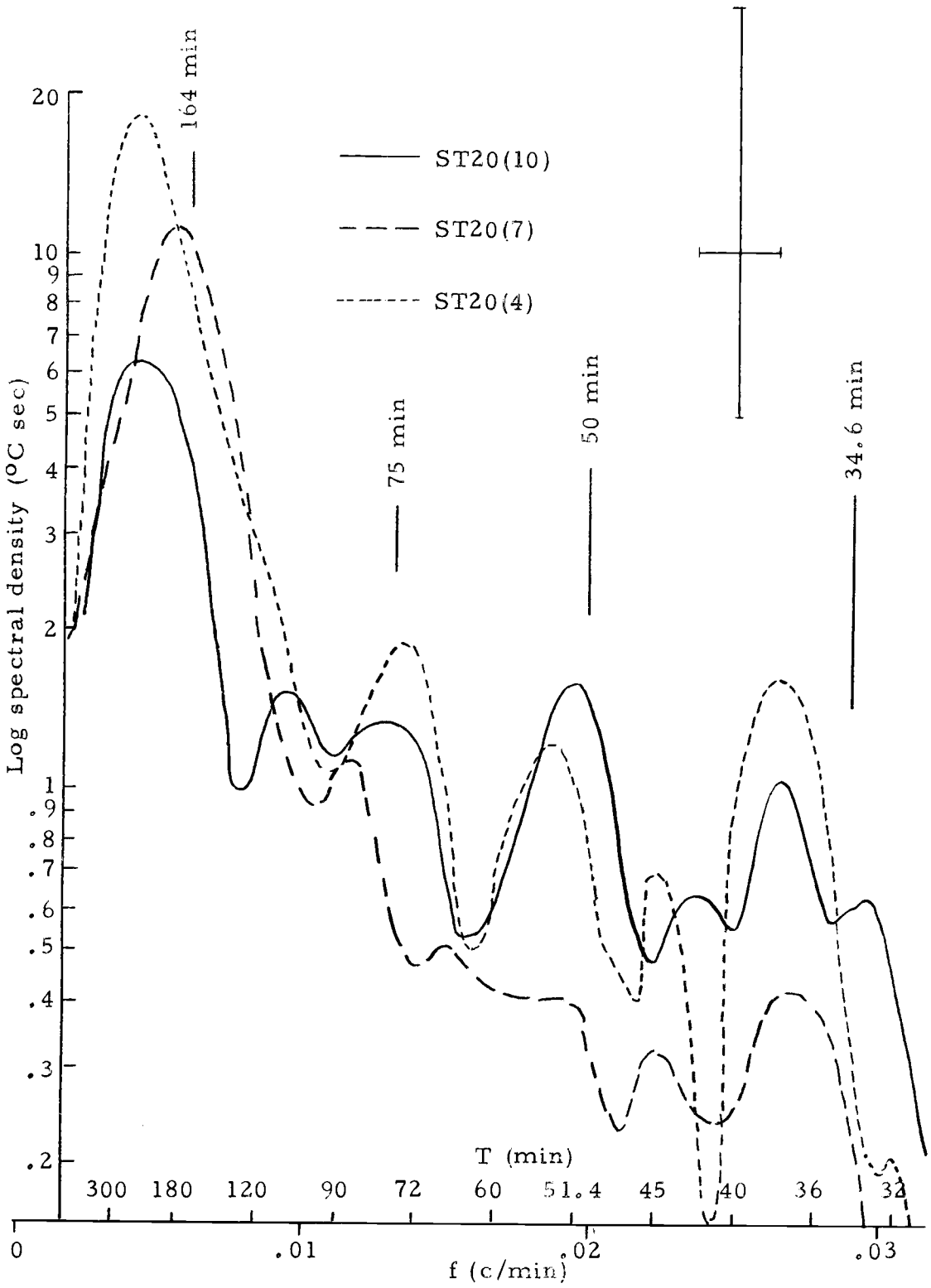

Figure 44. Spectra of ST20(10), ST20(7), and ST20(4) during 30 hours of prime interest from 2300 February 15, 1975 to 0500 February 17, 1975. 95% confidence interval bars indicated

The spectra of the four wind-rotated band-passed current components (Fig. 45) were inconsistent. There were peaks evident at periods near 75 minutes except in the CVE(10) spectra. At a period near 50 minutes there was no peak in the CUE(10) record and a definite peak for the CVE(10) spectra at a much higher energy level. This supports the idea that at station 10 the current response was aligned 25^{o} to the right of the wind. At station 7 the two components have the same amount of energy at 50 minutes but the CUE(7) peak is more significant. In the 40 to 60 minute period band there is generally more energy present in the CVE components at both stations than in the CUE components which was expected from the alignment of the components with respect to the wind. This was particularly true at station 10 where the CVE component dominates the CUE component for all periods less than 120 minutes.

Cross-spectral analyses were made between MSI and all the oceanic parameter records for the 30 hour prime period. The analyses were performed on 30 hours of five minute data with 10.2 degrees of freedom. The calculated coherence squared between two records needed to be greater than 0.691 in order to be significant at the 90% level (Jenkins and Watts, 1968). Very few significant coherences were found in these analyses. There were some that were interesting but they were not statistically significant. The coherence squared of the cross-spectra involving MSI are displayed in Figure 46.

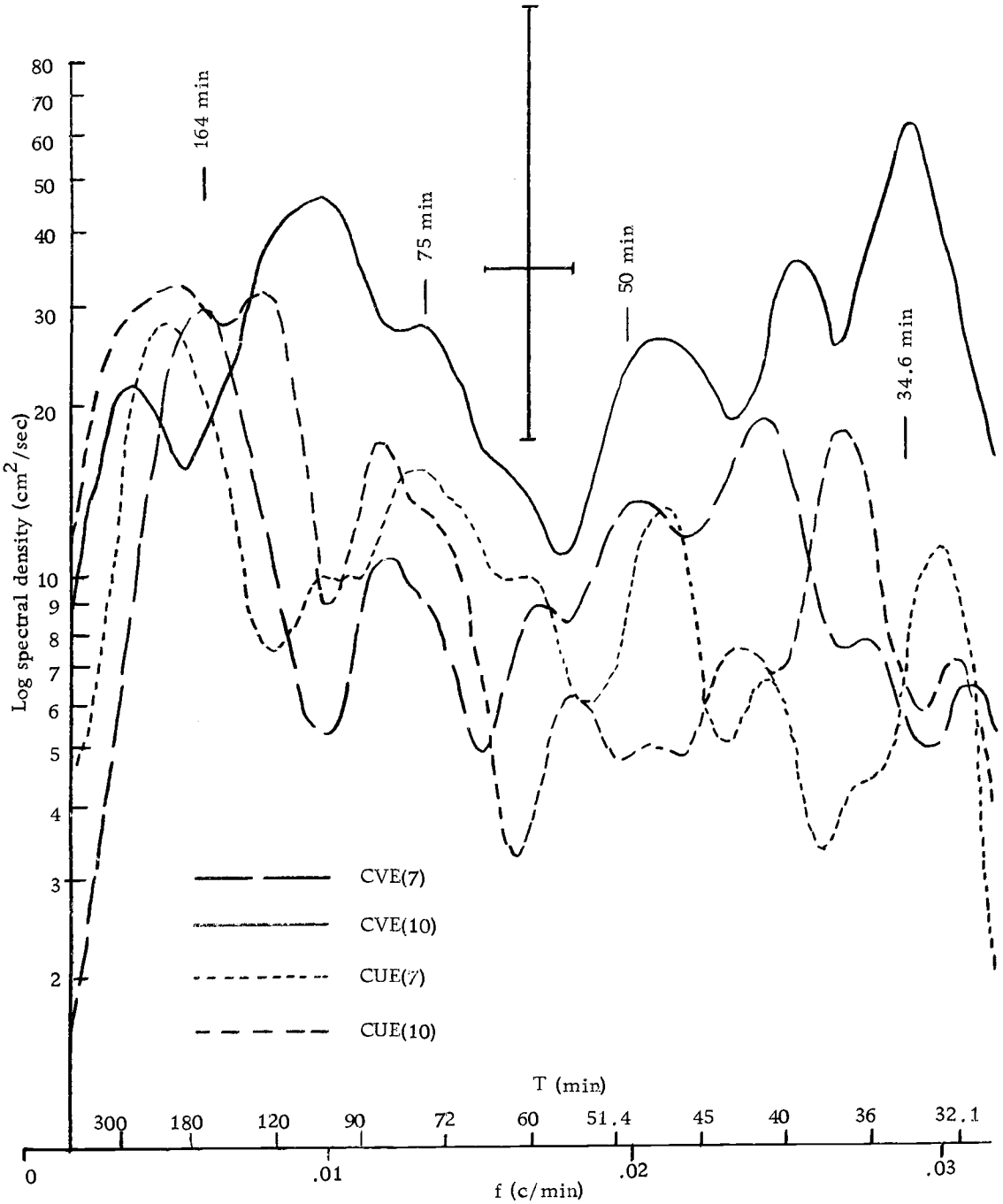

Figure 45. Spectra of CUE(10), CVE(10), CUE(7) , and CVE(7) during 30 hours of prime interest from 2300 February 15, 1975 to 0500 February 17, 1975. 95% confidence interval bars indicated

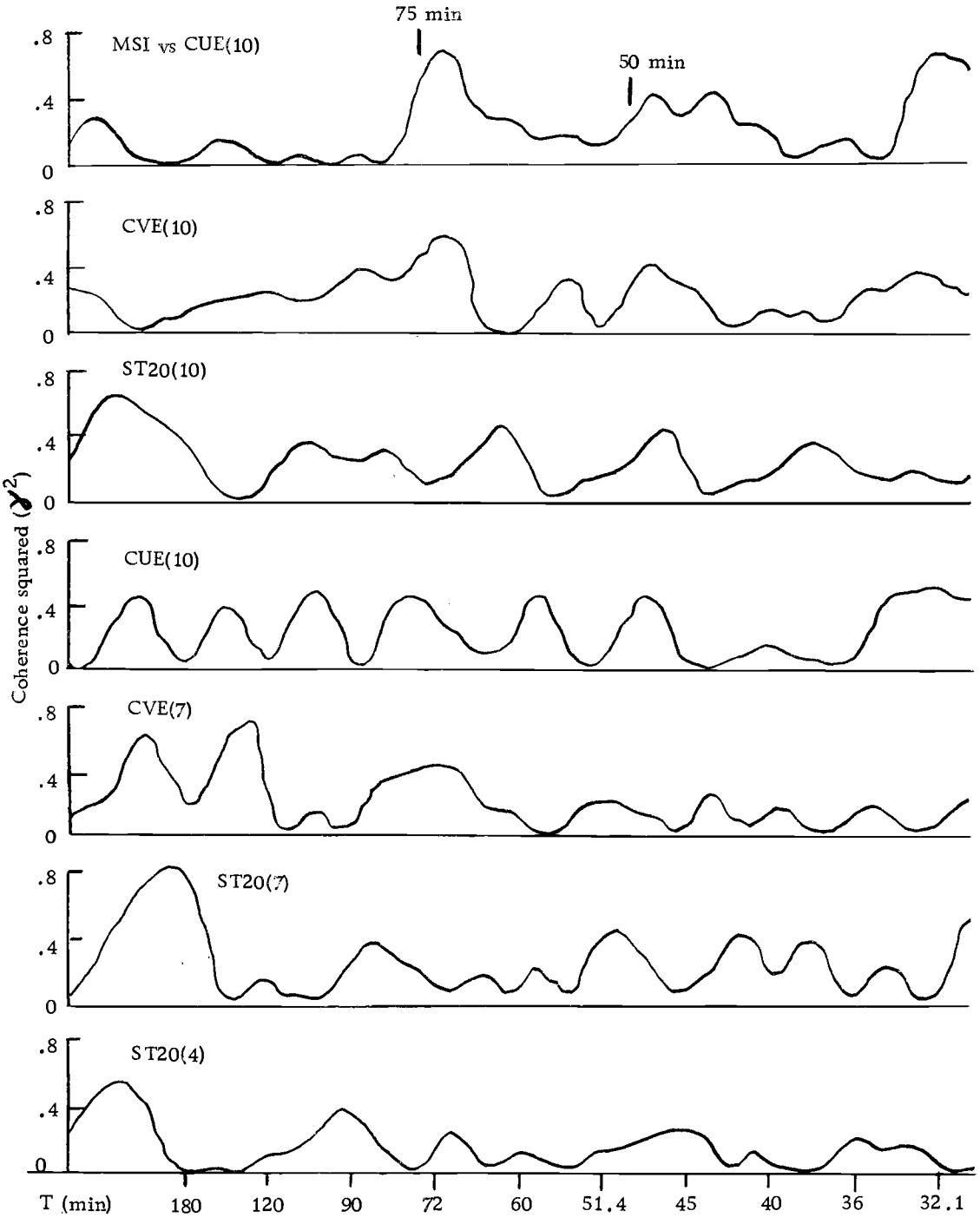

Figure 46. Squared coherence from cross-spectral analyses of MSI versus ST20(10), CUE(10), CVE(10), ST20(7), CUE(7), CVE(7), and ST20(4). .90 significant γ^2 is .691.

The cross-spectra between MSI and the sea temperature fluctuations at station 4 [ST20(4)] indicate no relationship exists, since for periods less than 90 minutes the coherence squared was less than 0.3. There are peaks in the coherence squared of MSI versus the four current components ranging from 0.4 to 0.6 for periods around 75 minutes, but there were no similar peaks in the coherence squared of MSI versus the sea temperature fluctuations at stations 7 and 10. In the 45 to 50 minute period band there were peaks greater than 0.4 in the coherence squared for MSI versus all the ocean parameter fluctuations at stations 7 and 10 except CVE(7).

In all, while the results of the spectral analyses are not conclusive, they add credence to the previously discussed conclusions that the cells pass over the spar buoy with an average period of around 50 minutes and that the ocean responds to these cells with fluctuations in temperature and currents.

VII. DISCUSSION OF OCEANIC RESPONSE TO MESOSCALE CELLS

The results of the previous section indicate that sea temperature fluctuations and current fluctuations are influenced by the passage of mesoscale atmospheric cells. From these results it can be concluded that some response occurred, but the actual processes involved are unclear. Some speculations concerning possible mechanisms follow.

First, a summary of the results to be discussed will be given. A cold air outbreak began on February 14, 1975, which produced well-developed mesoscale atmospheric cells by February 16. For 30 hours (2300 February 15 to 0500 February 17) the cells were of the closed variety and the air temperature and absolute humidity fluctuations correlated very well. Thereafter the cellular development appeared to lessen slightly, with some resurgences. During the passage of a cell over the spar buoy wind speed and turbulent heat fluxes varied by approximately 12.5%. If the clear, downdraft part of the cell is considered the reference point (a minimum in the MSI record), then the wind speed maximum occurred about 15 minutes before the passage of this reference point and the maximum heat flux occurred about five to ten minutes before the passage of the reference point. The oceanic responses tended to show up as sea

temperature fluctuations about 45 minutes after the passage of an MSI minimum and current surges to the right of the mean wind about 50 minutes after the passage of an MSI minimum. The average periodicity of MSI minima passing over the spar buoy was about 50 minutes.

Mixing Model

The simplest model to explain the sea temperature fluctuations would be for the cooler air temperatures associated with an MSI minimum to mix downward, with the 45 minute lag representing the mixing time. This idea was rejected for two main reasons: (1) the water column was unstable due to extensive surface cooling that was only modulated by the passage of cells, and mixing models require some degree of stable stratification (Hoeber, 1972); and (2) if it was a mixing process, then the sea temperature fluctuations at shallower depths should have occurred at intermediate lags. This was not the case. The three thermistors on the spar buoy all indicated the response occurred at the same lag and this lag was the same, or greater, than the lag found for the deeper current meter temperature response.

Wind Forced Model

If the increased cooling just before the passage of an MSI

minimum forms a layer of cooler water on the surface that is not quite unstable enough to sink, then the passage of the next wind maximum about 40 minutes later could give this layer a critical push and cause the layer to sink precipitously. The wind speed maxima were generally 12.5% greater than the minima, therefore the difference in surface wind energy was nearly 30%. This would not only explain the similar lags in the temperature responses, but also the increase in water momentum to the right of the wind as the wind increase itself would impart momentum and the abrupt sinking of the surface water would transport surface momentum with it. This idea appears feasible and cannot be rejected by the data.

Intermittent Convection

Foster (1971) described a process of intermittent convection in a fluid colled from above. This is a cyclic process involving the formation of a surface boundary layer by diffusive cooling, the increasing thickness and instability of this layer, the destruction of this layer by a localized convective plume, and the reformation of the surface boundary layer. He limited his discussion to a laboratory fluid with molecular diffusion coefficients. Using a simplified linear model (which required extensive computer time to analyze) he found that for fluids with a high Rayleigh number (greater than 10^7) intermittent convection occurs with fairly definite time and horizontal space

scales. He also found that, beyond some critical depth, this process was independent of depth. Applying molecular results to a turbulent fluid is questionable and applying a simplified linear molecular model to a turbulent ocean is even more so. But doing so provides an interesting possible explanation of the observed oceanic responses.

The results of Foster's (1971) model, a turbulent viscosity coefficient found by Hoeber (1972), and an average value of the turbulent heat fluxes found on February 16 at the spar buoy, were used to make an order of magnitude estimate of the characteristic time and horizontal space scales. These values were 100 minutes and 120 meters. If a process like intermittent convection occurs and if the above variation of Foster's model has any validity, then the time scale of the convective plumes is about the same as the time scale of the mesoscale cells, while the horizontal space scale of the plumes is much smaller than the horizontal space scale of the cells.

Intermittent Convection Plus Wind Forcing

The author believes that the process occurring on February 16, 1975 involved the cooled surface layer being drained by periodic convective plumes. The periods of the plumes were not free periods as discussed by Foster (1971), but periods forced by the passage of mesoscale cells. The forcing aspect of the cells could be the maximum heat flux associated with the MSI minimum, or, more

likely, the maximum wind speed at approximately the same time. These plumes are visualized as having a much smaller space scale than the mesoscale cells, which could explain the apparent 360^{o} phase shifts in the lag correlation analyses.

VIII. CONCLUSION

The main conclusion drawn from this research is that the passage of well-developed, closed, mesoscale atmospheric convective cells over the ocean causes fluctuations in the sea temperatures and currents at a depth of 20 meters on a time scale similar to that of the cells. During 30 hours of the outbreak studied, the passage of a clear area of a cell, when upward heat fluxes and wind speeds were greatest, was followed in 45 to 50 minutes by a drop in sea temperature and an increase in current motion to the right of the wind. Evidence for the above conclusions consists of the significant lag correlations found between a dimensionless index [MSI] formed from fluctuations of air temperature and absolute humidity (of $\approx 0.4^{\circ}C$ and ≈ 0.4 g/kg respectively) and fluctuations in the sea temperatures (of $\approx 0.03^{\circ}C$) and in the magnitudes of the current component aligned 25° to the right of the mean wind (of ≈ 15 cm/sec). The data suggest this interaction was a result of the variations in upward heat fluxes ($\approx 12.5\%$) and surface wind speed ($\approx 12.5\%$) associated with the passage of mesoscale atmospheric cells. Such an air-sea interaction has not, to the knowledge of the author, been previously measured or discussed. It must be emphasized that, though significant, the observed sea temperature and current fluctuations are only partially

explained by this interaction. The overall importance of this type of interaction must be determined by further research.

In arriving at the above conclusions other conclusions about mesoscale atmospheric cells were made. The presence and configuration of clouds, as shown by satellite emagery and solarimeter data, are not the only indicators of cellular activity. Fluctuations in the surface air temperature and absolute humidity can be correlated to indicate the development of mesoscale cellular activity and can be combined, as in MSI, to indicate the passage of mesoscale atmospheric cells over a given point. In some ways, the use of surface air temperature and absolute humidity fluctuations is superior to the use of cloud related data in that atmospheric conditions are measured at the surface, not 2000 meters above, and can be measured 24 hours a day, and not just during daylight hours.

Using correlations of surface air temperature and absolute humidity fluctuations to indicate the development of mesoscale cellularactivity and satellite imagery to indicate the type of cells present, it is suggested that there is a maturation process in mesoscale atmospheric cellular development. Open cells represent less development, and closed cells represent greater development. This result and the observation that open and closed cells were both present in the AMTEX area during outbreaks are seemingly contradictory to previous hypotheses wherein the magnitude of the surface

heat fluxes was felt to determine whether cells would be open or closed. It was also noted that the mesoscale cellular activity was persistent since air temperature and absolute humidity fluctuations were still highly correlated on the 18th of February after the cold air outbreak had apparently ceased.

In analyzing the current records the author found that the currents in the East China Sea, at least in the buoy area, were heavily dominated by the semi-diurnal tides, with a weak mean flow towards the northeast parallel to the Kuroshio. Using a technique developed by the author to combine mean flow data from two current meters it was found that the mean flow meandered. At least once this meandering approached a closed loop current.

The shorter period fluctuations (less than five hours) in the current records tended to orientate 25^{o} to the right of the mean wind flow in a manner indicative of Ekman veering. The author has no knowledge that short period fluctuations have ever been examined for Ekman veering. A string of current meters in near neutral waters, such as the East China Sea, might reveal an Ekman spiral. It was also noted that the current meter records were noisier during cold air outbreaks possibly indicative of increased instability of the water column, increased winds, or of mesoscale atmospheric cellular forcing of current fluctuations. The current meter noise was greater

in the V component which was generally to the right of the outbreak winds.

STD's and the thermistor chains indicated that the waters were basically isothermal to 70 meters during the AMTEX program. Short period fluctuations in the thermistor chain records tended to show up simultaneously at all depths, probably reflecting the instability and sinking of the waters. Vertical temperature gradients appeared and disappeared in the thermistor chain data with periods of 12.4 and 24 hours. The 12.4 hour periods are significantly coherent with the tidal currents, indicating that tidal advection combined with a horizontal temperature gradient could explain the 12.4 hour periodicity. The solar heating cycle apparently provides the best explanation for the 24 hour periodicity. At this time no definite conclusions can be made about the periodic appearance of vertical gradients in the water column.

The above conclusions were based on what has to be considered a minimal data base. Some of the evidence is not truly conclusive, though it is felt that the conclusions provide a valid, and exciting, basis for future research.

BIBLIOGRAPHY

Agee, E.M., T.S. Chen, and K.E. Dowell. 1973. A review of mesoscale cellular convection. Bulletin American Meteorological Society 54(10):1004-1012.

Box, G.E.P. and G.M. Jenkins. 1970. Time series analysis, forecasting and control. Holden-Day, San Francisco. 553 p.

Bunker, A.F. 1972. Wintertime interactions of the atmosphere with the Mediterranean Sea. Journal of Physical Oceanography 2:225-238.

Foster, T.D. 1971. Intermittent convection. Geophysical Fluid Dynamics 2:201-217.

Foster, T.D. 1972. Haline convection in polynyas and leads. Journal of Physical Oceanography 2:462-469.

Friehe, C.A. and K.F. Schmitt. Parameterization of air-sea interface fluxes of sensible heat and moisture by the bulk aerodynamic formulas. Undated manuscript. Scripps Institute of Oceanography, LaJolla, California. 30 p.

Gonella, J. 1972. A rotary-component method for analyzing meteorological and oceanographic vector time series. Deep Sea Research 19:833-846.

Hess, S.L. 1959. Introduction to theoretical meteorology. Holt, Rinehart and Winston, New York. 362 p.

Hoeber, H. 1972. Eddy thermal conductivity in the upper twelve meters of the tropical Atlantic. Journal of Physical Oceanography 2:303-304.

Hubert, L.F. 1966. Mesoscale cellular convection. Meteorological Satellite Laboratory report No. 37, Washington, D.C. 68 p.

Ichiye, T. and E.J. Zipser. 1967. An example of heat transfer at the air-sea boundary over the Gulf Stream during a cold air outbreak. Journal Meteorological Society of Japan 45(3):261-270.

Jenkins, G.M. and D.G. Watts. 1969. Spectral analysis and its applications. Holden-Day, San Francisco, California. 525 p.

Leetmaa, A. and C.S. Welch. 1972. A note on diurnal changes in momentum transfer in the surface layers of the ocean. Journal of Physical Oceanography 2:302-303.

Lenschow, D.H. 1972. The air mass transformation experiment (AMTEX). Bulletin American Meteorological Society 53(4):353-357.

Lenschow, D.H. and E.M. Agee. 1974. The air mass transformation experiment (AMTEX): Preliminary results from 1974 and plans for 1975. Bulletin American Meteorological Society 55(10):1228-1235.

List, R.J. 1949. Smithsonian meteorological tables, sixth revised edition. Smithsonian Institution Press, Washington, D.C. 527 p.

Longuet-Higgins, M.S. 1968. On the trapping of waves along a discontinuity of depth in a rotating ocean. Journal of Fluid Mechanics 31(3):417-434.

Malkus, J.S. 1962. Large scale interactions. The Sea. (M.N. Hill, ed.). Pergamon Press, Fairview, N.Y. Vol. 1, chapter 4, p. 88-294.

Manabe, S. 1957. On the modification of air-mass over the Japan Sea when the outburst of cold air predominates. Journal Meteorological Society of Japan 35:311-326.

Mooers, C.N.K. 1973. A technique for the cross spectrum analysis of pairs of complex-valued time series, with emphasis on the properties of polarized components and rotational invariants. Deep Sea Research 20:1129-1141.

Neuman, G. and W.J. Pierson. 1966. Principles of physical oceanography. Prentice-Hall, Englewood Cliffs, N.J. 545 p.

Niino, H. and K.O. Emery. 1961. Sediments of shallow portions of East China and South China Sea. Geological Society of America Bulletin 72:731-762.

Nitani, H. 1972. Kuroshio in the East China Sea. In: Kuroshio (H. Stommel and H.Yoshida, eds.). University of Washington Press, Seattle, Washington. 517 p.

Ninomiya, K. 1972. Heat and water-vapor budget over the East China Sea in the winter season. Journal Meteorological Society of Japan 50(1):1-17.

Nowlin, W.D., Jr. and C.A. Parker. 1974. Effects of a cold-air outbreak on shelf waters of the Gulf of Mexico. Journal of Physical Oceanography 4:467-486.

Reed, R.K. and D. Halpern. 1975. The heat content of the upper ocean during coastal upwelling: Oregon, August 1973. Journal of Physical Oceanography 5(2):378-383.

Robinson, A. 1973. Spar buoy. Exposure 1(2):12-13.

Snedecor, G.W. and W.G. Cochran. 1967. Statistical methods, sixth edition. The Iowa State University Press, Ames, Iowa. 593 p.

Stommel, H., A. Vorhis, and D. Webb. 1971. Submarine clouds in the deep ocean. American Scientist 59:716-722.

Worthington, L.V. 1971. Anticyclogenesis of the oceans as a result of outbreaks of continental polar air. Vol. 1, Studies in physical oceanography. Gordon Breach, New York. p. 169-178.

Worthington, L.V. 1972. Negative oceanic heat flux as a cause of water-mass formation. Journal of Physical Oceanography 2(3):205-211.

APPENDIX

APPENDIX

Calculation of Heat and Mass Fluxes

Turbulent Fluxes

The heat and mass fluxes reported in this thesis were calculated by the bulk aerodynamic method. This method approximates the fluxes over a given interval of time by the use of the average "bulk" parameters of wind speed and air-sea surface temperature and vapor density differences.

The basic formulas are (Friehe and Schmitt, undated):

$$HS = D_a \cdot C_p \cdot C_h \cdot \overline{U} \cdot (T_s - T_a) \tag{1}$$

$$E = C_e \cdot \overline{U} \cdot (Q_s - Q_a) \tag{2}$$

where:

HS = the sensible heat flux ($cal/cm^2 sec$)

D_a = density of the air (g/cm^3)

C_p = isobaric specific heat of moist air ($cal/g\,^oC$)

C_h = sensible heat transfer coefficient (empirical)

$\overline{U}$ = mean wind speed at reference height h (cm/sec)

T_s = sea surface potential temperature, usually obtained about one meter below the surface (^oC)

T_a = potantial air temperature at reference height h (^oC)

E = evaporative mass flux ($g/cm^2 sec$)

C_e = evaporative mass transfer coefficient (empirical)

Q_s = water vapor density near sea surface, obtained by assuming the air to be saturated at the sea surface temperature (g/m^3)

Q_a = water vapor density at reference height h (g/m^3)

Then the latent heat flux is calculated by

$$HL = L(E) \tag{3}$$

where:

HL = latent heat flux ($cal/cm^2 sec$)

L = latent heat of evaporation (cal/g)

These formulas are straightforward but complicated to use because air is a thermodynamic fluid and most of the parameters must be calculated from basic measurements. These basic measurements are the dry-bulb and wet-bulb air temperatures (DB and WB in ^oC), wind speed (U in m/sec) all measured at a given height (h in meters), and sea surface temperature (ST in ^oC). Also some data concerning the sea surface air pressure (P in mb) and salinity (S in $^o/_{oo}$) are needed.

The wind speed is used as measured. The potential temperatures T_s, T_a, and the latent heat of evaporation are simple functions of ST, DB, and P (List, 1949):

$$T_s = ST \cdot (1000/P)^{2/7} \tag{4}$$

$$T_a = DB \cdot (1000/P)^{2/7} \tag{5}$$

$$L = 5.973 - (0.565 \cdot ST) \tag{6}$$

The calculations of D_a, Q_s and Q_a are all dependent upon the saturated vapor pressure (ES in atm) over pure water at appropriate temperatures (T in ^oK) found by the Goff-Gratch equation (List, 1949):

$$\begin{aligned} \text{Log}_{10}(ES) = {} & -7.90208\,[(373.16/T) - 1] \\ & + 5.0208\,[\text{Log}_{10}(373.16/T)] \\ & - 1.3816\,(10^{-7})\,[10^{11.344(1-T/373.16)} - 1] \\ & + 8.1328\,(10^{-3})\,[10^{-3.19149(373.16/T-1)} - 1] \end{aligned} \tag{7}$$

Then formulas derived from Hess (1959) give the vapor pressure (EV in atm), the absolute humidity (AH in g/g), and the mixing ratio (r in g/g):

$$EV = ES - (DB - WB)\,[C_p/(.622 \cdot L)] \tag{8}$$

$$AH = 0.622\,[EV/(1 - .378 \cdot EV)] \tag{9}$$

$$r = AH/(1 - AH) \tag{10}$$

and formulas from List (1949) give the specific heat of moist air (C_p in cal/g^oK) and the density of moist air (D_a in g/m^3):

$$C_p = 0.2402 + 0.4409(r) \tag{11}$$

$$D_a = 1292.9\,[273.13/(T+273.23)] \cdot [(P - .3783)/1013.25] \tag{12}$$

The sea surface vapor density (Q_s) is found by first calculating the saturated vapor pressure at the sea surface by using ST in equation (7), then this is converted into saturated absolute humidity by equation (9), and finally this is multiplied by the air density calculated by using ST in equation (12) to give Q_s. The vapor density at height

$h(Q_a)$ is found by first calculating the saturated vapor pressure at height h by using WB in equation (7), then the actual vapor pressure at height h is calculated by using DB and WB in equation (8),[1] then this is converted into absolute humidity by equation (9) and finally the absolute humidity is multiplied by the air density calculated by using DB in equation (12) to give Q_a. The specific heat of the sea surface air (C_p) is calculated by converting the absolute humidity at the sea surface to a mixing ratio (r) by using equation (10) and then calculating C_p by equation (11).

All that remains to be calculated in order to use equations (1) and (2) are values for the empirical constants C_h and C_e. Friehe and Schmitt (undated) have compared data of turbulent flux measurements taken simultaneously with "bulk" parameters. They found that $C_e = 1.32 \times 10^{-3}$ adequately fits the moisture flux data but that three values of C_h were needed for different situations:

$$C_h = 0.86 \times 10^{-3} \text{ for } U(T_s - T_a) < 0$$

$$C_h = 0.97 \times 10^{-3} \text{ for } 0 < U(T_s - T_a) < 2500 \text{ cm}^{\circ}\text{K/sec}$$

$$C_h = 1.46 \times 10^{-3} \text{ for } U(T_s - T_a) > 2500 \text{ cm}^{\circ}\text{K/sec}$$

These coefficients assume the temperature and wind speed data are taken at h = 10 m. For $h \neq 10$ m the coefficients are adjusted by assuming logarithmic profiles and constant fluxes. Use of the

---

[1] In equation (8), C_p is approximated by 0.240 and the latent heat calculated by using WB instead of ST in equation (6).

logarithmic profile implies that:

$$C_{10} = k^2/[\ln(10/z_o)]^2 \tag{13}$$

where k = von Karmans constant (0.4) and z_o = a roughness parameter dependent on surface conditions, and C_{10} is the coefficient at h = 10 m. Assuming constant flux implies that:

$$C = k^2/[\ln(h/z_o)]^2 \tag{14}$$

where the value of z_o is the same as in equation (13). Therefore C can be calculated by solving equation (13) for z_o in terms of C_{10} and k and then solving equation (14) for C in terms of k and z_o.

For the data at AMTEX station 10 used in this thesis $U(T_s-T_a)$ was consistently large so $C_h = 1.46 \times 10^{-3}$ was used as the proper coefficient for h = 10 m. The atmospheric data were collected at an average height of 4 m. Therefore the coefficients used were:

$$C_e = 1.57 \times 10^{-3}$$

$$C_h = 1.75 \times 10^{-3}$$

With the above coefficients and previously calculated parameters, equations (1), (2), and (3) were used to calculate the evaporative mass transfer, evaporative heat transfer and sensible heat transfer from the ocean to the atmosphere for five minute intervals throughout the available data record.

Of the basic data used in these calculations WS, DB, and WB were measured on the spar buoy at h = 4 m, the air pressure was measured on a weather ship located about 80 km to the southeast of

the spar buoy and at one hour intervals, the salinity was assumed constant at $34^{o}/_{oo}$ which is a characteristic figure for this area at this time of year (Niino and Emery, 1961), and ST was measured at a depth of 20 m on a current meter about 200 meters from the spar buoy.